

**A STUDY OF OPTICAL RESOLUTION OF
METHIONINE HYDROCHLORIDE BY
PREFERENTIAL CRYSTALLIZATION**

Watcharakarn Srimahaprom

A Thesis Submitted in Partial Fulfillment of the Requirements for the

Degree of Master of Engineering in Chemical Engineering

Suranaree University of Technology

Academic Year 2011

ศึกษาการแยกสารเมไทโอนีนไฮโดรคลอไรด์โดยการตกผลึกรูปแบบที่ต้องการ

นายวัชรกานต์ ศรีมหาพรหม

วิทยานิพนธ์นี้เป็นส่วนหนึ่งของการศึกษาตามหลักสูตรปริญญาวิศวกรรมศาสตรมหาบัณฑิต

สาขาวิชาวิศวกรรมเคมี

มหาวิทยาลัยเทคโนโลยีสุรนารี

ปีการศึกษา 2554

**A STUDY OF OPTICAL RESOLUTION OF METHIONINE
HYDROCHLORIDE BY PREFERENTIAL CRYSTALLIZATION**

Suranaree University of Technology has approved this thesis submitted in partial fulfillment of the requirements for a Master's Degree.

Thesis Examining Committee



(Dr. Terasut Sookkumnerd)

Chairperson



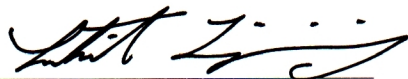
(Prof. Dr. Adrian Flood)

Member (Thesis Advisor)



(Asst. Prof. Dr. Atichat Wongkoblap)

Member



(Prof. Dr. Sukit Limpijumnong)

Vice Rector for Academic Affairs



(Assoc. Prof. Ft. Lt. Dr. Kontorn Chamniprasart)

Dean of Institute of Engineering

วัชรกานต์ ศรีมหาพรหม : ศึกษาการแยกสารเมไทโอนีนไฮโดรคลอไรด์โดยการตกผลึก
รูปแบบที่ต้องการ (A STUDY OF OPTICAL RESOLUTION OF METHIONINE
HYDROCHLORIDE BY PREFERENTIAL CRYSTALLIZATION) อาจารย์ที่ปรึกษา :
ศาสตราจารย์ ดร.เอเดรียน พลัด, 199 หน้า.

โปรตีนเป็นสิ่งที่จำเป็นในการบำรุงเสริมสร้างและซ่อมแซมส่วนที่สึกหรอของร่างกาย
อีกทั้งยังเป็นสารประกอบอินทรีย์ที่เป็นส่วนประกอบสำคัญของเนื้อเยื่อและอวัยวะของร่างกาย
มนุษย์และสิ่งมีชีวิตทุกชนิด โครงสร้างของโปรตีนมีโมเลกุลของกรดอะมิโน (amino acid) เป็น
องค์ประกอบที่สำคัญโดยมีลักษณะเป็นสารชีวโมเลกุล กรดอะมิโนจากการสังเคราะห์โปรตีนใน
ร่างกายมีอยู่ 20 ชนิด แบ่งได้เป็น 2 ประเภท คือ กรดอะมิโนที่ไม่จำเป็น (non-essential amino acids)
12 ชนิด และกรดอะมิโนจำเป็น (essential amino acids) 8 ชนิด

เมไทโอนีน (methionine, met) เป็นหนึ่งในกรดอะมิโนที่จำเป็นต่อร่างกาย แต่ร่างกายไม่
สามารถสังเคราะห์ขึ้นได้เอง จึงมีการสังเคราะห์เมไทโอนีนขึ้นมาด้วยกระบวนการทางเคมี
ซึ่งกรดอะมิโนที่ได้จะอยู่ในรูปของดีแอลเมไทโอนีน (DL-methionine) แต่มีเฉพาะรูปของแอล
(L-form) เท่านั้นที่จำเป็นและมีประโยชน์ต่อร่างกาย ดังนั้นจึงต้องทำการสกัดแยกเฉพาะ
แอลเมไทโอนีน (L-methionine) ออกจากดีแอลเมไทโอนีนด้วยวิธีการตกผลึก เนื่องจากเป็น
กระบวนการแยกสารที่มีประสิทธิภาพค่อนข้างสูงและสะดวก วิธีการตกผลึกที่ใช้ในงานวิจัยนี้ คือ
การตกผลึกแบบที่ต้องการ (preferential crystallization) เพราะสามารถแยกแอลเมไทโอนีนออก
จากดีเมไทโอนีน (D-methionine) ได้ แต่การแยกด้วยวิธีนี้จะต้องทำเมไทโอนีนให้อยู่ในรูปของ
เกลือไฮโดรคลอไรด์ (HCl salt) ก่อน จึงจะสามารถแยกด้วยกระบวนการตกผลึกแบบที่ต้องการ
ได้ เนื่องจากเมไทโอนีนในรูปของเกลือไฮโดรคลอไรด์ (met-HCl) จะอยู่ในรูปแบบของ
คอลลอยด์เมอรัเรท (conglomerate forming) ในขณะที่ผลึกของเมไทโอนีนบริสุทธิ์ซึ่งอยู่ในรูปแบบ
ของราซีเมท (racemate forming) ไม่สามารถทำการแยกด้วยกระบวนการนี้ได้

จากการทดลองพบว่าความสามารถในการละลายในน้ำของเมไทโอนีนไฮโดรคลอไรด์
(met-HCl) มีค่าแปรผันโดยตรงกับอุณหภูมิ ซึ่งค่าความสามารถในการละลายในน้ำของเมไทโอนีน
ไฮโดรคลอไรด์จะมีค่าเพิ่มขึ้นเมื่ออุณหภูมิเพิ่มสูงขึ้น จากผลของค่าความสามารถในการละลาย
ในน้ำ เมื่อแสดงด้วยแผนภาพเฟสไดอะแกรมสำหรับระบบสารผสมสามองค์ประกอบ (ternary
phase diagram) ของ แอลเมไทโอนีนไฮโดรคลอไรด์ (L-met-HCl) + ดีเมไทโอนีนไฮโดรคลอไรด์
(D-met-HCl) + น้ำ พบว่าสอดคล้องเป็นไปตามแผนภาพเฟสไดอะแกรมของสารประกอบ
คอลลอยด์เมอรัเรท

การศึกษาอัตราการเติบโตของผลึกแบบกระจาย (growth rate distribution) และจุดเริ่มต้นของการเกิดนิวคลีเอชัน (nucleation threshold) มุ่งเน้นเพื่อใช้ในการออกแบบสภาวะการทดลองและดำเนินการทดลองสำหรับการตกผลึกแบบที่ต้องการให้เหมาะสมที่สุด จุดเริ่มต้นของการเกิดนิวคลีเอชันแบบปฐมภูมิ (primary nucleation threshold) และจุดเริ่มต้นของการเกิดนิวคลีเอชันแบบทุติยภูมิ (secondary nucleation threshold) ถูกวัดก่อนการทดลองหาอัตราการเติบโตของผลึกเพื่อให้แน่ใจว่าไม่มีนิวคลีเอชันเกิดขึ้นในกระบวนการตกผลึก ด้วยวิธีการหาค่าความสัมพันธ์ระหว่างเวลาการเหนี่ยวนำให้เกิดนิวคลีเอชัน (induction time) กับค่าความเข้มข้นยิ่งยวดสัมพัทธ์ (relative supersaturation) ของเมไทโอนีนไฮโดรคลอไรด์ที่มีค่าความเข้มข้นต่างๆ ซึ่งผลการทดลองพบว่าค่าเวลาการเหนี่ยวนำให้เกิดนิวคลีเอชันจะมีค่าเพิ่มขึ้น เมื่อค่าความเข้มข้นยิ่งยวดสัมพัทธ์ของเมไทโอนีนไฮโดรคลอไรด์มีค่าลดลง ซึ่งเหมือนกันทั้งค่าจุดเริ่มต้นของการเกิดนิวคลีเอชันแบบปฐมภูมิและทุติยภูมิ

อัตราการเติบโตของผลึกแอลเมไทโอนีนไฮโดรคลอไรด์จะเติบโตได้ดีมากในสารละลายความเข้มข้นยิ่งยวดของแอลเมไทโอนีนไฮโดรคลอไรด์ แต่เติบโตไม่ดีในสารละลายความเข้มข้นยิ่งยวดของดีแอลเมไทโอนีนไฮโดรคลอไรด์ (DL-met·HCl) นอกจากนี้ยังพบว่าทั้งในสารละลายความเข้มข้นยิ่งยวดของแอลเมไทโอนีนไฮโดรคลอไรด์ และสารละลายความเข้มข้นยิ่งยวดของดีแอลเมไทโอนีนไฮโดรคลอไรด์ จะมีอัตราการเติบโตของผลึกแบบกระจายที่ค่อนข้างกว้างด้วยกันทั้งคู่ ในเวลาและค่าความเข้มข้นที่เท่ากัน

การตกผลึกแบบที่ต้องการของสารละลายดีแอลเมไทโอนีนไฮโดรคลอไรด์ที่อุณหภูมิ 10 องศาเซลเซียส ถูกศึกษาโดยกระบวนการตกผลึกแบบกะโดยใช้ตัวล่อ (seeded batch crystallization) เพื่อแยกสารอีแนนทิโอเมอร์ที่ต้องการ (L-met·HCl) ออกจากสารละลายราซิเมท (DL-met·HCl) ซึ่งผลความสำเร็จของงานวิจัยนี้แสดงด้วยค่าเปอร์เซ็นต์ความบริสุทธิ์ของผลึกแอลเมไทโอนีนไฮโดรคลอไรด์ โดยใช้วิธีการวัดสมบัติการหมุนแสง (optical activity) ผลการทดลองพบว่าเปอร์เซ็นต์ความบริสุทธิ์ของผลึกแอลเมไทโอนีนไฮโดรคลอไรด์มีค่าลดลงอย่างรวดเร็วเข้าสู่ภาวะสมดุล ณ ค่าหนึ่งๆ เมื่อเวลาผ่านไป ที่เป็นเช่นนี้เนื่องจากอิทธิพลของจุดเริ่มต้นของการเกิดนิวคลีเอชันของสารอีแนนทิโอเมอร์ที่ไม่ต้องการ (D-met·HCl) โดยสรุปการแยกสารอีแนนทิโอเมอร์ที่ต้องการ ออกจากสารละลายราซิเมทด้วยวิธีการตกผลึกแบบที่ต้องการ ไม่สามารถแยกสารอีแนนทิโอเมอร์ที่ต้องการที่มีความบริสุทธิ์ 100 เปอร์เซ็นต์ได้

สาขาวิชา วิศวกรรมเคมี
ปีการศึกษา 2554

ลายมือชื่อนักศึกษา

ลายมือชื่ออาจารย์ที่ปรึกษา

WATCHARAKARN SRIMAHAPROM : A STUDY OF OPTICAL
RESOLUTION OF METHIONINE HYDROCHLORIDE BY
PREFERENTIAL CRYSTALLIZATION. THESIS ADVISOR :
PROF. ADRIAN E. FLOOD, Ph.D., 199 PP.

OPTICAL RESOLUTION/PREFERENTIAL CRYSTALLIZATION/AMINO
ACID/METHIONINE HYDROCHLORIDE

Proteins are important for the treatment and repair of organs in the body. They are organic compounds that are the components of the cells and tissues of humans. Proteins consist of many amino acids bonded together with peptide bonds. Thus proteins and/or amino acids are essential for human and animal nutrition. Methionine (met) is an amino acid which is essential in the human diet. Methionine is not synthesized in humans, hence we must consume sufficient amounts of methionine or methionine-containing proteins.

For this reason, methionine has been chemically synthesized for commercial benefit and for other industrial users. Methionine from chemical synthesis is DL-methionine, however only the L-form is essential and beneficial for the humans; the D-form is not essential for the body. Therefore a crystallization process called preferential crystallization can be used to separate the D- and L-forms of methionine. The separation must be done on the HCl salt of methionine since this crystallizes as a conglomerate, while methionine crystallizes as a racemic crystal.

The experimental results reveal the solubility of methionine hydrochloride (met·HCl) in water is strongly dependent on the temperature and solubility increased with increasing temperature. The ternary solubility diagram of L-met·HCl + D-

met·HCl + water is in accordance with the typical ternary phase diagram for a conglomerate type compound. The growth rate distributions together with the nucleation thresholds data can be used to optimize operation of the preferential crystallization. The primary nucleation threshold (PNT) and secondary nucleation threshold (SNT) were determined by induction time measurement with relative supersaturations of DL-met·HCl solution, to ensure that growth of crystal was measured under convenient non-nucleating conditions. The induction time increasing as the relative supersaturation of the PNT and SNT decreases. The crystal growth rate of L-met·HCl depends strongly on the relative supersaturation from supersaturated solutions of pure L-met·HCl but not from racemic solutions (DL-met·HCl). Also there is a wide crystal growth rate distribution from both types of supersaturated solutions.

The preferential crystallization of DL-met·HCl aqueous solution at 10°C was studied via a seeded batch crystallization process, that will be used to separate the desired enantiomer (L-met·HCl) from the racemic solution (DL-met·HCl). The percent purity of L-met·HCl crystal was evaluated by means the optical activity measurement. The purity of L-met·HCl crystal decreased rapidly to the equilibrium value over time, due to the influence of the nucleation threshold of the counter-enantiomer (D-met·HCl) being small. Using preferential crystallization to separate the enantiomers of met·HCl from an aqueous solution to obtain a high purity product appears to be very difficult; this study cannot separate the desired enantiomer to close to 100% purity.

School of Chemical Engineering

Academic Year 2011

Student's Signature



Advisor's Signature



ACKNOWLEDGEMENT

First, I would like to thank Prof. Dr. Adrian E. Flood and Dr. Terasut Sookkumnerd for providing me with the opportunity to study the Master of Engineering Program in Chemical Engineering at Suranaree University of Technology (SUT). Foremost, I would like to express my sincere gratitude to Prof. Dr. Adrian E. Flood, my thesis advisor. I am grateful to him for all of his supporting information and invaluable advice, as well as his kindness, which helped me pass through my difficult times. I also thank him for his tireless effort in correcting my English grammar, and encouraging me to complete my work. I would not have achieved this far and this thesis would not have been accomplished without all the great support from him.

Also, I would like to thank all the lecturers at the School of Chemical Engineering, SUT, for their good attitude and advice. I would also like to thank all the thesis examination committee, Dr. Terasut Sookkumnerd, Asst. Prof. Dr. Atichat Wongkoblaph, and my advisor, for their insightful comments and supportive questions during the thesis examination. I would like to take this opportunity to sincerely thank to all the academic staffs, lab technicians, and secretaries in the School of Chemical Engineering for their encouragement and guidance, and also including thank all the members of the technical staffs in the Center for Scientific and Technological Equipment (CSTE), SUT, for their support and guidelines for use of the laboratory equipment, and occasional help in characterization of the properties of samples.

I gratefully acknowledge the funding sources that made my master research work possible, especially the SUT Research and Development Fund, grant number SUT7-706-51-36-31 for sponsoring my study and support for research through the Master of Chemical Engineering Program. I am also grateful to Suranaree University of Technology where I studied and conducted my research.

In addition, I would like to thank all my colleagues who are graduate students and undergraduate students in the School of Chemical Engineering, SUT, for all their supported and shared the research experiences and pleasure in life throughout the period of graduate education. Especially, I would like to thank from my heart to Miss Wanida Potong (Kluay), who is the best close friend for encouragement, heartiness, entertainment, and best always to take care of each other all along. Thank you for always standing beside each other in tough times of my life.

The finally important, I most gratefully acknowledge my dear family for all their unconditional love, understanding, and support, especially for my parents who raised me with love, supported me in the pursuit of success, and persistent confidence in me. Without these two most beloved people I could never have imagined achieving this goal.

Watcharakarn Srimahaprom

TABLE OF CONTENTS

	Page
ABSTRACT (THAI).....	I
ABSTRACT (ENGLISH).....	III
ACKNOWLEDGEMENTS.....	V
TABLE OF CONTENTS.....	VII
LIST OF TABLES.....	XIV
LIST OF FIGURES.....	XIX
SYMBOLS AND ABBREVIATIONS.....	XXVII
CHAPTER	
I INTRODUCTION.....	1
1.1 Background and Significance of the Problem.....	1
1.2 Research Objectives.....	5
1.3 Scope and Limitations.....	5
1.3.1 Thermodynamic Properties of DL-met·HCl on Preferential Crystallization.....	5
1.3.2 Kinetic Properties of DL-met·HCl on Preferential Crystallization.....	6
1.4 Outputs.....	6
1.5 References.....	7

TABLE OF CONTENTS (Continued)

	Page
II SOLUBILITY OF ENANTIOMERIC METHIONINE HYDROCHLORIDE IN AQUEOUS SOLUTION.....	8
2.1 Abstract.....	8
2.2 Introduction.....	9
2.3 Theory.....	12
2.3.1 Racemic Mixtures.....	12
2.3.2 Classical Solubility Measurement.....	14
2.3.3 Binary and Ternary Phase Diagrams and System Types.....	16
2.4 Experimental Procedure.....	22
2.4.1 Materials.....	22
2.4.2 Determination of the Concentration Calibration Curve of DL-met·HCl.....	24
2.4.3 Determination of the Solubility of met·HCl in Aqueous Solution for Pure Enantiomer and Racemic Conglomerate.....	24
2.4.4 Determination of the Solubility of Mixture Compositions of met·HCl Enantiomers in Aqueous Solution.....	26

TABLE OF CONTENTS (Continued)

	Page
2.5 Results and Discussion.....	28
2.5.1 DL-met·HCl Solubility Calibration Curve.....	28
2.5.2 Solubility of the met·HCl Species in Aqueous Solution.....	30
2.5.3 Ternary Solubility Diagram of the met·HCl Enantiomers in Water System.....	34
2.6 Conclusions.....	38
2.7 References.....	40
III CRYSTAL GROWTH RATES AND GROWTH RATE DISTRIBUTIONS FOR L-METHIONINE HYDROCHLORIDE SINGLE CRYSTALS IN SUPERSATURATED SOLUTIONS OF METHIONINE HYDROCHLORIDE.....	44
3.1 Abstract.....	44
3.2 Introduction.....	46
3.3 Theory.....	49
3.3.1 Fundamentals of Nucleation.....	50
3.3.2 Fundamental of Induction Time Measurement.....	51
3.3.3 Methodology to Study the Crystal Growth.....	52

TABLE OF CONTENTS (Continued)

	Page
3.4 Experimental Procedure.....	54
3.4.1 Materials.....	54
3.4.2 Determination of the Induction Times of Primary and Secondary Nucleation Threshold for DL-met·HCl in Aqueous Solution.....	55
3.4.3 Determination of the Mean Crystal Growth Rates and Growth Rate Distribution of L-met·HCl Single Crystals in DL- and L- met·HCl Supersaturated Solution by Small-Cell Crystallizer.....	58
3.5 Results and Discussion.....	62
3.5.1 Effect of DL-met·HCl Supersaturated Solution to the Induction Time for Primary and Secondary Nucleation Threshold Measurement.....	62
3.5.2 Growth Rate Distribution of L-met·HCl Single Crystals in DL- and L-met·HCl Supersaturated Solution.....	67

TABLE OF CONTENTS (Continued)

	Page
3.5.3 Mean Growth Rates of L-met·HCl Single Crystals in DL- and L-met·HCl Supersaturated Solution.....	87
3.6 Conclusions.....	91
3.7 References.....	93
IV THE PURIFICATION OF L-METHIONINE HYDROCHLORIDE VIA OPTICAL RESOLUTION OF DL-METHIONINE HYDROCHLORIDE BY PREFERENTIAL CRYSTALLIZATION.....	96
4.1 Abstract.....	96
4.2 Introduction.....	98
4.3 Theory.....	101
4.3.1 Principle of Preferential Crystallization.....	101
4.3.2 Optical Activity Measurement.....	103
4.4 Experimental Procedure.....	106
4.4.1 Materials.....	106
4.4.2 Preferential Crystallization of DL-met·HCl Aqueous Solution.....	106
4.4.3 Optical Activity of L-met·HCl by Polarimetry.....	108

TABLE OF CONTENTS (Continued)

	Page
4.5 Results and Discussion.....	111
4.5.1 The Suspension Density of DL-met·HCl Aqueous Solution on Preferential Crystallization.....	111
4.5.2 Determination of the Percent Purity of L-met·HCl Crystals.....	119
4.6 Conclusions.....	129
4.7 References.....	131
V CONCLUSIONS AND RECOMMENDATIONS	135
5.1 Conclusions.....	135
5.2 Recommendations.....	139
5.3 Reference.....	141
 APPENDICES	
APPENDIX A. CALCULATION OF THE METHIONINE HYDROCHLORIDE CONCENTRATION IN SOLUBILITY EXPERIMENTS.....	142
APPENDIX B. CALCULATION OF CONFIDENCE INTERVAL FOR MEAN VALUES.....	160
APPENDIX C. CALCULATION OF THE SUSPENSION DENSITY AT EQUILIBRIUM CONDITION.....	166

TABLE OF CONTENTS (Continued)

	Page
APPENDIX D. DETERMINATION OF THE DENSITY OF DL-METHIONINE HYDROCHLORIDE AQUEOUS SOLUTION AT 25°C.....	175
APPENDIX E. DETERMINATION OF THE PERCENT PURITY OF L-METHIONINE HYDROCHLORIDE IN THE CRYSTAL PHASE.....	182
APPENDIX F. PUBLICATIONS.....	187
BIOGRAPHY.....	199

LIST OF TABLES

Table	Page
2.1 The results of the concentration calibration curve for the met·HCl solution at 25°C.....	29
2.2 Average value of solubility results (C_{Avg}^* , g met·HCl/100 g water), and error limit (95% confidence interval, C.I.) for the racemic conglomerate mixture, pure enantiomer, and 75 : 25 mixture of met·HCl enantiomers in water at four temperatures.....	31
2.3 Average solubility results in mass fraction (\bar{w}) and error limit (95% confidence interval, C.I.) for the racemic conglomerate mixture, pure enantiomer, and 75 : 25 mixture of met·HCl enantiomers in water at four temperatures.....	35
3.1 Experimental conditions of the primary nucleation threshold experiments and the induction time values (t_{ind}).....	63
3.2 Experimental conditions of the secondary nucleation threshold experiments and the induction time values (t_{ind}).....	64

LIST OF TABLES (Continued)

Table	Page
3.3 Experimental results of crystal growth of a L-met·HCl crystals in L-met·HCl supersaturated solution ($\sigma = 0.005$) at 10°C, magnification 25x (From Figure 3.14).....	73
3.4 Crystal growth rates of L-met·HCl crystals in L-met·HCl supersaturated solution ($\sigma = 0.005$), 10°C, magnification 25x (From Figure 3.15).....	74
3.5 Results of crystal growth rate (G) of L-met·HCl crystals (total 45 crystal particles) in DL-met·HCl solution ($\sigma = 0.005$) at 10°C.....	75
3.6 Results of crystal growth rate (G) of L-met·HCl crystals (total 43 crystal particles) in DL-met·HCl solution ($\sigma = 0.01$) at 10°C.....	76
3.7 Results of crystal growth rate (G) of L-met·HCl crystals (total 60 crystal particles) in DL-met·HCl solution ($\sigma = 0.02$) at 10°C.....	77
3.8 Results of crystal growth rate (G) of L-met·HCl crystals (total 38 crystal particles) in L-met·HCl solution ($\sigma = 0.005$) at 10°C.....	78

LIST OF TABLES (Continued)

Table	Page
3.9 Results of crystal growth rate (G) of L-met·HCl crystals (total 57 crystal particles) in L-met·HCl solution ($\sigma = 0.01$) at 10°C.....	79
3.10 Results of crystal growth rate (G) of L-met·HCl crystals (total 78 crystal particles) in L-met·HCl solution ($\sigma = 0.02$) at 10°C.....	80
3.11 Mean and standard deviation (S.D.) of the crystal growth rate distributions of L-met·HCl crystals in DL- and L-met·HCl solutions at 10°C.....	89
4.1 The experimental conditions and results of the preferential crystallization of DL-met·HCl aqueous solution at 10°C ($\sigma = 0.005$).....	113
4.2 The experimental conditions and results of the preferential crystallization of DL-met·HCl aqueous solution at 10°C ($\sigma = 0.01$).....	114
4.3 Suspension density results for preferential crystallization of DL-met·HCl aqueous solution at 10°C ($\sigma = 0.005$).....	115
4.4 Suspension density results for preferential crystallization of DL-met·HCl aqueous solution at 10°C ($\sigma = 0.01$).....	116

LIST OF TABLES (Continued)

Table	Page
4.5	The optical activity results of preferential crystallization of DL-met·HCl aqueous solution at 10°C ($\sigma = 0.005$).....121
4.6	The optical activity results of preferential crystallization of DL-met·HCl aqueous solution at 10°C ($\sigma = 0.01$).....122
A.1	Conversion factor for brix scale (sucrose).....144
A.2	Raw data of solubility measurement of DL-met·HCl aqueous solution at 5°C.....146
A.3	Raw data of solubility measurement of DL-met·HCl aqueous solution at 10°C.....147
A.4	Raw data of solubility measurement of DL-met·HCl aqueous solution at 25°C.....148
A.5	Raw data of solubility measurement of DL-met·HCl aqueous solution at 40°C.....149
A.6	Raw data of solubility measurement of L-met·HCl aqueous solution at 5°C.....150
A.7	Raw data of solubility measurement of L-met·HCl aqueous solution at 10°C.....151
A.8	Raw data of solubility measurement of L-met·HCl aqueous solution at 25°C.....152
A.9	Raw data of solubility measurement of L-met·HCl aqueous solution at 40°C.....153

LIST OF TABLES (Continued)

Table	Page
A.10 Raw data of solubility measurement of the mixture compositions (75% L-met·HCl : 25% D-met·HCl) aqueous solution at 5°C.....	154
A.11 Raw data of solubility measurement of the mixture compositions (75% L-met·HCl : 25% D-met·HCl) aqueous solution at 10°C.....	155
A.12 Raw data of solubility measurement of the mixture compositions (75% L-met·HCl : 25% D-met·HCl) aqueous solution at 25°C.....	156
A.13 Raw data of solubility measurement of the mixture compositions (75% L-met·HCl : 25% D-met·HCl) aqueous solution at 40°C.....	157
A.14 The change of concentration unit of the DL-met·HCl aqueous solution at 5°C (from Table A.2).....	158
A.15 Average solubility data in mass fraction (\bar{w}) of the DL-met·HCl aqueous solution at 5°C (from Table A.2).....	159
B.1 The percentage points $t_{\alpha/2, n-1}$ of the t-distribution (Doebelin, 1995).....	163
D.1 The experimental results of density of DL-met·HCl aqueous solution at 25°C.....	179

LIST OF FIGURES

Figure	Page
1.1 The general chemical structure of α -amino acids.....	2
2.1 The racemic mixtures can crystallize as: (a) racemic compounds where both enantiomers crystallize together into the DL crystal, or as (b) conglomerates where both enantiomers when crystallize from a solution and form separate D or L crystals, and more rarely as (c) pseudoracemates where the two enantiomers coexist in a disordered manner in the same crystal.....	13
2.2 Different types of enantiomer systems represented by binary phase diagrams: (a) conglomerate, (b) racemic compound, and (c) the three types of solid solution forming system; T_A is the melting point of the enantiomer, T_R is the melting point of the racemic compound, and T_E is the eutectic melting temperature (Mitchell, 1998).....	17
2.3 Illustration of typical solubility ternary phase diagrams of enantiomeric systems under isothermal conditions: (a) conglomerate, (b) racemic compound, and (c) pseudoracemate (Wang and Chen, 2008).....	20

LIST OF FIGURES (Continued)

Figure	Page
2.4	The 0.5 liter glass batch crystallizer for preparing the methionine hydrochloride.....23
2.5	The designed experimental setup to study the solubility of three fixed enantiomeric mixtures of met·HCl in pure water.....26
2.6	Refractive index for the calibration curve of methionine hydrochloride (met·HCl) aqueous solution at 25°C.....30
2.7	Solubility data for the conglomerate DL-methionine hydrochloride (DL-met·HCl) in water.....32
2.8	Solubility data for the pure enantiomer L-methionine hydrochloride (L-met·HCl) in water.....33
2.9	Solubility data of the (○) conglomerate DL-met·HCl (from this work) and (●) L-/D-met·HCl (from this work) in water to compared with solubility literature data of (△) DL-met (replotted from Dalton and Schmidt, 1935) and (▲) L-/D-met (replotted from Polenske and Lorenz, 2009) in water.....34

LIST OF FIGURES (Continued)

Figure	Page
2.10 Ternary solubility diagram of L-methionine hydrochloride (L-met·HCl) + D-methionine hydrochloride (D-met·HCl) + water; the phase diagram is shown for isotherms at 5°C, 10°C, 25°C, and 40°C (from top to bottom); the isotherm lines are just guides to the eye.....	36
3.1 Mechanisms of nucleation (Randolph and Larson, 1988).....	50
3.2 Temperature changes and definitions of (a) MSZW and (b) induction time (Kobari, Kubota, and Hirasawa, 2010).....	52
3.3 Photomicrograph of L-met·HCl seed crystals on magnification 25x.....	54
3.4 Experimental setup schematic for the primary and secondary nucleation threshold measurement of DL-met·HCl in water.....	56
3.5 Schematic diagram of the 0.4 L glass batch crystallizer with jacket used to observe primary and secondary nucleation thresholds; (a) top view and (b) side view are shown.....	57

LIST OF FIGURES (Continued)

Figure	Page
3.6 Schematic diagram of the single crystal growth, small-cell crystallizer using an optical microscope (a) top view, (b) side view; (1) glass cover-slip, (2) single crystals, (3) supported rod, (4) thermometer, (5) cover glasses, (6) O-ring seal, (7) sample solution compartment, and (8) constant temperature water circulation compartment.....	60
3.7 The design of L-met·HCl single crystals growth in DL- and L-met·HCl supersaturated solutions by a small-cell crystallizer and optical microscope experimental setup schematic; (1) thermostat, (2) digital camera, (3) stereomicroscope, (4) small-cell crystallizer, (5) thermometer, (6) supported rod, (7) DP11 hand switch, and (8) computer.....	61
3.8 An example of measuring the primary nucleation threshold experiments for DL-met·HCl supersaturated solution ($\sigma = 0.02$), at 10°C.....	65
3.9 Effect of supersaturation on the induction time for the primary nucleation threshold (PNT) of DL-met·HCl solution at 10°C.....	66

LIST OF FIGURES (Continued)

Figure	Page
3.10 Effect of supersaturation on the induction time for the secondary nucleation threshold (SNT) of DL-met·HCl solution at 10°C.....	66
3.11 Photomicrographs of crystal growth of L-met·HCl single crystals in DL-met·HCl solution ($\sigma = 0.005$) at 10°C, magnification 40x.....	68
3.12 Photomicrographs of crystal growth of L-met·HCl single crystals in L-met·HCl solution ($\sigma = 0.005$) at 10°C, magnification 25x.....	69
3.13 The photomicrographs and dimensions of the standard wire at four magnifications that were used to measure the size of crystals.....	71
3.14 An example of measuring the size of L-met·HCl crystals in L-met·HCl solution ($\sigma = 0.005$) at 10°C, sample time 50 minutes, and magnification 25x.....	73
3.15 Crystal growth of L-met·HCl crystals in L-met·HCl supersaturated solution solution ($\sigma = 0.005$) at 10°C (plotted form Table 3.3).....	74
3.16 Growth rate distribution of L-met·HCl crystals in DL-met·HCl solution ($\sigma = 0.005$).....	83

LIST OF FIGURES (Continued)

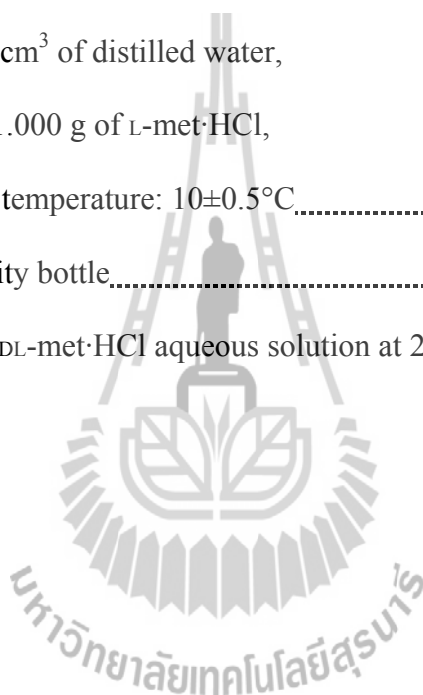
Figure	Page
3.17 Growth rate distribution of L-met·HCl crystals in DL-met·HCl solution ($\sigma = 0.01$).....	84
3.18 Growth rate distribution of L-met·HCl crystals in DL-met·HCl solution ($\sigma = 0.02$).....	84
3.19 Growth rate distribution of L-met·HCl crystals in L-met·HCl solution ($\sigma = 0.005$).....	86
3.20 Growth rate distribution of L-met·HCl crystals in L-met·HCl solution ($\sigma = 0.01$).....	86
3.21 Growth rate distribution of L-met·HCl crystals in L-met·HCl solution ($\sigma = 0.02$).....	87
3.22 Mean growth rates of L-met·HCl crystals in DL-met·HCl supersaturated solution at 10°C with three relative supersaturations.....	88
3.23 Mean growth rates of L-met·HCl crystals in L-met·HCl supersaturated solution at 10°C with three relative supersaturations.....	88
3.24 Mean growth rates for L-met·HCl crystals as a function of relative supersaturation of DL- and L-met·HCl supersaturated solution at 10°C.....	90

LIST OF FIGURES (Continued)

Figure	Page
4.1 Illustration of the principle of preferential crystallization for conglomerate forming system in ternary phase diagram (Qamar, Angelov, Elsner, Ashfaq, Seidel-Moegenstern, and Warnecke, 2009).....	102
4.2 Schematic diagram of a polarimeter (Hornback, 2005).....	104
4.3 Experimental setup schematic for preferential crystallization of DL-met·HCl aqueous solution.....	107
4.4 The P20 polarimeter used to measure the optical rotation of chiral compound solution.....	109
4.5 Suspension density results for preferential crystallization of DL-met·HCl ($\sigma = 0.005$).....	118
4.6 Suspension density results for preferential crystallization of DL-met·HCl ($\sigma = 0.01$).....	118
4.7 The relationship between specific rotation and amount of L-met·HCl in mixtures of D- and L-met·HCl.....	124
4.8 Optical purity of the produced L-met·HCl crystal during resolution by preferential crystallization from DL-met·HCl aqueous solution ($\sigma = 0.005$); Total solution: 40 g, Solvent: 10.45 cm ³ of distilled water, Seed crystals: 1.000 g of L-met·HCl, Crystallization temperature: 10±0.5°C.....	127

LIST OF FIGURES (Continued)

Figure		Page
4.9	Optical purity of the produced L-met·HCl crystal during resolution by preferential crystallization from DL-met·HCl aqueous solution ($\sigma = 0.01$); Total solution: 40 g, Solvent: 10.30 cm ³ of distilled water, Seed crystals: 1.000 g of L-met·HCl, Crystallization temperature: 10±0.5°C.....	128
D.1	A 2 ml of density bottle.....	176
D.2	The density of DL-met·HCl aqueous solution at 25°C.....	180



SYMBOLS AND ABBREVIATIONS

Symbols

C	=	Methionine hydrochloride concentration, g met·HCl/g solution
$C_{crystal}$	=	The concentration of crystal solution, g met·HCl/100 ml solution
$C_{DL-met-HCl}$	=	DL-met·HCl concentration at any temperature, g DL-met·HCl/g solution
C_o, c_o	=	Initial concentration of DL-met·HCl, g DL-met·HCl/g solution
C_{actual}^*	=	Actual concentration of met·HCl aqueous solution, g met·HCl/g solution
$C_{actual, Avg}^*$	=	An average actual concentration of met·HCl aqueous solution, g met·HCl/g solution
$C_{calibrated}^*$	=	Calibrated concentration of met·HCl aqueous solution, g met·HCl/100 g water
$C_{DL-met-HCl}^*$	=	Solubility concentration of DL-met·HCl, g DL-met·HCl/100 g water
$C_{DL-met-HCl, Avg}^*$	=	An average solubility concentration of DL-met·HCl, g DL-met·HCl/100 g water
$C_{L-met-HCl}^*$	=	Solubility concentration of L-met·HCl, g L-met·HCl/100 g water

SYMBOLS AND ABBREVIATIONS (Continued)

c	=	Solution concentration, g solute/g solvent or kg solute/m ³ solution
	=	Concentration of the chiral compound solution sample, g/100 ml solution
c^*	=	Equilibrium saturation concentration, g solute/g solvent or kg solute/m ³ solution
Δc	=	Concentration driving force, g solute/g solvent or kg solute/m ³ solution
D	=	Dextrorotatory rotation (right, according to Fischer convention)
DL	=	Racemic mixture
f	=	Degree of freedom defined by $f = n - 1$
G	=	Crystal growth rate defined by $\Delta \text{width} / \Delta t$, m/s or $\mu\text{m}/\text{min}$
	=	Independent growth rate variable, m/s or $\mu\text{m}/\text{min}$
$\overline{G'}$	=	Geometric mean growth rate, m/s or $\mu\text{m}/\text{min}$
\overline{G}	=	Mean growth rate, $\mu\text{m}/\text{min}$
L	=	Levorotatory rotation (left, according to Fischer convention)
l	=	Length of the polarimeter tube, dm
M_T	=	Suspension density, g of crystal/g of solution
$M_{T,(t=\infty)}$	=	Suspension density at equilibrium, g of crystal/g of solution
N	=	Number of small crystal, #
n	=	The sample size
n_D	=	Refractive index, -

SYMBOLS AND ABBREVIATIONS (Continued)

R	=	Designing the configuration of a stereocenter, R is indicated as rectus, meaning in Latin for right (in clockwise direction)
S	=	Supersaturation ratio, -
S	=	Designing the configuration of a stereocenter, S is indicated as sinister, meaning in Latin for left (in counter-clockwise direction)
s_x	=	The standard deviation of measured values
T	=	Experimental temperature, °C
	=	Temperature at any time, °C or K
T_A	=	Melting point of the enantiomer, °C
T_E	=	Eutectic melting temperature, °C
T_{cryst}	=	Crystallization temperature, °C
T_m	=	Temperature of detection of first nuclei or metastable limit is calculated from the measured MSZWs by using the relation of $T_m = T_o - \Delta T_m, \text{ °C or K}$
T_o	=	Initial saturation temperature of solution, °C or K
T_R	=	Melting point of the racemic compound, °C
ΔT	=	Supercooling defined by $(T_o - T)$, °C or K
	=	Temperature gradient at any time, °C
ΔT_m	=	Metastable zone width or MSZW, °C or K
t	=	Resolution time, minute
t_{ind}	=	Induction time, minute or second

SYMBOLS AND ABBREVIATIONS (Continued)

t_m	=	Time needed for the metastable zone width or induction time is reached, minute or second
\bar{w}	=	Average solubility data in mass fraction, -
$\bar{w}_{DL\text{-met}\cdot HCl}$	=	Average solubility data of DL-met·HCl in mass fraction, -
$w_{D\text{-met}\cdot HCl}$	=	Mass fraction of D-met·HCl, -
$w_{DL\text{-met}\cdot HCl}$	=	Mass fraction of DL-met·HCl, -
$w_{L\text{-met}\cdot HCl}$	=	Mass fraction of L-met·HCl, -
w_{water}	=	Mass fraction of water, -
\bar{x}	=	The sample mean
(+)	=	Direction rotates the plane of polarized light turned to the right (in clockwise direction)
(-)	=	Direction rotates the plane of polarized light turned to the left (in counter-clockwise direction)

Greek Symbols

α	=	Angle of rotation of plane-polarized light of the chiral compound solution, degrees (°)
$[\alpha]_{\lambda}^T$	=	Specific rotation of the chiral compound, degrees
$\sigma_{\bar{x}}$	=	The standard error of the mean
$[\alpha]_D^{25}$	=	Specific rotation of the met·HCl solution at 25°C and sodium D-line wavelength, degrees

SYMBOLS AND ABBREVIATIONS (Continued)

Δ	=	Change in a variable
$\rho_{DL-met\cdot HCl@25^{\circ}C}$	=	The density of DL-met·HCl aqueous solution at 25°C, g solution/ml solution
σ	=	Relative supersaturation, -
σ'	=	Geometric standard deviation, depends on variable
Superscripts		
*	=	Equilibrium
T	=	Temperature at any time, °C
25	=	Temperature used in polarimetry measurement is 25°C
Subscripts		
A	=	Enantiomer
Avg	=	Average value
$cryst$	=	Crystallization
D	=	Light source used in polarimeter is the sodium D-line which $\lambda = 589 \text{ nm}$, λ is indicated as D
E	=	Eutectic
ind	=	Induction
m	=	Metastable zone width or metastable limit
R	=	Racemic compound
λ	=	Wavelength of the incident light, nm

SYMBOLS AND ABBREVIATIONS (Continued)

0 = Initial

Abbreviations

α -amino acid	=	Alpha-amino acid
α -carbon	=	Alpha-carbon
CD	=	Circular dichroism
C.I.	=	Confidence interval
CSD	=	Crystal size distribution
-COOH	=	Carboxylic acid group
DSC	=	Differential scanning calorimetry
DTA	=	Differential thermal analysis
D-met	=	D-methionine
D-met·HCl	=	D-methionine hydrochloride
DL-met	=	DL-methionine
DL-met·HCl	=	DL-methionine hydrochloride
exp	=	Exponential function
GRD	=	Growth rate distribution
HCl	=	Hydrochloric acid
-H	=	Hydrogen atom
L-met	=	L-methionine
L-met·HCl	=	L-methionine hydrochloride
MMP	=	beta-methylmercapto-propionaldehyde

SYMBOLS AND ABBREVIATIONS (Continued)

m.p.	=	Melting point, °C
MSZW	=	Metastable zone width
met	=	Methionine
met·HCl	=	Methionine hydrochloride
-NH ₂	=	Amino group
ORD	=	Optical rotator dispersion
PNT	=	Primary nucleation threshold
RI	=	Refractive index
SAM	=	S-Adenosyl methionine
S.D.	=	Standard deviation
SIPC	=	Seeded isothermal preferential crystallization
SLE	=	Solid-liquid equilibrium
SNT	=	Secondary nucleation threshold

CHAPTER I

INTRODUCTION

1.1 Background and Significance of the Problem

Proteins are complex organic compounds of high molecular weight which can be found in every living thing. The basic structure of a protein consists of a chain of various amino acids connected by peptide bonds, and which are typically folded into a globular-shape. Most proteins are linear polymers built from a series of up to 20 different L- α -amino acids. All amino acids possess common structural features, including an α -carbon to which an amine group ($-\text{NH}_2$), a carboxyl group ($-\text{COOH}$), a proton ($-\text{H}$), and a variable side chain are bonded as shown in Figure 1.1. The amino acids in a polypeptide chain are linked by peptide bonds. Once linked in the protein chain, an individual amino acid is called a residue, and the linked series of carbon, nitrogen, and oxygen atoms are known as the main chain or protein backbone.

Amino acids are the building blocks of all proteins and are therefore vital nutrients for humans and animals. Many of the common amino acids are essential for survival. Amino acids are critical to life, and have many functions in metabolism, and also important in many other biological molecules, such as forming parts of coenzymes, in S-Adenosylmethionine (SAM), or as precursors for the biosynthesis of molecules such as heme. Due to this central role in biochemistry, amino acids are important in nutrition. Besides, amino acids are commonly used in food technology and industrial chemicals, and are important reagents in the production of other

chemicals, including food additives, cosmetics and toiletries, surfactants and pharmaceuticals, among many other applications as reagents or intermediates, feed (animal nutrition) and other materials (optical material, biomaterial, etc.).

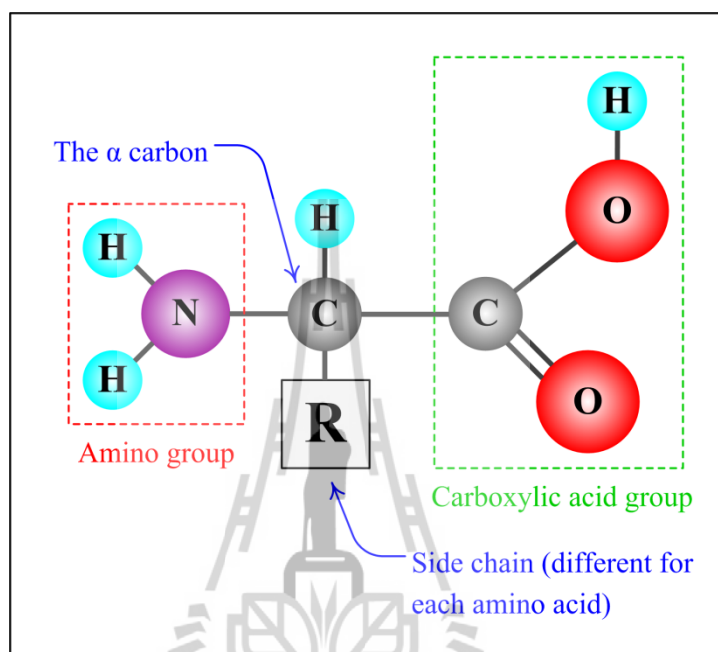


Figure 1.1 The general chemical structure of α -amino acids.

Methionine (met) is an essential sulfur containing amino acid. It is found in nature as the L-enantiomer. Poultry and pigs need significant amounts of L-methionine (L-met) in their food but the L-met occurring naturally in the feedstuff (e.g., in soya grains, cereals) is often insufficient. Thus, it is necessary to add industrially manufactured methionine (Polenske and Lorenz, 2009). All industrial producers of DL-methionine (DL-met) start with the same raw materials, acrolein (a 3-carbon aldehyde) derived from propylene, methyl mercaptan (methanethiol) derived from methanol and various sulfur sources, hydrogen cyanide, and ammonia or ammonium carbonate. Methyl mercaptan is reacted with acrolein to produce beta-

methylmercaptopropionaldehyde, known as MMP. The MMP is then reacted with hydrogen cyanide to produce alpha-hydroxy-gamma-methylthiobutyonitrile, which on treatment with ammonia followed by hydrolysis yields DL-met (Aldrich, 2007). Usually it is not necessary to separate the racemic mixture of methionine into two enantiomers since DL-met can be transformed into the desired form, which is pure L-met, by the animal organism. However, the enantiomer(s) of methionine can be gained by preferential crystallization using methionine derivatives or the hydrochloride as a feed material (Polenske and Lorenz, 2009).

Resolution of optical isomers by crystallization has been performed mainly in two ways. The first, preferential crystallization, is a method to separate racemic mixtures of the group of conglomerate forming systems into their pure enantiomers. It occurs when seed crystals of an optically active compound are allowed to grow in an aqueous solution (supersaturated solution) of racemic compounds, where only the same enantiomer as that of the seed crystal can be deposited on to the seed surface. However, the direct crystallization of pure enantiomers from racemic solutions is limited to conglomerates (5–10% of all chiral systems). Unfortunately, the majority of chiral substances belong to the racemic compound forming systems (including 90–95% of all chiral systems) (Polenske, Lorenz, and Seidel-Morgenstern, 2007). Typical examples that have been successfully resolved by preferential crystallization are S-carboxymethyl-DL-cysteine, DL-threonine, and DL-glutamic acid. The other resolution process involving crystallization, optical resolution via diastereoisomeric salt formation or the diastereomer method, also has great importance and is suitable for the production of optically active chiral compounds both on the lab scale and the industrial scale. In the diastereomer method, diastereomer compounds are derived

from the enantiomers to be separated. Unlike enantiomers, diastereomers have significantly different solubilities, and therefore, optical resolution with higher separation efficiency is possible. From thermodynamic considerations based on the solubility diagram, the diastereomer method can produce a 100% pure diastereomer as an intermediate product, which is easily decomposed to the final required enantiomer (Yokota, Takahashi, Sato, Kubota, Masumi, and Takeuchi, 1998). However, it is usually more expensive and complex than preferential crystallization due to the chiral separating agent required.

In this research, DL-met will be chosen as the model substance because it is one of the essential amino acids that are required by animals and humans, especially because it is not synthesized by the human body. Besides, DL-met is used as a dietary component in poultry and animal feed, and only a very limited proportion of the literature on the issue of preferential crystallization concerns it. DL-met has the chemical formula is $C_5H_{11}NO_2S$. Being a principal supplier of sulfur, it prevents disorders of the hair, skin and nails. It helps to lower cholesterol levels by increasing the liver's production of lecithin, thus reducing liver fat and protecting the kidneys. It serves as a natural chelating agent for heavy metals and regulates the formation of ammonia and creates ammonia-free urine, which reduces bladder irritation. Further, it also influences hair follicles and promotes hair growth. Studies in rat urolithiasis have proven that methionine feeding leads to protection from stone formation (Ramachandran and Natarajan, 2006). Moreover, DL-met is used in production of medicines and active pharmaceutical ingredients, and also as a precursor to other amino acids.

1.2 Research Objectives

This research aims to determine a method to separate the pure L-enantiomer from DL-methionine compound by reacting the methionine with hydrochloric acid (HCl) to form methionine hydrochloride (met·HCl). DL-met·HCl will be separated via preferential crystallization with seeding of L-methionine hydrochloride (L-met·HCl) to obtain pure crystals of L-met·HCl. This current project will investigate the influence of the crystallization parameters on the preferential crystallization. The operating parameters varied in the studies are the crystallization temperature, supersaturation, seeding, and batch time. Finally, the nucleation thresholds, crystal growth rates, particle size distribution and crystal purity will be determined, described and discussed.

1.3 Scope and Limitations

1.3.1 Thermodynamic Properties of DL-met·HCl on Preferential Crystallization

a) The solubility data as a function of temperature will be measured by total solids concentration determination using refractive index in order to model the ternary phase diagram boundaries of both enantiomer(s) and the racemic mixture of methionine hydrochloride.

b) The density of methionine hydrochloride solutions as a function of temperature will be measured in order to convert concentration units from g met·HCl/g solution to g met·HCl/ml solution, since the latter form is required for accurate knowledge of the polarimeter reading and percent purity calculation.

c) The nucleation threshold for primary nucleation and secondary nucleation as a function of the concentration gradient and temperature gradient will be determined for DL-met·HCl in water using isothermal measurement in order to estimate a suitable batch time for preferential crystallization to obtain high purity of the crystalline product.

1.3.2 Kinetic Properties of DL-met·HCl on Preferential Crystallization

a) Crystal growth rates and growth rate distributions will be determined as a function of supersaturation as the time rate of change of the number mean crystal size.

b) Evaluation and characterization of the optically active compounds for L-met·HCl and D-met·HCl in water by measuring their specific rotation and comparing these values with the theoretical values found in the literature.

c) Investigating the kinetics of the preferential crystallization through changes in concentration and purity, by measuring optical rotation and refractive index of the crystal and solution as a function of batch time.

1.4 Outputs

An understanding of the behavior of the optical resolution of DL-met·HCl by preferential crystallization of the pure L-enantiomer product through crystallization will be achieved. This study will especially benefit the chemical industry, and the food and pharmaceutical industries. Knowledge of preferential crystallization is necessary to reliably produce these very important products, and also to help industry produce an important industrial commodity suitable for sale and the specified applications.

1.5 References

- Aldrich, G. (2007). DL-methionine: several vital functions. **Petfood Industry; Ingredient Issues** 49(11): 42-43.
- Polenske, D., Lorenz, H., and Seidel-Morgenstern, A. (2007). Separation of propranolol hydrochloride enantiomers by preferential crystallization: Thermodynamic basis and experimental verification. **Crystal Growth & Design** 7(9): 1628-1634.
- Polenske, D. and Lorenz, H. (2009). Solubility and metastable zone width of the methionine enantiomers and their mixtures in water. **Journal of Chemical and Engineering Data** 54: 2277-2280.
- Ramachandran, E. and Natarajan, S. (2006). Gel growth and characterization of β -DL-methionine. **Crystal Research and Technology** 41(4): 411-415.
- Yokota, M., Takahashi, Y., Sato, A., Kubota, N., Masumi, F., and Takeuchi, H. (1998). Purity drop in optical resolution of DL-methionine by the diastereomer method. **Chemical Engineering Science** 53(8): 1473-1479.

CHAPTER II

SOLUBILITY OF ENANTIOMERIC METHIONINE HYDROCHLORIDE IN AQUEOUS SOLUTION

2.1 Abstract

The solubility data is the first property that requires measurement in this research. Results of solubility must be used in the study of the mechanisms involved in the crystallization process, for example primary and secondary nucleation thresholds, mean growth rate of crystals, and in the current study this includes the optimization of preferential crystallization. The solubilities in pure water of the hydrochloride salt form of the amino acid, DL-methionine hydrochloride (a racemic conglomerate), L-methionine hydrochloride (the pure enantiomer), and an intermediate mixture composition (75% L-met-HCl : 25% D-met-HCl) have been measured in the temperature range between 5°C and 40°C using an isothermal solubility method. Moreover, the ternary solubility diagram of enantiomeric methionine hydrochloride species in water solvent has been created, and uses the solubility data from the solubility measurement mentioned above. The result shows that the solubility of both forms is strongly dependent on temperature. The ternary solubility diagram of L-methionine hydrochloride + D-methionine hydrochloride + water shows mirror image symmetry with respect to the racemic compound axis.

2.2 Introduction

The synthesis and separation of the enantiomers of organic compounds into the pure chiral species has received increasing interest recently, especially because of their importance in the biochemistry and pharmaceuticals industry (Collins, Sheldrake, and Crosby, 1992; Davankov, 1997). More than 50% of active pharmaceutical ingredients produced are known to be chiral, and hence enantioseparation and recovery of the solid enantiomer from solution are of large interest (Lorenz and Seidel-Morgenstern, 2002; Tulashie, Lorenz, Malwade, and Seidel-Morgenstern, 2010). The market volume for chiral drugs (single enantiomers) rose from 26% in 1983 to 55% in 2004 (Caner, Groner, Levy, and Agranat, 2004). The volume of the market for single enantiomer chiral drugs was approximately 100 billion US\$ in 2000 (Maier, Franco, and Lindner, 2001) and it was assumed that it would reach a volume of 200 billion US\$ in 2008. These numbers show that the separation of enantiomers has gained increasing importance in the last decade.

Manufacturing processes in the pharmaceutical industry often use crystallization processes which can achieve high purity and produce the desired crystal form. To design crystallization processes it is necessarily describe the physical properties of the crystal products, such as solubility, density, crystal purity, crystal size, and size distribution. In specialty chemicals, solubility and polymorphism play key roles in the initial design of a crystallization process. Moreover, several operational parameters such as temperature and impeller speed need to be understood and controlled to achieve constant desupersaturation, consistent narrow particle size distribution around the desired product mean, minimal attrition, and homogeneous growth conditions (Schmidt, Patel, Ricard, Brechtelsbauer, and Lewis 2004; Fujiwara,

Nagy, Chew, Braatz, 2005). Therefore, physical properties and operating parameters are essential for controlling and designing crystallization processes.

The application of crystallization processes for the separation or purification of enantiomers requires a detailed knowledge of fundamental solid-liquid equilibria (SLE) data expressed in phase diagrams describing the melting behavior of two enantiomers (binary melting point phase diagram) and/or the solubility behavior of the system (L)-enantiomer/(D)-enantiomer/solvent (the ternary solubility diagram) (Lorenz, Perlberg, Sapoundjiev, Elsner, and Seidel-Morgenstern, 2006). Knowledge of the SLE data can allow for optimization of the separation processes and also for increases in the productivity. Thermodynamic data for construction of the ternary phase diagrams for chiral systems are usually not available, particularly in the stage of screening different solvents or solvent mixtures which is in contrast with inorganic and organic products (Lorenz and Seidel-Morgenstern, 2002).

This chapter will focus on solubility data of the two enantiomers in mixtures of D-, L-, and solvent. This allows construction of a ternary solubility phase diagram. A ternary phase diagram can show how this mixture of components behaves thermodynamically. A solubility equilibrium method based on the classical isothermal method and the refractive index technique was used to study the solubility.

Consequently, the aim of this chapter is to determine the solubility data as a function of temperature for methionine hydrochloride (met·HCl) in pure water for three compositions; pure enantiomer (L-met·HCl), racemic conglomerate (DL-met·HCl), and a mixture composition (75% L-met·HCl : 25% D-met·HCl). The study neglects the effect of pH on the solubility of methionine hydrochloride, using the natural pH of the system at the equilibrium as the basis. This will explain the thermodynamic behavior

of this system, with these data being necessary to predict and model any crystallization properties in the next chapter.



2.3 Theory

2.3.1 Racemic Mixtures

A mixture of compounds (solid, liquid, or a gas) containing an equal amount of both enantiomers and for which the physical state is not a repeating unit containing the two enantiomers, is called a racemic mixture. A racemic mixture has the same boiling point, refractive index, and density in the liquid state as the pure individual enantiomers (Červinka, 1995). Categories of racemic mixtures are distinguished by the nature of the properties of crystals with which they are in equilibrium. There are racemic compounds, racemic conglomerates, and pseudoracemates (racemic solid solutions), as shown in Figure 2.1 (a), (b), and (c), respectively.

Racemic compounds form crystals in which the two enantiomers of opposite chirality are paired in a well-defined arrangement in the crystal lattice (Jacques, Collet and Wilen, 1981; Moss, 1996). In such compounds, the enantiomer has greater affinity to the mirror image type than to its own species. Thus, the melting point of a racemic compound is decreased a small amount if one enantiomer is added to them. However, the melting point of a pure enantiomer can be higher or lower than the racemic compound (Roozeboom, 1899). Unfortunately, about 90–95% of racemic mixtures form a racemic compound in the solid phase, which is the most difficult for achieving a certain enantiomeric enrichment by preferential crystallization (Lorenz, Perlberg, Sapoundjiev, Elsner, and Seidel-Morgenstern, 2006).

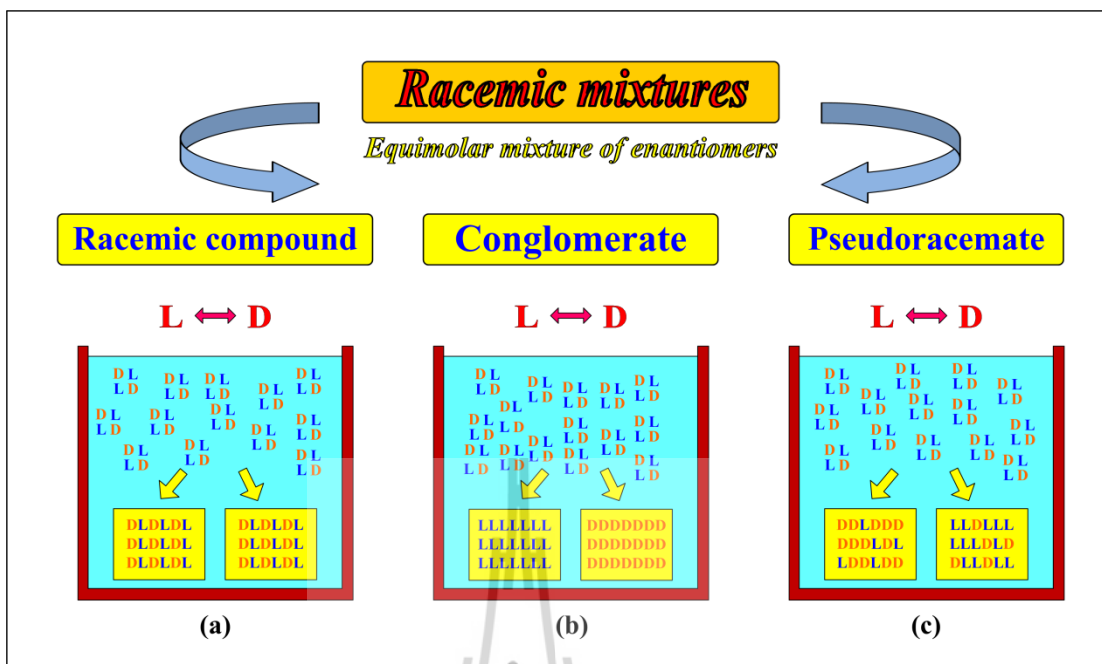


Figure 2.1 The racemic mixtures can crystallize as: (a) racemic compounds where both enantiomers crystallize together into the DL crystal, or as (b) conglomerates where both enantiomers when crystallize from a solution and form separate D and L crystals, and more rarely as (c) pseudoracemates where the two enantiomers coexist in a disordered manner in the same crystal.

On the other hand, if each enantiomer has greater attraction to its own kind than the opposite, two enantiomers crystallize as an equimolar mixture of two homochiral crystals, in other words, a physical mixture of pure crystals of each enantiomer. This mixture is called a racemic conglomerate, and corresponds to the species addressed in this work: methionine hydrochloride (met-HCl). The melting point of a racemic conglomerate is always lower than of the pure enantiomer, and if a

small amount of one enantiomer was added to the conglomerate with increases the melting point (Roozeboom, 1899). The racemic mixures that are conglomerate forming are very few, only 5–10% (Jacques, Collet, and Wilen, 1981).

If differences in the affinity between enantiomers of like and opposite kinds are small, two enantiomers exist more or less randomly in the same crystal lattice as a solid solution. The term pseudoracemate is used to designate this case, which is rather rare. The properties of racemic solid solutions, which includes the melting points and solubility, are either identical or only slightly different from those of pure enantiomers (Roozeboom, 1899; Červinka, 1995).

2.3.2 Classical Solubility Measurement

Of the various properties which determine the separation or purification of enantiomer(s) in a crystallization process, solubility is of the greatest importance. Solubility provides the concentration at which the solute can dissolve into a given solvent at a specific temperature, and this property has a great influence on the choice of the method of crystallization. It will also allow evaluation of the supersaturation region and the undersaturated region. Moreover, it allows calculation of the maximum yield of product crystals. In the majority of cases the solubility increases with temperature but solubility may also be a function of pressure at low to moderate pressure. Generally, the effect can be ignored in the systems normally found in crystallization from solution.

Methods for determining the solubilities of solids in liquids vary in accuracy and convenience and in the types of systems to which they are best suited. The traditional methodology for determining solubilities of ternary and higher order amino acid systems have generally employed the isothermal analytic method

(Kurosawa, Teja, and Rousseau, 2005; Tamagawa, Martins, Derenzo, Bernardo, Rolemberg, Carvan, and Giulietti, 2006). This form of solubility measurement has an accuracy of 1% to 10%, depending on the analytical procedure performed on the saturated solution. More accurate solubility measurements require more elaborate procedures. This is especially true for rapidly re-equilibrating systems where sampling errors may become significant (Capewell, Hefter, and May, 1999).

Currently the aqueous solubility data of amino acids are obtained by means of the classical solubility measurement techniques, which are broadly classified into isothermal and non-isothermal methods (polythermal or dynamic). In a classical isothermal method the solubility is determined at a constant controlled temperature with agitation. There are two main isothermal techniques. In the first technique, a known mass of solvent is heated or cooled to the desired temperature. Excess solute is added into the solvent and the solution is agitated for a long time period to ensure that the solution is already saturated, because the dissolution rate of solute is slowed when approaching the saturation points. A clear sample is removed and analyzed for the amount of solute. The experiment is carried out in a closed vessel to prevent solvent loss by evaporation. In the second isothermal technique, an exactly known amount of solute is added to a predetermined amount of solvent at the desired temperature. A small droplet of solvent is added to the solution every hour until all solid particles of solute have disappeared (which could be observed using light scattering techniques); at this point the solution is saturated at the desired temperature. This method can be used to determine the solubility to a precision of approximately $\pm 0.5\%$.

For the polythermal or dynamic method, the objective is to have some of the solid formed when the lowest temperature is used, and all components forming a liquid solution at the highest temperature used. A mixture of solute and solvent is prepared by mass in proportions corresponding approximately to the composition of a saturated solution in the middle of the operating temperature range. The mixture of solution is placed in a closed glass vessel immersed in a glass thermostat with continuous agitation. The mixture is first heated gradually until all solids have been dissolved, and then cooled to obtain a nucleate in the solvent. The mixture is heated again very slowly ($\leq 0.2^\circ\text{C}/\text{min}$) with continuous agitation until the last crystal dissolves. The temperature at which the last crystal disappears is the saturation temperature. The procedure is repeated to obtain a saturation temperature within $\pm 0.1^\circ\text{C}$. The isothermal method for solubility estimation tends to be more accurate (Mohan, Lorenz, and Myerson, 2002).

2.3.3 Binary and Ternary Phase Diagrams and System Types

The essential phase diagrams which have to be known are the binary phase diagram that describes the melting behavior of the two enantiomers, and for crystallization from solution, the ternary phase diagram describing the solubility behavior of the two enantiomers in the presence of a suitable solvent. Binary phase diagrams are usually determined by thermal analysis techniques. Particularly, differential thermal analysis (DTA) and differential scanning calorimetry (DSC) can be used to determine the phase transitions and are widely applied as analytical tools for pharmaceutical development. Their applicability and efficiency has been confirmed over many years (Lorenz and Seidel-Morgenstern, 2002). The enantiomeric mixtures can be differentiated from one another on the basis of their

melting point behavior that corresponds to either racemate crystalline forming, conglomerate forming, or solid solution forming systems. They have been divided into three fundamental types of binary phase diagram, which are presented in Figure 2.2 (Roozeboom, 1899). The upper lines in Figure 2.2(a) and 2.2(b) indicate the melting temperature for an enantiomer composition. The lower horizontal line in Figure 2.2(a) and 2.2(b) indicate the eutectic temperature (Srisanga and ter Horst, 2010).

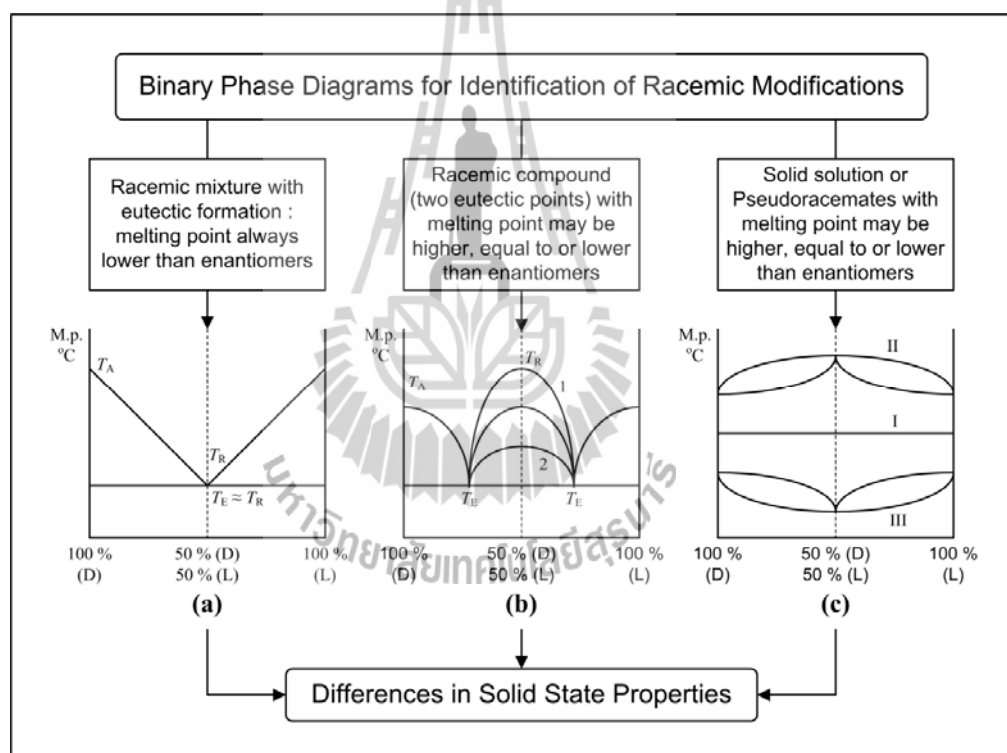


Figure 2.2 Different types of enantiomer systems represented by binary phase diagrams: (a) conglomerate, (b) racemic compound, and (c) the three types of solid solution forming system; T_A is the melting point of the enantiomer, T_R is the melting point of the racemic compound, and T_E is the eutectic melting temperature (Mitchell, 1998).

Figure 2.2(a) shows a simple eutectic which is the melting point of a conglomerate that always occurs at 50:50 enantiomeric composition. The melting point of one enantiomer decreases after continuous addition of the other enantiomer down to the minimum at the point of equivalence (the eutectic temperature) and then increases in the same manner. From such a characteristic, the solubility of a racemic mixture is always higher than that of the pure enantiomer. This is only true when the racemic solid mixture is actually a conglomerate.

The melting point diagram of a racemic compound in Figure 2.2(b) shows two minimum (eutectic points) and a maximum at the point of equivalence. The melting point of the racemic compound is always greater than eutectic temperature, but may be higher or lower than the melting point of the pure enantiomers. When the racemic species is a racemic compound that melts at a higher temperature than the corresponding enantiomers, as in curve number 1, it is impossible to resolve the racemic species and is difficult to purify single enantiomers by crystallization. In curve number 2, where the melting temperature of the racemic species as a racemic compound is lower than of the enantiomers, the purification is facilitated and resolution is possibly by entrainment (preferential crystallization induced by seeding) (Li, Ojala, Grant, 2001). The solubility of a racemic compound may be greater or less than that of individual enantiomers, which is unlike the solubility of a conglomerate.

Finally, Figure 2.2(c) presents the binary melting point diagram of enantiomers forming solid solutions (or pseudoracemate) at all concentrations which is divided into three types. Type I shows an ideal solid solution, which is a mixtures of the two enantiomers in all ratios melting at the same temperature as the pure

enantiomers. The melting temperature is constant and not depending on the enantiomer fraction. Type II shows the curve of the phase diagram is convex, which indicates positive deviations from ideality and also indicates a maximum melting point for the pseudoracemate, while Type III shows a minimum melting point or negative deviations from ideality, and the phase diagram is concave (Mitchell, 1998; Wang and Chen, 2008).

Figure 2.3 shows typical solubility phase diagrams for conglomerates, racemic compounds, and solid solution forming systems in an equilateral triangular form. These diagrams consist of the three vertexes of the triangles which represent the pure components: the solvent on top, the (D)- and (L)-enantiomers on left and right respectively. The concentration units can be mole or weight fractions of the component represented on the axis. Each point inside the diagram indicates a ternary mixture consisting of all three components. Figure 2.3(a) presents the ternary solubility diagram of conglomerates that consists of (i) a 1-phase region which is an unsaturated (clear solution) on the solvent top corner, (ii) below the equilibrium conditions which will contain two 2-phase regions of a saturated solution and crystals of one of the two enantiomers, and (iii) a 3-phase region under the equilibrium conditions which consists of the saturated solution (a racemic or near racemic mixture of the two enantiomers, and the crystals which will be a mechanical mixture of crystals of the two pure enantiomers.

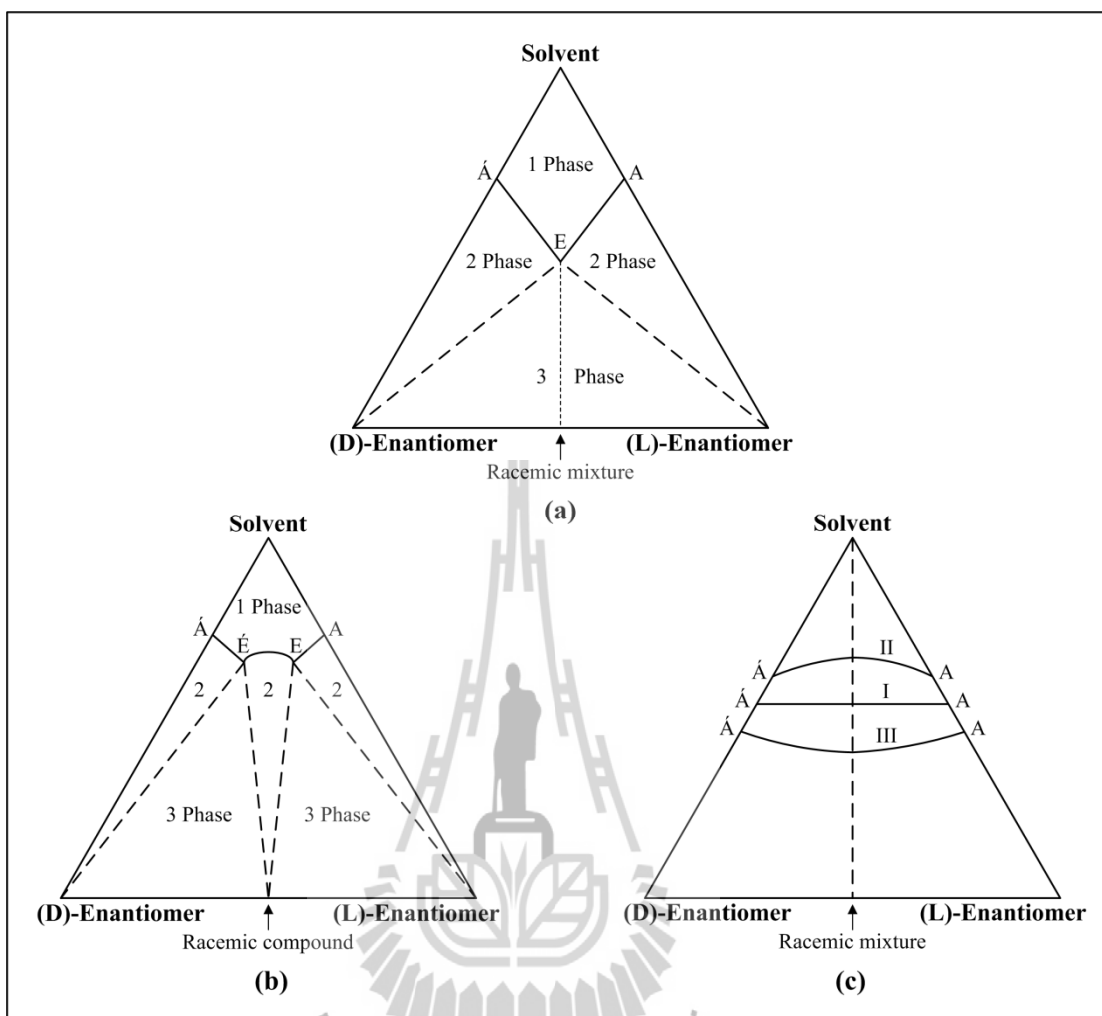


Figure 2.3 Illustration of typical solubility ternary phase diagrams of enantiomeric systems under isothermal conditions: (a) conglomerate, (b) racemic compound, and (c) pseudoracemate (Wang and Chen, 2008).

Figure 2.3(b) presents the majority of enantiomeric systems (up to 90% of the systems found in nature). It presents the ternary phase diagram of a racemic compound, which is more complicated than the conglomerate system due to the existence of two eutectic points (E and E') in the binary (D)/(L) enantiomeric system.

The diagram shows differences to the conglomerate system with respect to (i) the shape of 1-phase region of the undersaturated solution, (ii) the shape of the 2-phase regions (crystals of one of the two enantiomers and saturated solution), (iii) another 2-phase region appears due to the solid phase of the racemic crystals in the saturated solution, and (iv) there are two separate 3-phase regions in which the solid phase will be a mechanical mixture of one enantiomer and the racemate (Lorenz, Perlberg, Sapoundjiev, Elsner, and Seidel-Morgenstern, 2006).

The ternary phase diagram of a pseudoracemate is illustrated in Figure 2.3(c), which corresponds to the three types of solid solutions shown in Figure 2.2(c). The solubilities of the pure enantiomers are represented by points A and A' . In the case of type I, the solubility of the pseudoracemate is equal to the enantiomers and the solubility curve is the horizontal line AA' . In the types II and III, the pseudoracemate is more and less soluble than the enantiomers, respectively (Jacques, Collet, and Wilen, 1981).

2.4 Experimental Procedure

2.4.1 Materials

DL-methionine (DL-met) and L-methionine (L-met) were purchased from Acros Organics with purity greater than 99% and 98% respectively. Hydrochloric acid 37% (HCl) analytical reagent grade was purchased from Carlo Erba. These two methionine amino acids were reacted to form methionine hydrochloride in the batch crystallizer shown in Figure 2.4, using hydrochloric acid 37% as a reagent. 5.97 g of DL-met or 5.97 g of L-met was dissolved in 10 cm³ of hydrochloric acid 37% in a 0.5 L glass vessel with a sealed glass lid (to reduce solvent loss) at higher than room temperature until dissolution was complete, and then the solution was kept in a water bath at a constant temperature of 10°C. The solution was agitated by a centrally located four-blade propeller for around 24 hours. The precipitated DL-methionine hydrochloride (DL-met·HCl) or L-methionine hydrochloride (L-met·HCl) was collected by filtration with a 110 mm diameter number 42 ashless filter paper (Whatman, USA). Solution was filtered through a buchner funnel using an aspirator (Eyela model A-3S, Tokyo Rikakikai Company Limited, Japan), and washed with 5 ml of hydrochloric acid 37% at 10°C (Shiraiwa, Miyazaki, Watanabe, and Kurokawa, 1997). Both solid products were dried over silica gel in a desiccator. Deionized water (18.2 MΩ·cm) was used as a solvent in the preparation of all aqueous solutions throughout the experiments.

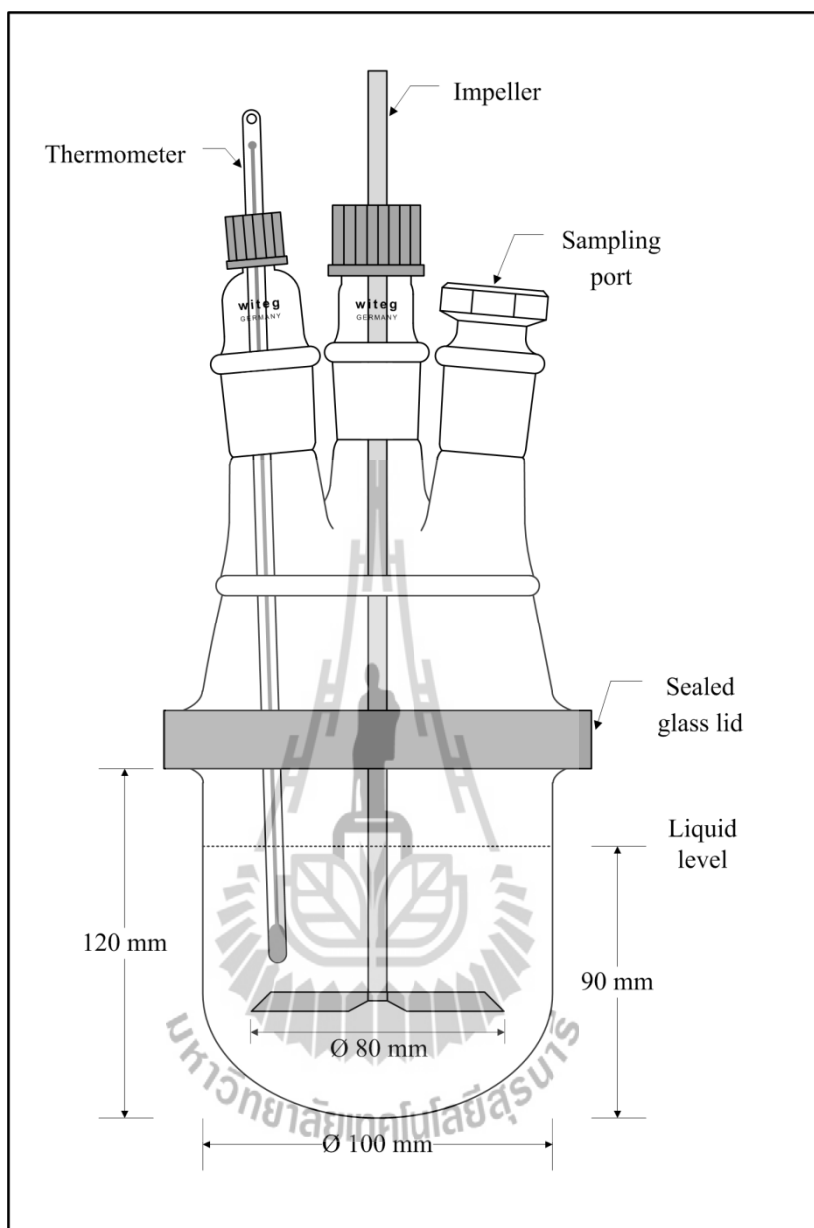


Figure 2.4 The 0.5 liter glass batch crystallizer for preparing the methionine hydrochloride.

2.4.2 Determination of the Concentration Calibration Curve of DL-met·HCl

The calibration curve for the concentration of DL-met·HCl in water was measured at 25°C using an automatic digital refractometer (Model RFM340, Bellingham and Stanley Limited, UK) with temperature control to within $\pm 0.3^\circ\text{C}$. The precision of the refractive index determination was ± 0.00001 refractive index unit. All solutions were prepared in the laboratory glass bottles with screw caps (Schott Duran, Germany) and varying the mass of DL-met·HCl to 2.5 g, 5.0 g, 7.5 g, 10 g, 12.5 g, 15.0 g, 17.5 g, and 20 g per 100 g solution. The bottle containing the solution was taken into a 3 L beaker (Schott Duran, Germany) on a magnetic stirrer plate (Model Yellowline MAG HS 7, Germany) with 25°C water circulating from a constant temperature water bath. The solutions were stirred constantly with a magnetic stirrer bar. The solution samples were removed after 24, 29, 34, and 39 hours and they were filtered through a 0.45 μm cellulose acetate membrane filter in a 47 mm filter holder (Millipore Swinnex Filter Holder, USA) connected to a 20 ml disposable syringe (Nipro Medical Corporation, Thailand). Solutions were analyzed for DL-met·HCl content by solution concentration measurement and pH values using a RFM340 automatic digital refractometer and pH meter (Model CyberScan pH510, Eutech Instrument Private Company Limited, Singapore), respectively.

2.4.3 Determination of the Solubility of met·HCl in Aqueous Solution for Pure Enantiomer and Racemic Conglomerate

The solubility data of the racemic conglomerate (DL-met·HCl) and pure methionine hydrochloride (L-met·HCl) in water were measured at 5°C, 10°C, 25°C, and 40°C by means of the isothermal solubility method using an RFM340 automatic

digital refractometer for analyzing met·HCl content. 20 ml of deionized water was added into a 100 ml laboratory glass bottle with a screw cap (Schott Duran, Germany) which was placed in a 3 L beaker on a magnetic stirrer plate. Constant temperature water at either 40°C, 25°C, 10°C, or 5°C (depending on the experimental temperature desired) was circulated through the 3 L beaker to maintain a constant solution temperature. The solubility experimental equipment setup is shown in Figure 2.5. The solubility experiments for DL-met·HCl were started at 40°C. The solid DL-met·HCl was added to water in a glass bottle with a screw cap in excess of the saturation condition at 40°C. The solution was stirred with a magnetic stirrer bar at all times for 48 hours, which is enough time to reach equilibrium. Secondly, around 2 ml of solution sample at 40°C was taken to separate the liquid from the solid using a 0.45 µm cellulose acetate membrane filter with a 250 ml filter holder with receiver (Nalgene Labware, USA) connected to an aspirator, through which solution could be filtered within a few seconds at room temperature. Then liquid samples, diluted at a ratio by mass of 1 : 4 (liquid solution : deionized water) were kept in a water bath at 25°C for an hour. Finally, the concentration of the solution was measured using refractive index at 25°C using a RFM340 automatic digital refractometer. To ensure DL-met·HCl and L-met·HCl solution concentrations were at equilibrium, measurements were repeated every hour for about 4 hours to check the concentration was constant. After measurement at 40°C the solution temperature was decreased to 25°C, 10°C, and 5°C respectively, and the saturation concentration measured at the new temperatures. The solubility of L-met·HCl was first determined at 5°C, then 10°C, 25°C, and 40°C respectively, using the same methods as used for the DL-met·HCl solubility experiments. Because of this it was possible to conserve the raw material (L-met·HCl).

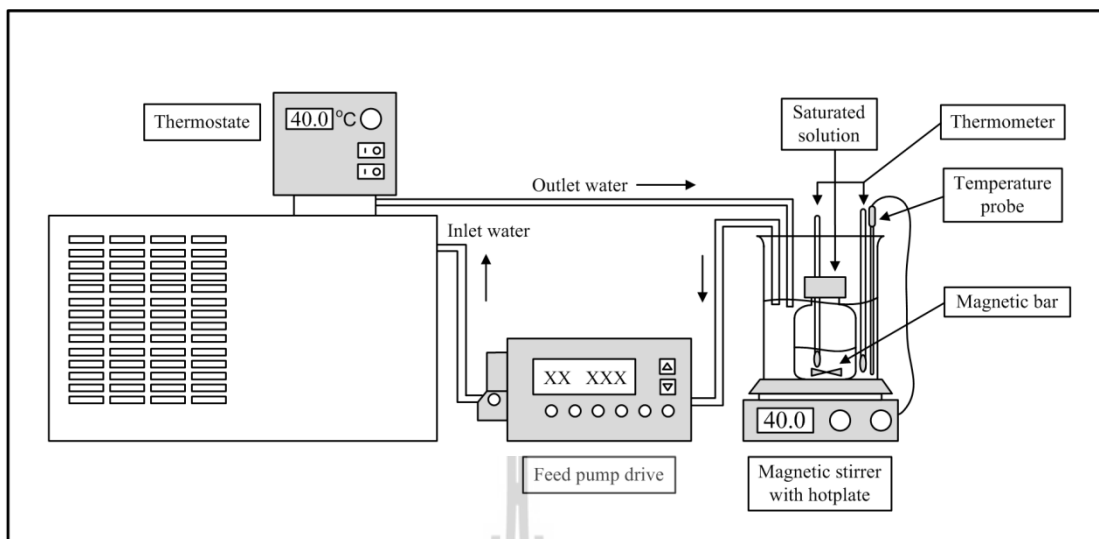


Figure 2.5 The designed experimental setup to study the solubility of three fixed enantiomeric mixtures of met·HCl in pure water.

2.4.4 Determination of the Solubility of Mixture Compositions of met·HCl Enantiomers in Aqueous Solution

A 75% L-met·HCl and 25% D-met·HCl enantiomeric mixture was used to study the solubility data for intermediate compositions of the met·HCl enantiomers in water. This was done by mixing DL-met·HCl and L-met·HCl in a 1 : 1 ratio. This system was also measured at 5°C, 10°C, 25°C, and 40°C using the same measurement techniques and an experimental procedure similar to those given in sections 2.4.3. The method starts at low temperature, as for L-met·HCl solubility measurement. The solid amino acids of DL-met·HCl and L-met·HCl were added into a 10 g of deionized water in a 100 ml of laboratory glass bottle with a screw cap at 1.00 g amounts at each time until it was in excess of the saturation condition at 5°C, and then the concentration measured. This method was repeated at the other saturation temperatures. The

solution concentration at each temperature was measured at 25°C using refractive index measured using a RFM340 automatic digital refractometer. This was repeated every hour for about 4 hours to ensure the solubility had been reached.



2.5 Results and Discussion

2.5.1 DL-met·HCl Solubility Calibration Curve

The experimental results for the calibration curve of DL-met·HCl concentration versus the refractive index at 25°C are listed in Table 2.1. The calibration curve of DL-met·HCl concentration at 25°C (used for calculation of met·HCl concentration during crystallization) is obtained from plotting the refractive index, n_D , against the concentration of DL-met·HCl, as shown in Figure 2.6. The calibration data in the concentration range of 0.0–20.0 g met·HCl/100 g solution was fitted using a linear polynomial equation, with the results shown in equation (2.1).

$$RI = 1.925 \times 10^{-3} C + 1.3330 \quad ; \quad r^2 = 0.9997 \quad (2.1)$$

where C represents the met·HCl concentration in g met·HCl/100 g solution, and RI represents the refractive index (n_D). The calibration curve has a y-intercept at a refractive index (n_D) at 1.3330 which is the refractive index of pure water. The concentration calibration curve of met·HCl was used to determine the unknown concentration of the solution of pure enantiomer (L-met·HCl) and mixture compositions of D-met·HCl and L-met·HCl since both enantiomers have the same refractive index. Because of this calibration curve is considered as a standard curve of met·HCl compounds, where the chirality prefixes (L-, D-, and DL-) of met·HCl compounds only refer to the properties of rotating plane polarized-light. However, L-/D-met·HCl, DL-met·HCl, and mixture compositions of met·HCl have a similar physical properties and chemical properties.

The refractive index of the met-HCl in water system is strongly dependent on the met-HCl compound concentration; the refractive index increases steadily with increasing met-HCl. This calibration curve can predict the trend of the relationship between met-HCl concentration and refractive index by extrapolation, but the results of extrapolations are often less meaningful and of greater uncertainty than interpolations. From Table 2.1, the measured pH value is strongly affected by the amount of met-HCl. The pH value decreases with an increasing amount of met-HCl in water due to the dissociation of the dissolved HCl, which makes met-HCl solutions strongly acidic.

Table 2.1 The results of the concentration calibration curve for the met-HCl solution at 25°C.

Sample number	Concentration (g met-HCl/100 g solution)	Refractive index (n_D)	pH
1	0.0	1.3330	7.00
2	2.5	1.3377	1.66
3	5.0	1.3423	1.42
4	7.5	1.3468	1.28
5	10.0	1.3520	1.19
6	12.5	1.3567	1.09
7	15.0	1.3613	1.02
8	17.5	1.3666	0.97
9	20.0	1.3715	0.89

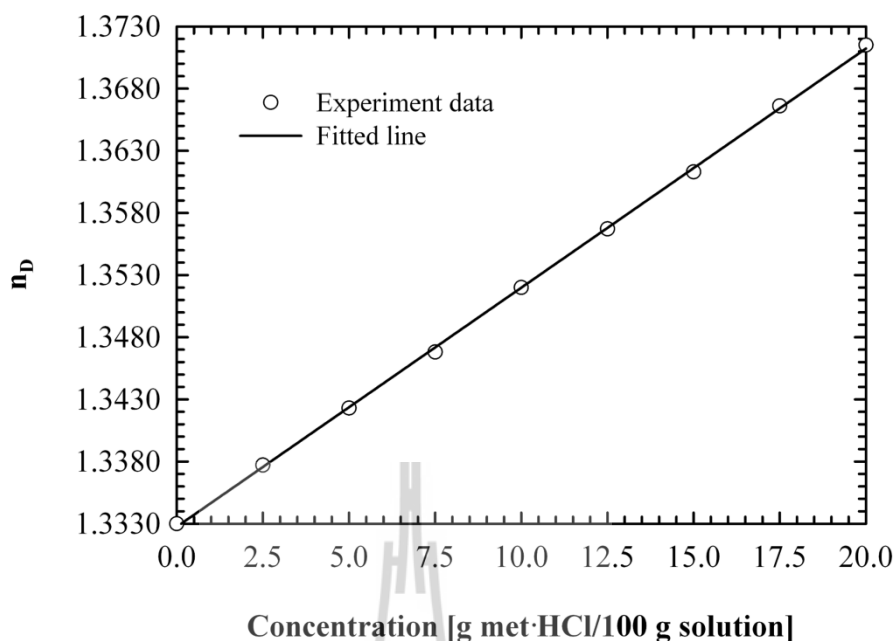


Figure 2.6 Refractive index for the calibration curve of methionine hydrochloride (met·HCl) aqueous solution at 25°C.

2.5.2 Solubility of the met·HCl Species in Aqueous Solution

The experimental data for solubilities of the three enantiomeric mixtures in water (racemic conglomerate, pure enantiomer, and mixture compositions) obtained in this work are summarized in Table 2.2., and the uncertainty limits are represented by 95% confidence intervals (see Appendix B). The example of an average solubility calculation of met·HCl aqueous solutions are shown in Appendix A. Solubilities of racemic conglomerate and pure enantiomeric methionine hydrochloride as a function of temperature are shown in Figure 2.7 and Figure 2.8, respectively. The solubility of a pure enantiomer of methionine hydrochloride in water is compared with the solubility of the racemic conglomerate mixture in Figure 2.9.

Table 2.2 Average value of solubility results (C_{Avg}^* , g met·HCl/100 g water), and error limit (95% confidence interval, C.I.) for the racemic conglomerate mixture, pure enantiomer, and 75 : 25 mixture of met·HCl enantiomers in water at four temperatures.

Temp. (°C)	DL-met·HCl		L-met·HCl		75% L- : 25% D- met·HCl	
	Run	$C_{\text{Avg}}^* \pm 95\% \text{ C.I.}$	Run	$C_{\text{Avg}}^* \pm 95\% \text{ C.I.}$	Run	$C_{\text{Avg}}^* \pm 95\% \text{ C.I.}$
5	3	258±54	3	156 ± 16	3	126± 25
10	3	278±44	3	163 ± 15	3	160 ± 29
25	3	300± 8	3	183 ±15	3	229 ± 18
40	3	361±66	3	216 ±29	3	281 ± 50

Figure 2.7 and Figure 2.8 show the relationship between the solubility of DL-met·HCl in water and L-met·HCl in water as a function of temperature respectively, where both solubility data show an increasing tendency with increasing temperature. Solid lines (DL-met·HCl and L-met·HCl) are best fitted trendlines of both met·HCl compound solubility data which fitted using a quadratic polynomial equation, with the relationship of the solubility data are being shown in equation (2.2) and (2.3).

For DL-met·HCl:

$$C_{\text{DL-met·HCl}}^* = 258.8019 + 0.6386T + 0.0471T^2 \quad ; \quad r^2 = 0.9811 \quad (2.2)$$

For L-met·HCl:

$$C_{L\text{-met}\cdot\text{HCl}}^* = 152.6917 + 0.6891T + 0.0220T^2 \quad ; \quad r^2 = 0.9986 \quad (2.3)$$

where C^* represents the solubility concentration in g met·HCl/100 g water, and T represents the solubility temperature in degree Celsius. Dashed-dot lines are the solubility relationship that can be observed from data with 95% confidence intervals, which shows a confidence region of DL-met·HCl and L-met·HCl solubility data along the solid lines.

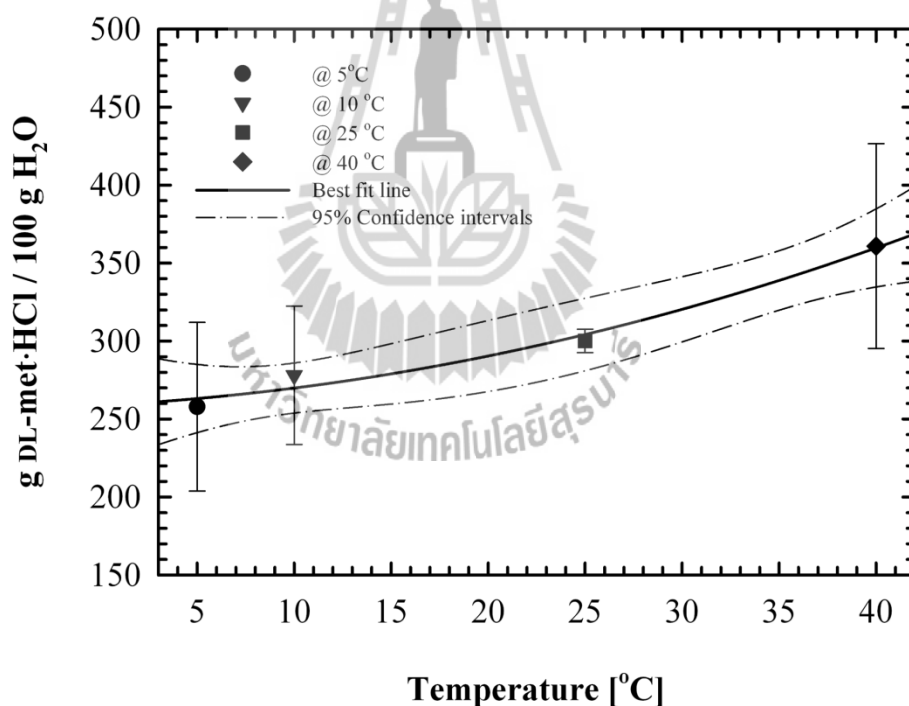


Figure 2.7 Solubility data for the conglomerate DL-methionine hydrochloride (DL-met·HCl) in water.

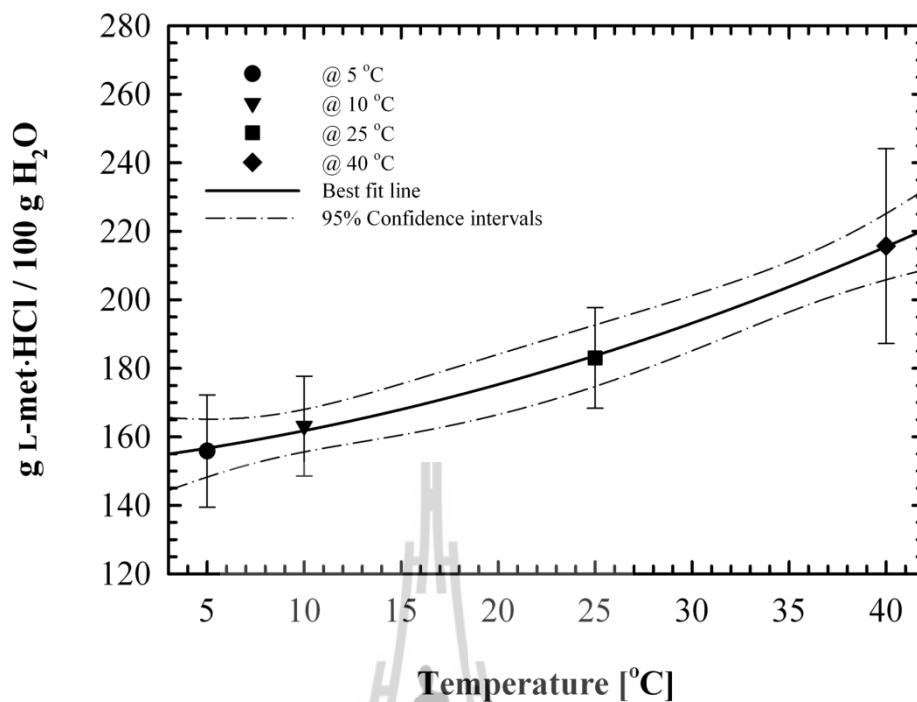


Figure 2.8 Solubility data for the pure enantiomer L-methionine hydrochloride (L-met·HCl) in water.

Figure 2.9 shows a comparison between the solubility of the conglomerate form of methionine hydrochloride in water and the racemic form of methionine in water in a temperature range of 0°C to 50°C. This shows that the solubility of DL-met is lower than the two enantiomers forms (L- and D-met), but the solubility of the racemic conglomerate DL-met·HCl form is higher than that of L- and D-met·HCl. Both the solubility of the conglomerate and racemic crystals increased with increasing temperature, and the solubility of the conglomerate of the hydrochloride form of methionine is very much higher than the solubility of the racemate form of methionine.

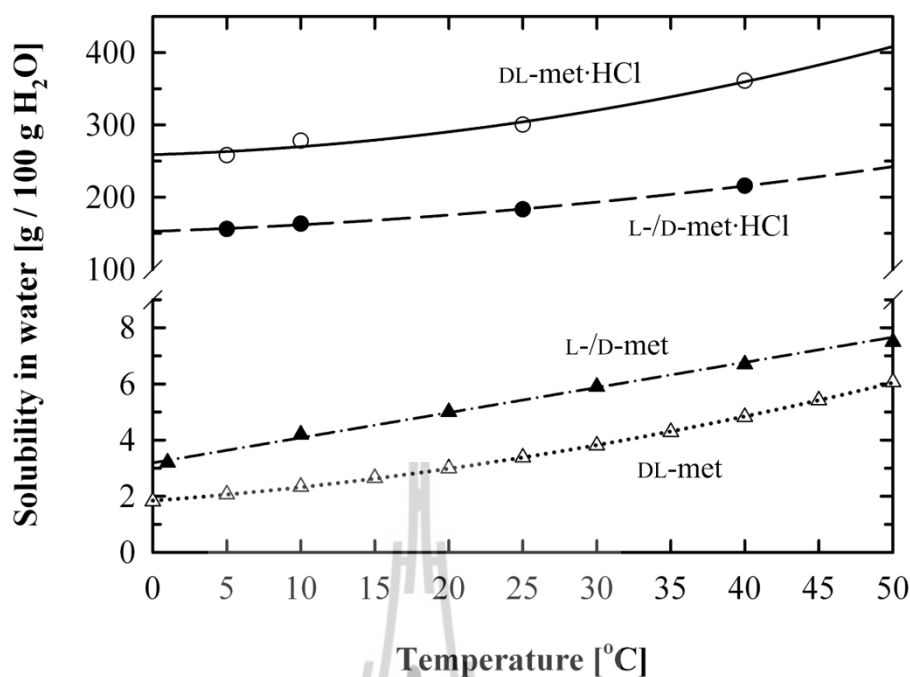


Figure 2.9 Solubility data of the (○) conglomerate DL-met·HCl (from this work) and (●) L-/D-met·HCl (from this work) in water to compared with solubility literature data of (△) DL-met (replotted from Dalton and Schmidt, 1935) and (▲) L-/D-met (replotted from Polenske and Lorenz, 2009) in water.

2.5.3 Ternary Solubility Diagram of the met·HCl Enantiomers in Water System

The appropriate solubility data for the ternary phase diagram of methionine hydrochloride enantiomers in water are presented in Table 2.3. They shows average solubility results of the racemic conglomerate, pure enantiomer, and mixture compositions of methionine hydrochloride aqueous solution in mass fraction units at 5°C, 10°C, 25°C, and 40°C which are plotted as a ternary phase diagram in Figure 2.10. The uncertainty limits are represented by 95% confidence interval (see Appendix B), and the example of an average solubility calculation in mass fraction of

met·HCl aqueous solutions were shown in Appendix A. 3 replicates of experiments in the ternary phase diagram L-met·HCl + D-met·HCl + water have been measured giving solubilities at temperature ranges between 5°C and 40°C covering the whole range of enantiomeric compositions.

Table 2.3 Average solubility results in mass fraction (\bar{w}) and error limit (95% confidence interval, C.I.) for the racemic conglomerate mixture, pure enantiomer, and 75 : 25 mixture of met·HCl enantiomers in water at four temperatures.

Temp. (°C)	DL-met·HCl		L-met·HCl		75% L- : 25% D- met·HCl	
	Run	$\bar{w} \pm 95\% \text{ C.I.}$	Run	$\bar{w} \pm 95\% \text{ C.I.}$	Run	$\bar{w} \pm 95\% \text{ C.I.}$
5	3	0.720 ± 0.041	3	0.609 ± 0.025	3	0.557 ± 0.049
10	3	0.735 ± 0.032	3	0.620 ± 0.021	3	0.614 ± 0.044
25	3	0.750 ± 0.005	3	0.647 ± 0.018	3	0.696 ± 0.016
40	3	0.783 ± 0.030	3	0.683 ± 0.029	3	0.737 ± 0.034

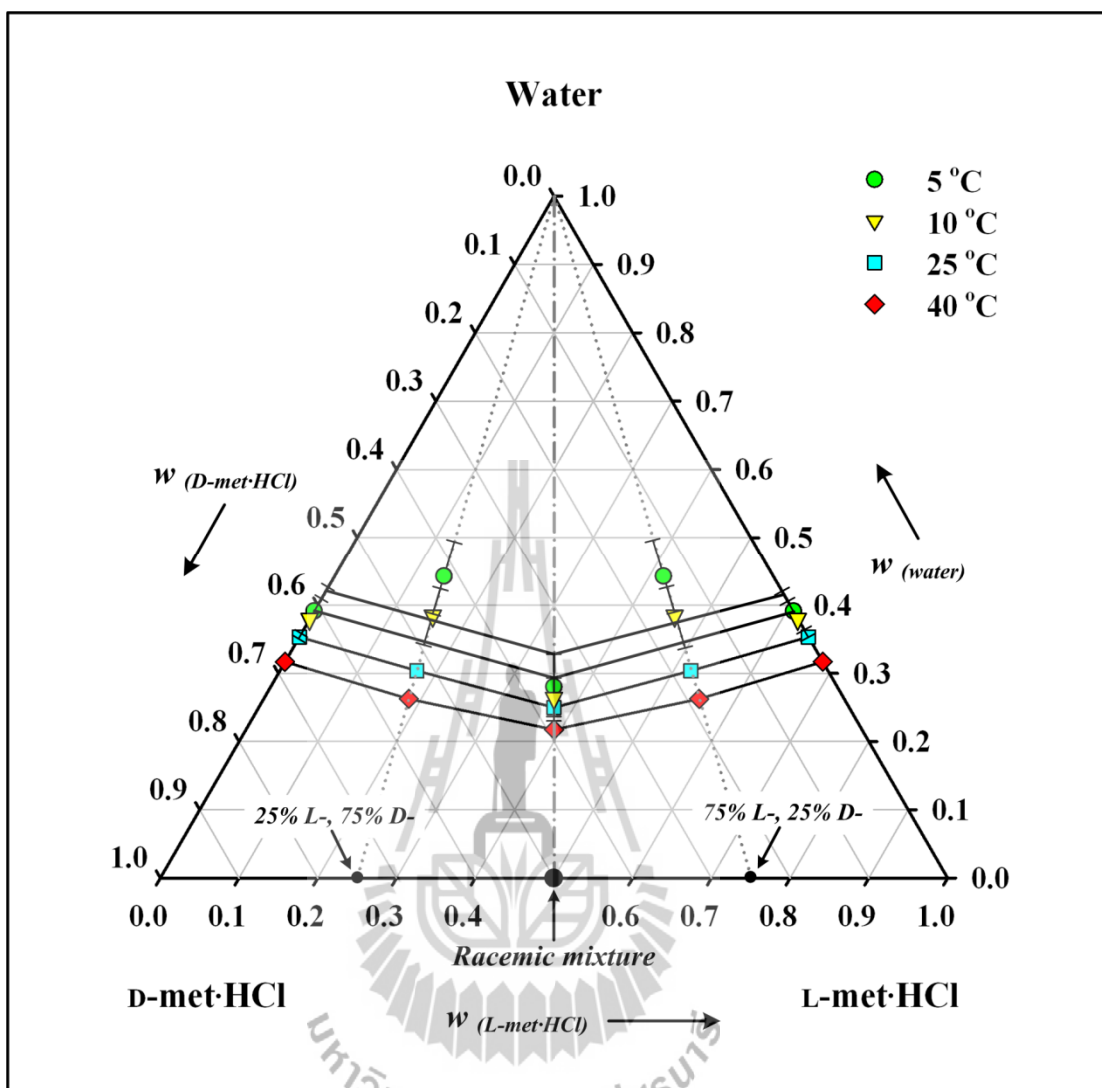


Figure 2.10 Ternary solubility diagram of L-methionine hydrochloride (L-met·HCl) + D-methionine hydrochloride (D-met·HCl) + water. The phase diagram is shown for isotherms at 5°C, 10°C, 25°C, and 40°C (from top to bottom). The isotherm lines are just guides to the eye.

Figure 2.10 presents the ternary solubility diagram of enantiomeric methionine hydrochloride in water in mass fraction units. These consist of all measured solubility data of the pure enantiomers (L-met·HCl), the racemic

conglomerate (DL-met·HCl), and the mixture compositions (75% L-met·HCl : 25% D-met·HCl) in the water solvent. The solubility isotherms of enantiomeric methionine hydrochloride exhibit the typical shape of a conglomerate forming chiral system with a maximum solubility at the racemic mixture composition (DL-met·HCl). The four solubility isotherms at 5°C, 10°C, 25°C, and 40°C are strongly dependent on temperature with an increase in temperature resulting in a rapid rise in solubility.



2.6 Conclusions

This work measured the solubility of the enantiomeric methionine hydrochloride in three forms (racemic conglomerate, pure enantiomer, and 75% L-met·HCl : 25% D-met·HCl mixture compositions) in water over the temperature range of 5°C to 40°C using an isothermal solubility method based on a classical solubility measurement. The refractive index method is convenient and simple for solids content in liquids measurement, after which refractive index values were converted to solution concentration using a concentration calibration curve. This method shows that the refractive index can well determine the solubility values. The solubility of the three forms of enantiomeric methionine hydrochloride in water (racemic conglomerate, pure enantiomer, and mixture compositions) revealed that the solubility is strongly dependent on the temperature, with solubility increased with increasing temperature.

More specially, it has been found that, when DL-met is converted into crystals of DL-met·HCl the resulting species has a much higher solubility in water than the free form (see Figure 2.9). On the other hand, the L-form or D-form of met·HCl has a lower solubility in water than DL-met·HCl (see Figure 2.9). Thus, it is possible to separate crystals of L-met·HCl and D-met·HCl from DL-met·HCl using optical resolution by preferential crystallization. All solubility results of a conglomerate of methionine hydrochloride can be described based on the behavior of conglomerate solubility. The refractive index method is a suitable method to measure the solubility results of methionine hydrochloride in water.

The ternary solubility diagram of L-met·HCl + D-met·HCl + water solvent is in accordance with the typical ternary phase diagram for a conglomerate forming species. There is mirror image symmetry in the diagram, as with all chiral species in

non-chiral solvents. The ternary phase diagram contains the equilibrium data of racemic conglomerate, pure enantiomer, and mixture compositions of methionine hydrochloride in mass fraction unit for four temperatures at 5°C, 10°C, 25°C, and 40°C. All the points measured refer to an amount of methionine hydrochloride at equilibrium state, which between pure enantiomers and the racemic mixture is a mixture compositions of methionine hydrochloride can be identified for 75% L-met·HCl : 25% D-met·HCl. The solubility equilibrium points on the ternary phase diagram can define the phase regions of the phase diagram.



2.7 References

- Caner, H., Groner, E., Levy, L., and Agranat, I. (2004). Trends in the development of chiral drugs. **Drug Discovery Today** 9(3): 105-110.
- Capewell, S. G., Hefter, G. T., and May, P. M. (1999). Improved apparatus and procedures for the measurement of solubility of rapidly equilibrating solid-liquid systems to 90°C. **Review of Scientific Instruments** 70(2): 1481-1485.
- Červinka, O. (1995). **Enantioselective reactions in organic chemistry**. Hertfordshire, England: Ellis Horwood.
- Collins, A. N., Sheldrake, G. N., and Crosby, J. (1992). **Chirality in industry: The commercial manufacture and applications of optically active compounds**. Chichester: John Wiley & Sons.
- Dalton, J. B. and Schmidt, C. L. A. (1935). The solubilities of certain amino acids and related compounds in water, the densities of their solutions at twenty-five degrees, and the calculated heats of solution and partial molal volume. II. **Journal of Biological Chemistry** 109: 241-248.
- Davankov, V. A. (1997). Analytical chiral separation methods. **Pure and Applied Chemistry** 69(7): 1469-1474.
- Flood, A. E. (2008). Recent patents on the optical resolution of amino acid enantiomers by crystallization from solution. **Recent Patents on Materials Sciences** 1: 98-115.
- Fujiwara, M., Nagy, Z. K., Chew, J. W., and Braatz, R. D. (2005). First-principles and direct design approaches for the control of pharmaceutical crystallization. **Journal of Process Control** 15: 493-504.

- Jacques, J., Collet, A., and Wilen, S. H. (1981). **Enantiomers, racemates, and resolutions**. New York: John Wiley & Sons.
- Kurosawa, I., Teja, A. S., and Rousseau, R. W. (2005). Solubility measurements in the L-isoleucine + L-valine + water systems at 298 K. **Industrial and Engineering Chemistry Research** 44: 3284-3288.
- Li, Z. J., Ojala, W. H., and Grant, D. J. W. (2001). Molecular modeling study of chiral drug crystals: Lattice energy calculations. **Journal of Pharmaceutical Sciences** 90(10): 1523-1539.
- Lorenz, H., Perlberg, A., Sapoundjiev, D., Elsner, M. P., and Seidel-Morgenstern, A. (2006). Crystallization of enantiomers. **Chemical Engineering and Processing** 45: 863-873.
- Lorenz, H. and Seidel-Morgenstern, A. (2002). Binary and ternary phase diagrams of two enantiomers in solvent systems. **Thermochimica Acta** 382: 129-142.
- Maier, N. M., Franco, P., and Lindner, W. (2001). Separation of enantiomers: Needs, challenges, perspectives. **Journal of Chromatography A** 906(1-2): 3-33.
- Mitchell, A. G. (1998). Racemic drugs: Racemic mixture, racemic compound or pseudoracemate?. **Journal of Pharmacy & Pharmaceutical Sciences** 1(1): 8-12.
- Mohan, R., Lorenz, H., and Myerson, A. S. (2002). Solubility measurement using differential scanning calorimetry. **Industrial and Engineering Chemistry Research** 41: 4854-4862.
- Moss, G. P. (1996). Basic terminology of stereochemistry (IUPAC Recommendations 1996). **Pure and Applied Chemistry** 68(12): 2193-2222.

- Polenske, D. and Lorenz, H. (2009). Solubility and metastable zone width of the methionine enantiomers and their mixtures in water. **Journal of Chemical and Engineering Data** 54: 2277-2280.
- Roozeboom, H. W. B. (1899). Löslichkeit und Schmelzpunkt als Kriterien für Racemische Verbindungen, Pseudoracemische Mischkristalle und Inaktive Konglomerate. **Zeitschrift für Physikalische Chemie** 28: 494-517.
- Schmidt, B., Patel, J., Ricard, F. X., Brechtelsbauer, C. M., and Lewis, N. (2004). Application of process modeling tools in the scale-up of pharmaceutical crystallization processes. **Organic Process Research & Development** 8: 998-1008.
- Shiraiwa, T., Miyazaki, H., Watanabe, T., and Kurokawa, H. (1997). Optical resolution by preferential crystallization of DL-methionine hydrochloride. **Chirality** 9: 48-51.
- Srisanga, S. and ter Horst, J. H. (2010). Racemic compound, conglomerate, or solid solution: Phase diagram screening of chiral compounds. **Crystal Growth & Design** 10: 1808-1812.
- Tamagawa, R. E., Martins, W., Derenzo, S., Bernardo, A., Rolemberg, M. P., Carvan, P., and Giulietti, M. (2006). Short-cut method to predict the solubility of organic molecules in aqueous and nonaqueous solutions by differential scanning calorimetry. **Crystal Growth & Design** 6(1): 313-320.
- Tulashie, S. K., Lorenz, H., Malwade, C. R., and Seidel-Morgenstern, A. (2010). Ternary solubility phase diagrams of mandelic acid and *N*-methylephedrine in chiral solvents with different carbon chain lengths. **Crystal Growth & Design** 10: 4023-4029.

Wang, Y. and Chen, A. M. (2008). Enantioenrichment by crystallization. **Organic Process Research & Development** 12: 282-290.



CHAPTER III

CRYSTAL GROWTH RATES AND GROWTH RATE

DISTRIBUTIONS FOR L-METHIONINE

HYDROCHLORIDE SINGLE CRYSTALS

IN SUPERSATURATED SOLUTIONS OF

METHIONINE HYDROCHLORIDE

3.1 Abstract

In this chapter, basic properties of the crystallization of the L-enantiomer of DL-methionine hydrochloride (DL-met·HCl) were studied in order to assist in understanding and modeling of the preferential crystallization of DL-met·HCl. In this work, the primary nucleation threshold (PNT), secondary nucleation threshold (SNT), and the crystal growth rate distribution of L-methionine hydrochloride (L-met·HCl) crystals in methionine hydrochloride (met·HCl) solutions were studied. The experimental data in this chapter will help to efficiently operate preferential crystallization of L-met·HCl, and allow the optimization of the resolution time and operating condition of the preferential crystallization. The PNT and SNT of DL-met·HCl in aqueous solution were measured based on induction time measurements for relative supersaturations (σ) of 0.01, 0.02, 0.03, 0.04, and 0.05, which were performed isothermally at 10°C in an agitated glass batch crystallizer with

a constant temperature jacket. The method used gives a satisfactory experimental result for the PNT and SNT of D- or L-met·HCl in aqueous solution. The results show that the induction time dependence on the relative supersaturation is an increase in induction time as the relative supersaturation decreases for both nucleation thresholds. The crystal growth rate and growth rate distribution (GRD) of L-met·HCl single crystals in DL- and L-met·HCl solutions at 10°C were determined by means of a small-cell crystallizer connected to a stereomicroscope with a digital camera, using relative supersaturations (σ) of 0.005, 0.01, and 0.02. The experimental data shows that the crystal growth rate depends strongly on the relative supersaturation of the met·HCl solution, especially from pure L-met·HCl supersaturated solution, and there is a wide crystal growth rate distribution from both types of supersaturated solution. The results will be used to determine the experimental conditions of the preferential crystallization of DL-met·HCl.

3.2 Introduction

Nucleation is one of the most important factors to control in industrial crystallization processes, since it controls crystal product quality aspects such as the kind of solid state, crystal size distributions, and purity of the product crystals. In most cases, knowledge of nucleation will be used to control the crystal growth processes. Nucleation is the formation of new crystals suspended in the solution. Crystal growth is the growth of these crystals to larger sizes through deposition of solute from the solution. Both nucleation and crystal growth require a supersaturated environment in order to occur. Crystal nucleation has been classified as primary nucleation when it takes place without the help of seed crystals and as secondary nucleation when seed crystals are present in a supersaturated solution (Shimizu, Tsukamoto, Horita, and Tadaki, 1984). Although in industrial crystallization, the secondary nucleation mechanism is considered to be the more important for controlling the size distribution of product crystals, it has not been well understood, and in most cases nucleation is necessarily avoided or minimized in crystallization processes since it is difficult to control and gives a bad product size distribution. If possible, the operation is usually undertaken in the metastable zone or the nucleation threshold, and crystallization is initiated through the addition of seed crystals, thus avoiding large amounts of nucleation (Garside and Davey, 1980; Larson, 1981). Over the last several decades, nucleation in solution has been the subject of extensive study. The results obtained are numerous and provide insight into a particular aspect the process, but usually without showing its interrelation with other such aspects or its significance for nucleation in general.

The crystal growth process is a process in which molecules, ions, or atoms, are incorporated into the crystal lattice. Although growth of crystals in a supersaturated solution is a complex process and involves a large number of steps, it can usually be described by two successive mechanisms, mass transfer (by diffusion or convection) of solute molecules from the bulk solution to the crystal surface, and integration of solute molecules into the surface (a reaction step) (Randolph and Larson, 1988).

A technique to better understand nucleation of molecules involves the measurement of nucleation time by the induction time technique. The induction time, t_{ind} , refers to the time that elapses after the creation of supersaturation in solution until a new phase is detected, and is an experimentally accessible quantity (Kuldipkumar, Kwon, and Zhang, 2007). The induction time thus measured allows for a connection to be made between nucleation theory and experimental investigation. Therefore, reliable methods for the determination of induction time periods are important. Several techniques such as measurement of solution conductivity (Söhnel and Mullin, 1978), intensity of transmitted light (Kozlovskii, Wakita, and Masuda, 1983), electronic microscopy (Michinomae, Mochizuki, and Ataka, 1999), fluorescence (Crosio and Jullien, 1992), and turbidity (Hu, Hale, Yang, and Wilson, 2001) have been used for the experimental determination of the induction time.

This work aims to systematically study the primary and secondary nucleation threshold of DL-met·HCl in aqueous solution at various relative supersaturation by means of induction time by the turbidity technique, and also determine the growth rate distribution of L-met·HCl crystals in DL- and L-met·HCl solution with different relative supersaturation using a small-cell crystallizer. The work will elucidate the relationship between induction time and the relative supersaturation of DL-met·HCl solution and

also the relationship between the relative supersaturation and the crystal growth rate. The solubility data of DL- and L-met·HCl from the previous chapter will be used here to calculate the amount of met·HCl species required in the aqueous solutions for a particular supersaturation value. This should improve understanding of the kinetics of nucleation and crystal growth of L-met·HCl crystals in met·HCl solutions. Moreover, important crystallization parameters will be estimated in order to predict the suitable operating condition for preferential crystallization of DL-met·HCl and including the purity of desired crystal form.



3.3 Theory

Solution crystallization is considered to be a two-step process: nucleation, or the birth of crystals, and crystal growth, which involves subsequent growth of existing crystals. One of requirements for bulk crystallization is that the solution should exceed its solubility at a given temperature, i.e., the solution should be supersaturated (Chattopadhyay, Erdemir, Evans, Ilavsky, Amenitsch, Segre, and Myerson, 2005).

The supersaturation of a system can be expressed in several of different ways. Considerable confusion can be caused if the basic units of concentration are not clearly defined. Also, the temperature must be specified.

Among the most common expressions of supersaturation are the concentration driving force (Δc), the supersaturation ratio (S), and a quantity sometimes referred to as the absolute or relative supersaturation (σ), or percentage supersaturation (100σ). These quantities are defined by Mullin (2001):

$$\Delta c = c - c^* \quad (3.1)$$

$$S = \frac{c}{c^*} \quad (3.2)$$

$$\sigma = \frac{\Delta c}{c^*} = S - 1 \quad (3.3)$$

where c is the solution concentration and c^* is the equilibrium saturation at the given temperature.

3.3.1 Fundamentals of Nucleation

Nucleation is a key step in the crystallization process, since it can control crystal product quality aspects such as the kind of solid state, size, crystal size distribution (CSD) and purity of product particles. There is a statistical process of a new phase (nuclei) forming from a supersaturated existing phase (Funakoshi and Matsuoka, 2008; Jiang and ter Horst, 2011). Nucleation from solution can be divided into two distinct types, which are primary nucleation and secondary nucleation, as presented in Figure 3.1. Primary nucleation is the formation of nuclei that are able to grow without presence of any solute crystals, whereas secondary nucleation requires the presence of solute crystals.

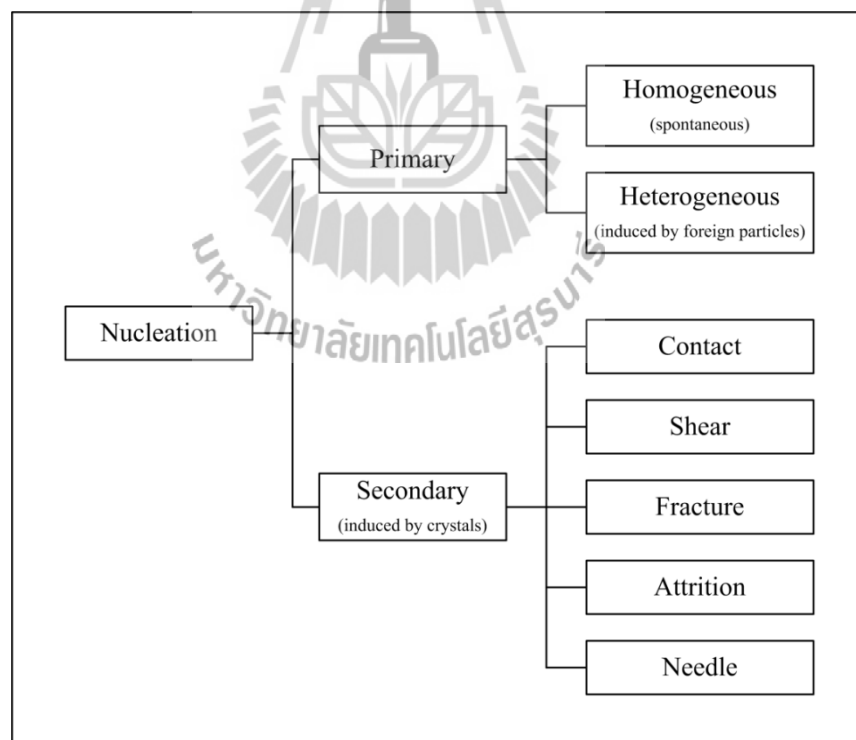


Figure 3.1 Mechanisms of nucleation (Randolph and Larson, 1988).

Primary nucleation is used to describe nucleation when the nucleation mechanism does not depend on the presence of suspended solute crystals in the solution. This is further divided into homogeneous mechanisms (where there are no external nucleation sites available, as could be caused by the walls of the vessel, dust particles, crystals or solids of other solute etc.) and heterogeneous mechanisms (where there is the presence of foreign suspended dust particles or apparatus surfaces). Secondary nucleation is more significant than primary nucleation, and can be called the main source of the nuclei occurring in the majority of industrial crystallization units, since the vessel is run continuously having solute crystals inside. Secondary nucleation can occur by contact nucleation, shear nucleation, fracture nucleation, attrition nuclei, and needle breeding. Randolph and Larson (1988) also propose an initial breeding nucleation mechanism, which is an important source of nuclei in a seeded system.

3.3.2 Fundamental of Induction Time Measurement

The induction time is usually defined as time needed for the first nucleation events to be detected in a solution kept at a constant supercooling (Kubota, 2008). It should be related to the metastable zone width (MSZW, ΔT_m), because the induction time and the MSZW are closely related with crystal nucleation kinetics. The MSZW has been defined as the supercooling at which the first crystals appear when the solution is cooled at a constant rate as shown in Figure 3.2(a). On the other hand, the induction time is defined as the time elapsed from attainment of a constant supersaturation to the appearance of first crystals as shown in Figure 3.2(b) (Kobari, Kubota, and Hirasawa, 2010). The induction time is affected by several parameters

such as the initial supersaturation, temperature, pH, agitation speed, and the presence of additives/impurities (Kuldipkumar, Kwon, and Zhang, 2007).

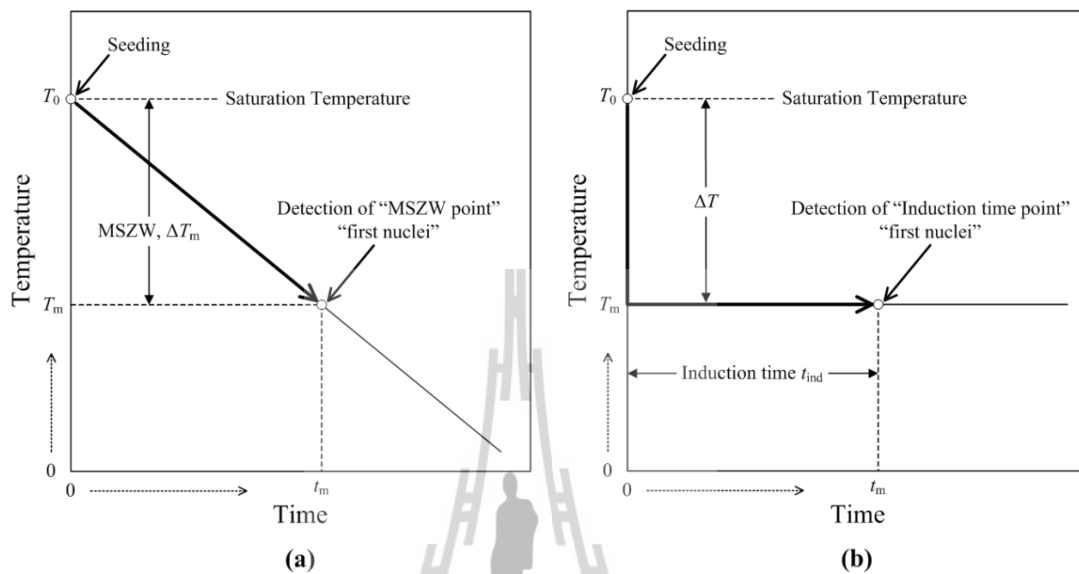
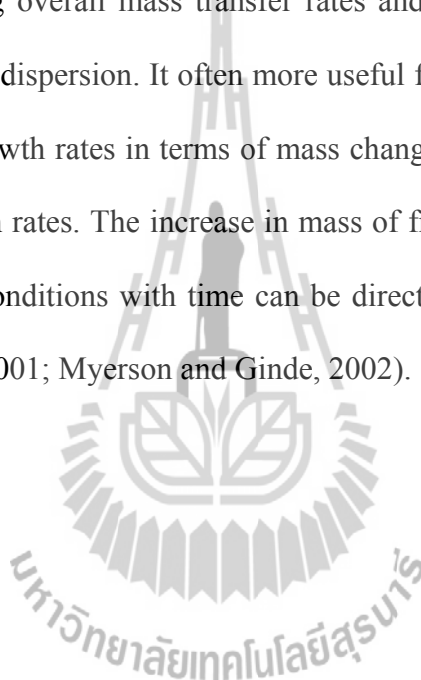


Figure 3.2 Temperature changes and definitions of (a) MSZW and (b) induction time (Kobari, Kubota, and Hirasawa, 2010).

3.3.3 Methodology to Study the Crystal Growth

Crystal growth rate (typically termed G and expressed in terms of micrometers per time) is a function of supersaturation, with higher supersaturations resulting in higher growth rates (Barrett, Smith, Worlitschek, Bracken, O'Sullivan, and O'Grady, 2005). In general, the crystal growth mechanism is determined by measuring the growth rates and then fitting the measured rates to the expressions describing the different crystal growth mechanisms (Kuldipkumar, Kwon, and Zhang, 2007). Crystal growth rate data can be obtained by a number of experimental methods. Two main groups can be differentiated. The first group comprises methods that measure the growth of a single crystal to obtain the needed data, e.g. recirculation

apparatus or flow apparatus (Myerson and Ginde, 2002), or microscopic cells (Rodriguez-Hornedo and Murphy, 1999). Single crystal growth techniques, which can focus on growth rates of individual faces, are predominantly used for fundamental studies relating to growth mechanisms. The second group of methods involves the growth of a suspension of crystals, e.g. in agitated vessels (Mullin, 2001), or fluidized beds (Phillips and Epstein, 2004). Measurements made on populations of crystals are useful for determining overall mass transfer rates and for observing size-dependent growth or growth rate dispersion. It is often more useful for crystallizer design purposes to measure crystal growth rates in terms of mass change of the crystals rather than as individual face growth rates. The increase in mass of fractionated seed crystals under carefully controlled conditions with time can be directly related to the overall linear growth rate (Mullin, 2001; Myerson and Ginde, 2002).



3.4 Experimental Procedure

3.4.1 Materials

DL- and L-met·HCl compounds were prepared by the method shown in section 2.4.1, Chapter II. The solutions of DL- and L-met·HCl in water were prepared in the relative supersaturation (σ) range between 0.005 and 0.05 (for experiments at 10°C) at a high temperature, around 45–50°C for about 30 to 40 minutes to ensure that no nuclei remained. The L-met·HCl crystals were prepared as seed crystals used in the secondary nucleation threshold experiments and also as single crystals in crystal growth rate experiments. The size of L-met·HCl crystals used in the experiments was 100–600 μm . An example of seed crystals for L-met·HCl is shown in Figure 3.3.



Figure 3.3 Photomicrograph of L-met·HCl seed crystals on magnification 25x.

3.4.2 Determination of the Induction Times of Primary and Secondary Nucleation Threshold for DL-met-HCl in Aqueous Solution

A schematic drawing of the nucleation threshold experimental setup is given in Figure 3.4. The apparatus comprises of a 400 ml glass batch crystallizer with a jacket, as shown in Figure 3.5 (schematic drawing), with a four-blade impeller and an overhead stirrer. The glass batch crystallizer with jacket was connected to circulating water at constant temperature from a cooling bath, and the solution temperature in the glass batch crystallizer was confirmed using a thermometer, and the temperature was controlled to within $\pm 0.5^\circ\text{C}$. The solution was agitated at 350 rpm at all times by a four-blade impeller connected to an overhead stirrer. The primary and secondary nucleation threshold experiments were modified from the method of Srisa-nga et al. and using the relationship between nucleation and induction time at a constant supercooling to determine both nucleation thresholds (Srisa-nga, Flood, and White, 2006; Kubota, 2010). 20 g of supersaturation solution of DL-met-HCl in water was prepared at 0.01, 0.02, 0.03, 0.04, and 0.05 of relative supersaturation (σ) based on solubility data at 10°C , which was dissolved at $45\text{--}50^\circ\text{C}$ for about 30 to 40 minutes in a 100 ml laboratory glass bottles with screw caps (Schott Duran, Germany) to ensure a homogenized solution, and that no nuclei existed in the solution. The clear solution was cooled down instantaneously to $10\pm 0.5^\circ\text{C}$ by pouring the solution (at $45\text{--}50^\circ\text{C}$) from a glass bottle to the glass batch crystallizer which was kept at a constant temperature (10°C).

The solution was held at 10°C until the induction time (t_{ind}) was reached. For SNT experiments, approximately 0.2 g of L-met-HCl as seed crystals was added into the solution before the start of the experiment, since secondary nucleation

is induced by the added seeds. Nucleation was observed by eye at particular time intervals, with nucleation being indicated by clouding due to the very fine nuclei particles. The timing was stopped when the solution began to change from a clear solution to become a turbid solution which was clearly visible. Primary nucleation threshold experiments were the same as the secondary nucleation threshold experiments, but the primary nucleation threshold experiment does not have seed crystals added before the start of the induction time measurement. The same steps were repeated for 0.01, 0.02, 0.03, 0.04, and 0.05 relative supersaturation (σ) of DL-met-HCl solution, for both primary and secondary nucleation threshold measurements.

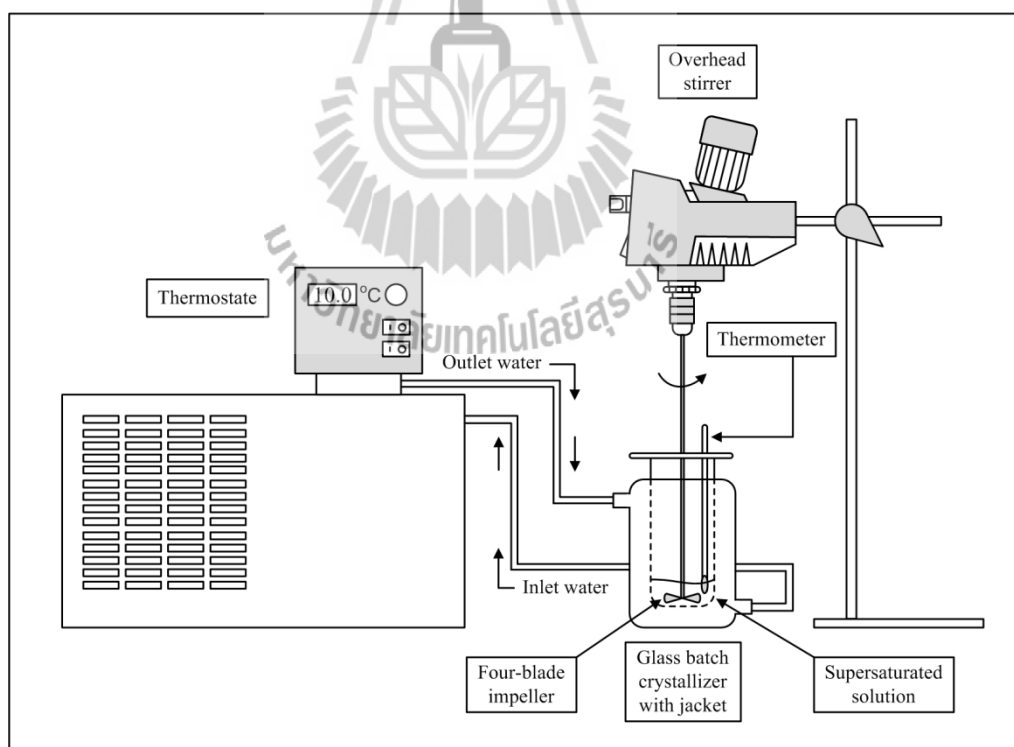


Figure 3.4 Experimental setup schematic for the primary and secondary nucleation threshold measurement of DL-met-HCl in water.

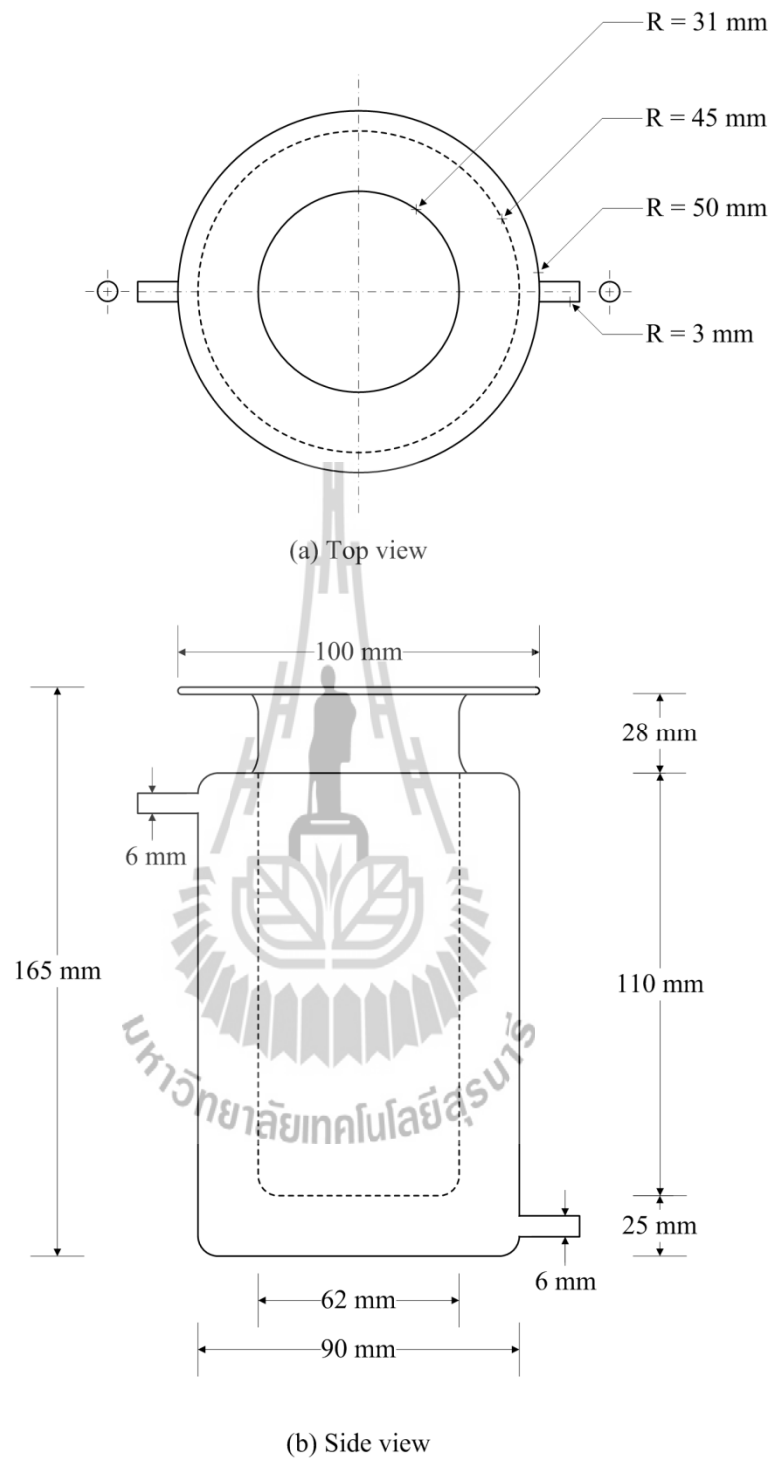


Figure 3.5 Schematic diagram of the 0.4 L glass batch crystallizer with jacket used to observe primary and secondary nucleation thresholds.

(a) Top view and (b) side view are shown.

3.4.3 Determination of the Mean Crystal Growth Rates and Growth Rate Distribution of L-met-HCl Single Crystals in DL- and L-met-HCl Supersaturated Solution by Small-Cell Crystallizer

The mean crystal growth rate and growth rate distribution measurement of L-met-HCl single crystals in DL- and L-met-HCl supersaturated solutions were studied via a small-cell crystallizer with a stereomicroscope. The small-cell crystallizer is depicted in Figure 3.6. The small-cell crystallizer was constructed of stainless steel and was of circular cross-section with an internal diameter of 60 mm. The supersaturated solution was held in the upper section (the growth section) which had a capacity of about 70 ml, and contains a glass cover slip upon which the single crystals grow. The lower section, which is separated from the growth section with an acrylic plate, is used for circulation of constant temperature water at 10°C from a water bath maintained to within $\pm 0.5^\circ\text{C}$, to hold the liquid solution in the growth section at 10°C; the solution temperature in the growth section was checked by a thermometer. Circular cover glasses (acrylic plates) were used to separate the supersaturated solution and water, and also used to close the solution chamber at the upper section and the circulating water chamber at the lower section from the atmosphere, sealing being achieved with O-rings (Garside, and Larson, 1978; Lowe, Ogden, McKinnon, and Parkinson, 2002).

70 ml of DL- and L-met-HCl solutions were prepared at 0.005, 0.01, and 0.02 of relative supersaturation (σ) (with reference to the saturation concentration at 10°C) at a high temperature (45–50°C), which is above the solubility temperature, to ensure that the solution is homogeneous and no ghost nuclei remained in the solution. Nine L-met-HCl single crystals were attached on the 20×20 mm glass cover slip. The

size of L-met-HCl seed crystals used in the experiment were 200–500 μm . The L-met-HCl single crystals on the glass cover slip were taken into the solution chamber (upper section) in the small-cell crystallizer in which met-HCl supersaturated solutions were maintained at $10\pm 0.5^\circ\text{C}$ by constant temperature water circulation. The crystal size was monitored directly throughout the experiment using a stereomicroscope (model SZX9, Olympus Optical Co., Ltd., Japan) equipped with a microscope digital camera (model DP11 type C-mount CCD camera plus hand switch, Olympus Optical Co., Ltd., Japan) connected to a computer to operate the software for image processing and analysis (Olympus Camedia Master version 1.11). The crystal size was measured by the changes in the dimensions of single crystals by measuring the scale calibrated by a standard wire at magnification 6.3x, 16x, 25x, and 40x as shown in Figure 3.13. In this experiment, the two visible dimensions of the single crystals can be observed, the width and the length, but measurement of the crystal size to determine the growth rate is done only on the crystal side that significantly changes and is most easily measured, that is the width of the single crystals. A schematic drawing of the crystal growth experimental setup is shown in Figure 3.7, and this was used for all experiments.

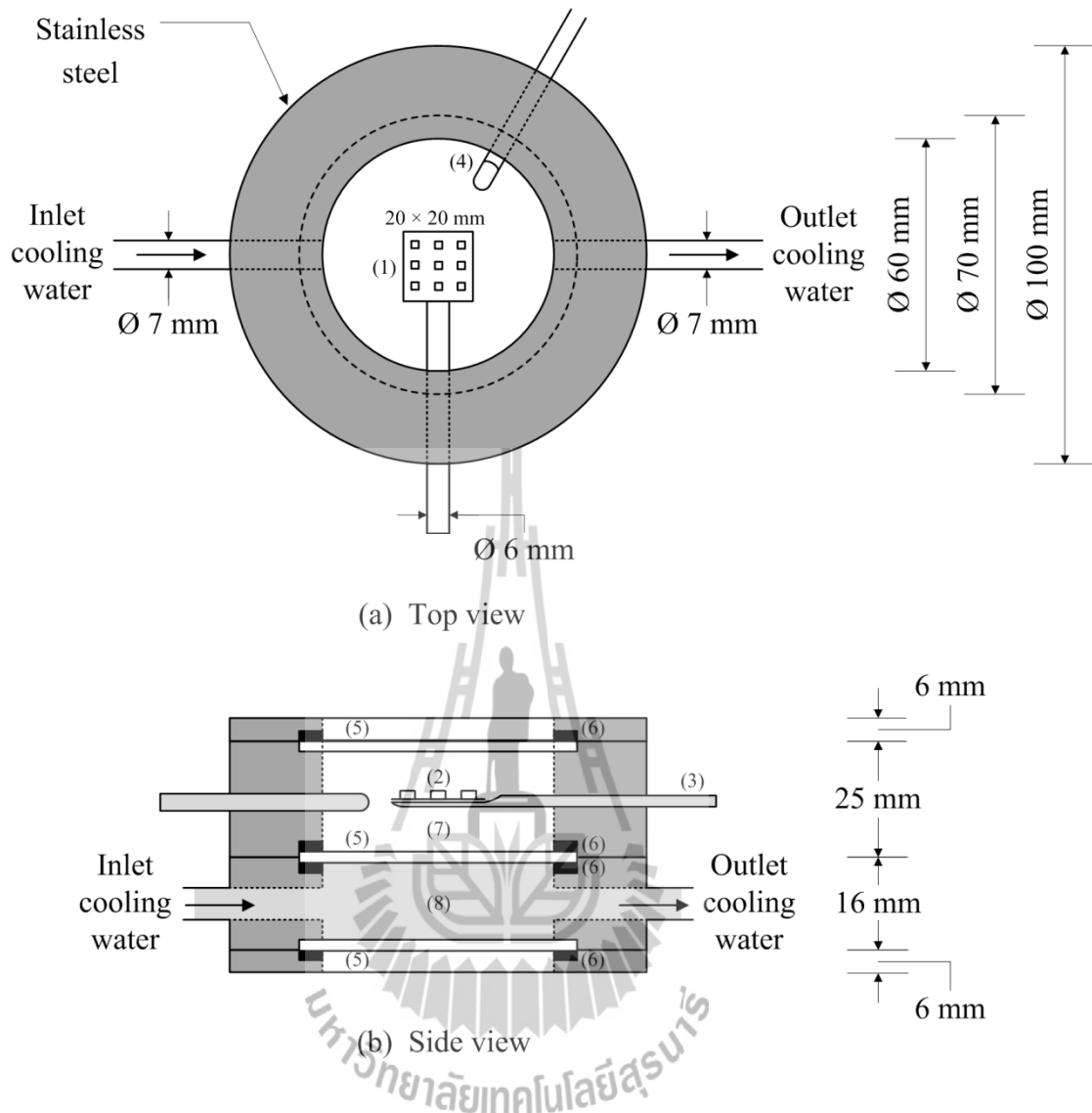


Figure 3.6 Schematic diagram of the single crystal growth, small-cell crystallizer using an optical microscope (a) Top view, (b) Side view; (1) glass cover-slip, (2) single crystals, (3) supported rod, (4) thermometer, (5) cover glasses, (6) O-ring seal, (7) sample solution compartment, and (8) constant temperature water circulation compartment.

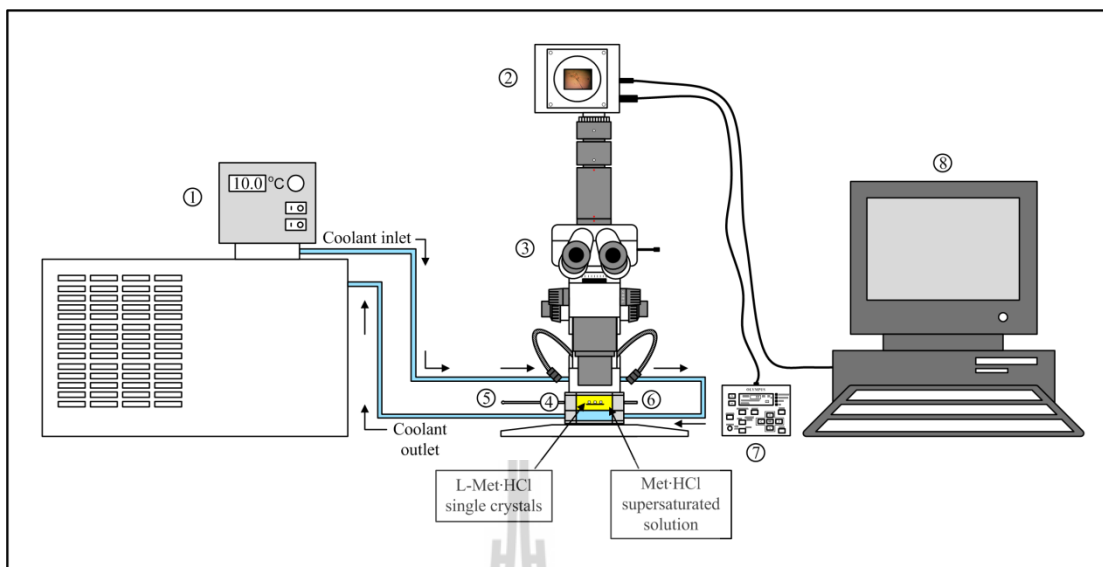


Figure 3.7 The design of L-met-HCl single crystals growth in DL- and L-met-HCl supersaturated solutions by a small-cell crystallizer and optical microscope experimental setup schematic; (1) thermostat, (2) digital camera, (3) stereomicroscope, (4) small-cell crystallizer, (5) thermometer, (6) supported rod, (7) DP11 hand switch, and (8) computer.

3.5 Results and Discussion

3.5.1 Effect of DL-met·HCl Supersaturated Solution to the Induction

Time for Primary and Secondary Nucleation Threshold

Measurement

Results of the induction time; t_{ind} for the primary nucleation threshold (PNT) and secondary nucleation threshold (SNT) of L-met·HCl in DL-met·HCl supersaturated solutions are shown in Table 3.1 and Table 3.2, respectively, for the experiment at 10°C. Figure 3.8 shows an example of the changes in the appearance of the DL-met·HCl solution during the induction time measurement. This figure shows the PNT of DL-met·HCl solution at 0.02 relative supersaturation (σ) by induction time measurement, where the primary nucleation began at 9 minutes (shown in picture (d)). At 9 minutes there is a slightly turbid (cloudy) solution. Hence, the timing was stopped at 9 minutes, when the solution changed from a clear transparent solution to become a turbid solution.

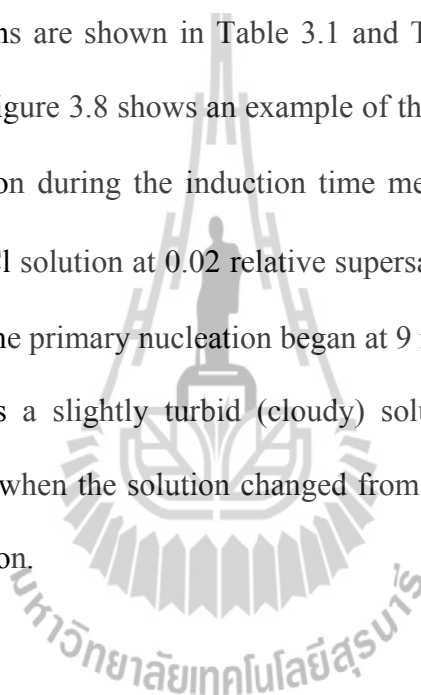


Table 3.1 Experimental conditions of the primary nucleation threshold experiments and the induction time values (t_{ind}).

Relative supersaturation (σ , [-])	Actual relative supersaturation [-]	Initial concentration (C_0) (g DL-met·HCl/g solution)	Mass of DL-met·HCl (g) (Theory / Actual)	Mass of H ₂ O (g) (Theory / Actual)	t_{ind} (minute)
0.01	0.009785	0.8021	16.0420 / 16.0468	3.9580 / 3.9624	11.0000
0.02	0.019935	0.8101	16.2020 / 16.2085	3.7980 / 3.8012	9.0000
0.03	0.029941	0.8180	16.3600 / 16.3685	3.6400 / 3.6424	7.5000
0.04	0.039800	0.8260	16.5200 / 16.5246	3.4800 / 3.4856	5.7667
0.05	0.049938	0.8339	16.6780 / 16.6803	3.3220 / 3.3234	4.4667



Table 3.2 Experimental conditions of the secondary nucleation threshold experiments and the induction time values (t_{ind}).

Relative supersaturation (σ ; [-])	Actual relative supersaturation [-]	Initial concentration (C_0) (g DL-met·HCl / g solution)	Mass of DL-met-HCl (g) (Theory / Actual)	Mass of H₂O (g) (Theory / Actual)	t_{ind} (minute)
0.01	0.009901	0.8021	16.0420 / 16.0456	3.9580 / 3.9598	1.4333
0.02	0.019746	0.8101	16.2020 / 16.2051	3.7980 / 3.8041	0.9500
0.03	0.029927	0.8180	16.3600 / 16.3614	3.6400 / 3.6411	0.7667
0.04	0.039831	0.8260	16.5200 / 16.5270	3.4800 / 3.4855	0.5667
0.05	0.049769	0.8339	16.6780 / 16.6792	3.3220 / 3.3264	0.5167



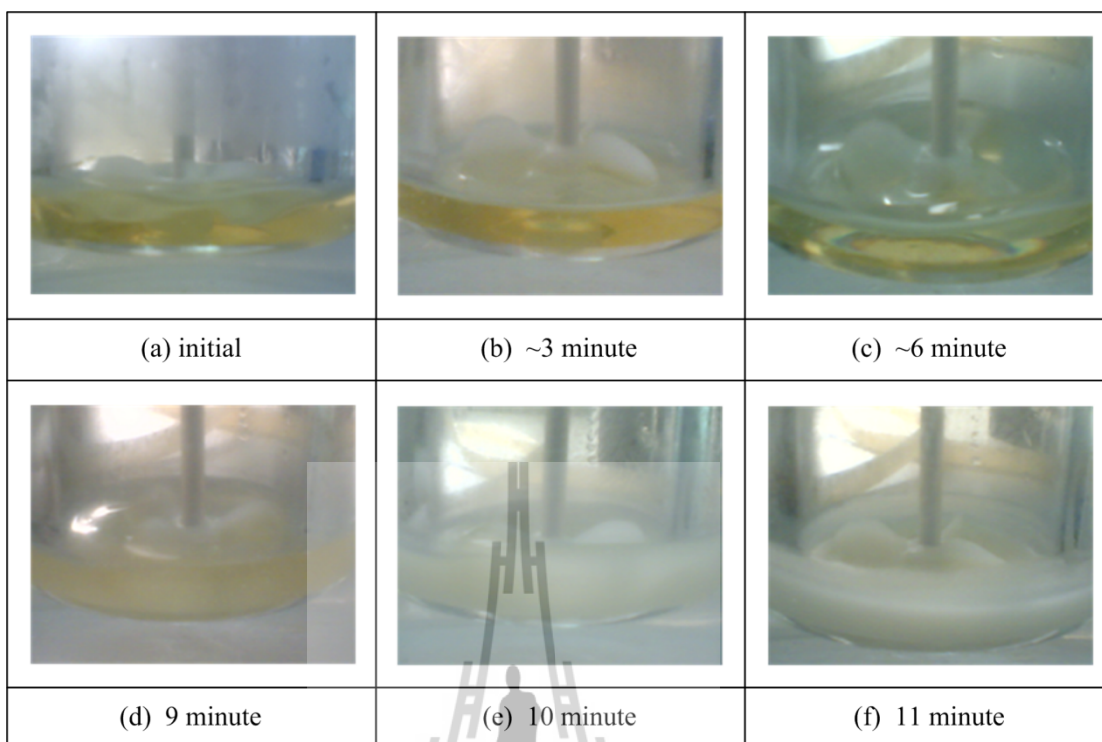


Figure 3.8 An example of measuring the primary nucleation threshold experiments for DL-met·HCl supersaturated solution ($\sigma = 0.02$), at 10°C.

The effect of various supersaturations on the induction time of the measured PNT and SNT of DL-met·HCl solution are shown in Figure 3.9 and Figure 3.10, respectively. These figures show the time dependence of the relative supersaturation of the PNT and SNT, with the induction time increasing as the relative supersaturation of the PNT and SNT decreases. The induction time of the SNT is less than the induction time of the PNT because of the influence of L-met·HCl seed crystals on the SNT experiment, which induced the birth of new crystals in the supersaturated solution.

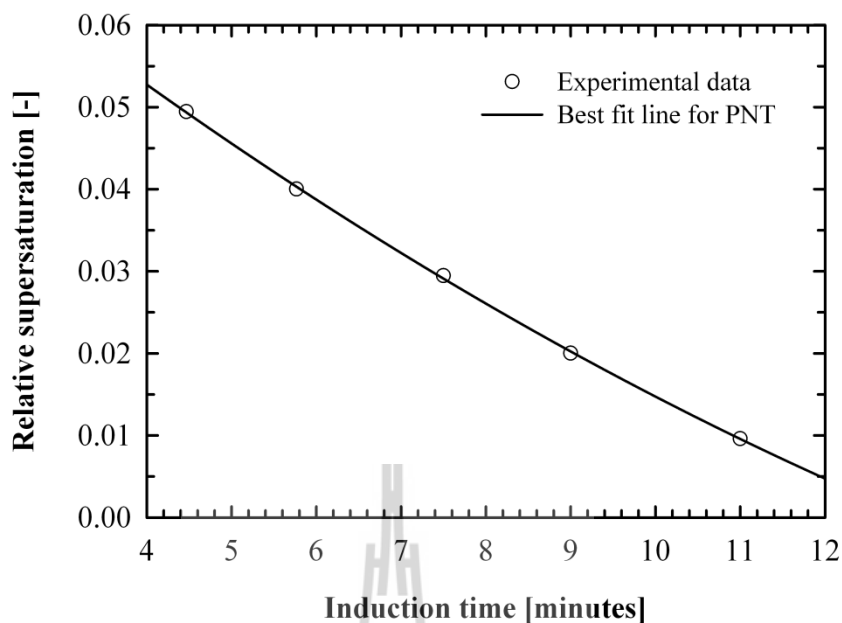


Figure 3.9 Effect of supersaturation on the induction time for the primary nucleation threshold (PNT) of DL-met·HCl solution at 10°C.

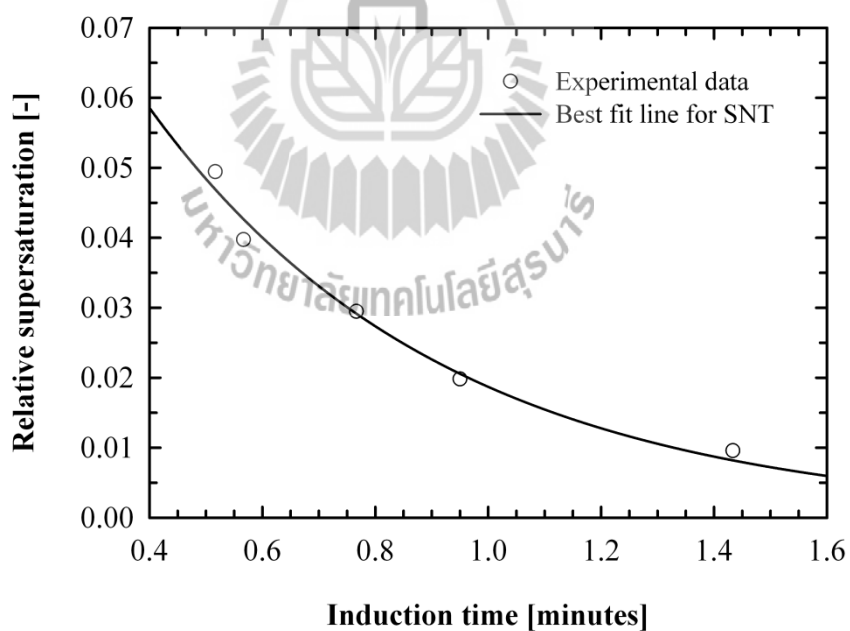


Figure 3.10 Effect of supersaturation on the induction time for the secondary nucleation threshold (SNT) of DL-met·HCl solution at 10°C.

3.5.2 Growth Rate Distribution of L-met·HCl Single Crystals in DL- and L-met·HCl Supersaturated Solution

The crystal growth rates of L-met·HCl single crystals in met·HCl solution were studied with a small-cell crystallizer, and the size of crystals were observed using a stereomicroscope equipped with a digital camera. Nine parent crystals of L-met·HCl were attached with latex glue onto a glass cover slip within the supersaturated solution of met·HCl at 10°C; the temperature was maintained by circulating constant temperature water from a cooling bath. The size of the small crystals was observed and recorded by a stereomicroscope with a digital camera, with each parent crystal being recorded every 10 minutes until 50 minute cycle times were completed. Examples of photomicrographs of crystal growth for L-met·HCl single crystals in DL-met·HCl solution and in L-met·HCl solution are shown in Figure 3.11 and Figure 3.12, respectively.

Figure 3.11 shows the crystal growth behavior of L-met·HCl parent crystal in DL-met·HCl supersaturated solution ($\sigma = 0.005$) at 10°C. The parent crystal was grown in the length direction significantly more than in the width direction, and also small particle which were attached on the single crystal at the initial time (which could not be seen with the naked eye) grew larger. They were grown mostly sideways from the surface of the parent crystals. The growth of small crystals on the surface of the parent crystal was quite disorganized, like a group of small needle-like crystals grown from the surface of parent crystal. Due to the imperfection of the crystal surface the growth is therefore not the growth of single crystals.

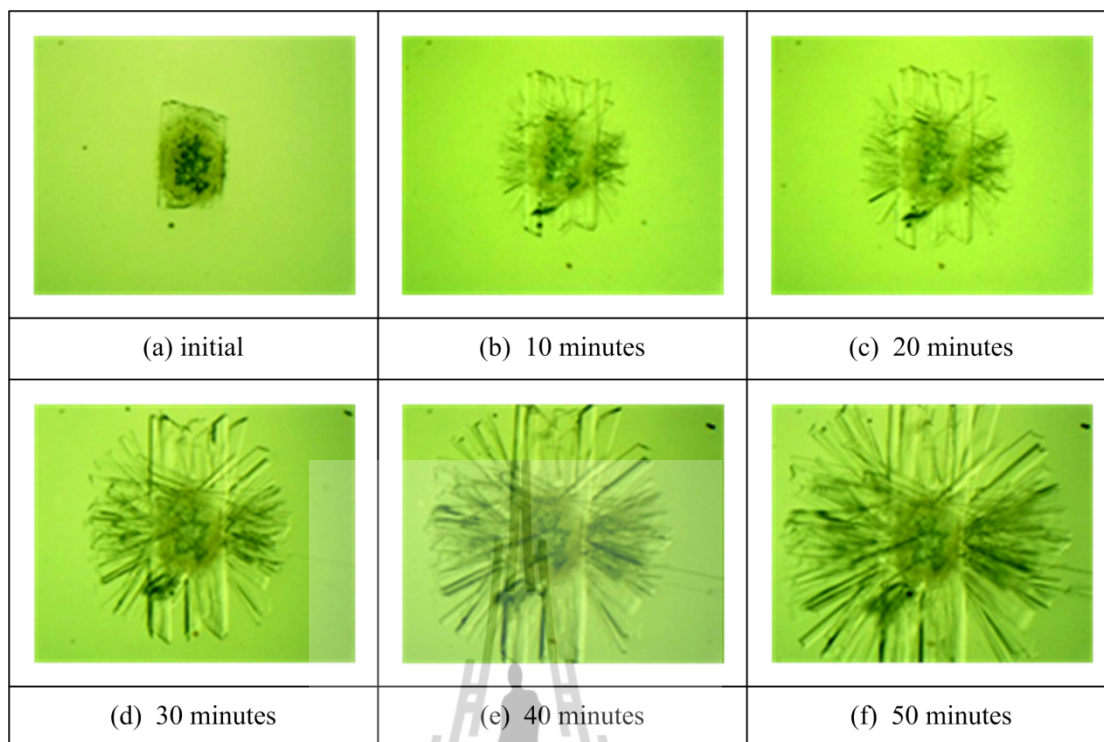


Figure 3.11 Photomicrographs of crystal growth of L-met·HCl single crystals in DL-met·HCl solution ($\sigma = 0.005$) at 10°C, magnification 40x.

Figure 3.12 shows the crystal growth behavior of L-met·HCl parent crystal in L-met·HCl supersaturated solution ($\sigma = 0.005$) at 10°C. The parent crystal was grown in both directions (the width and the length) similar to the growth in DL-met·HCl supersaturated solution, and also the small crystals were grown sideways from the parent crystal as well.

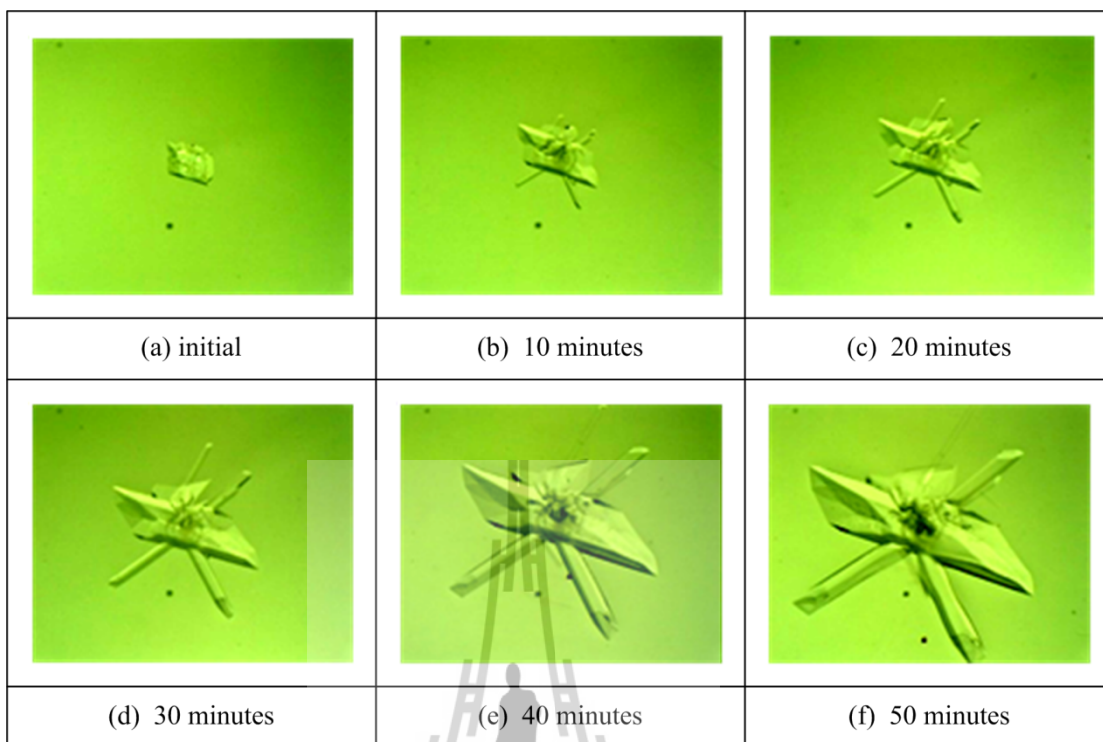
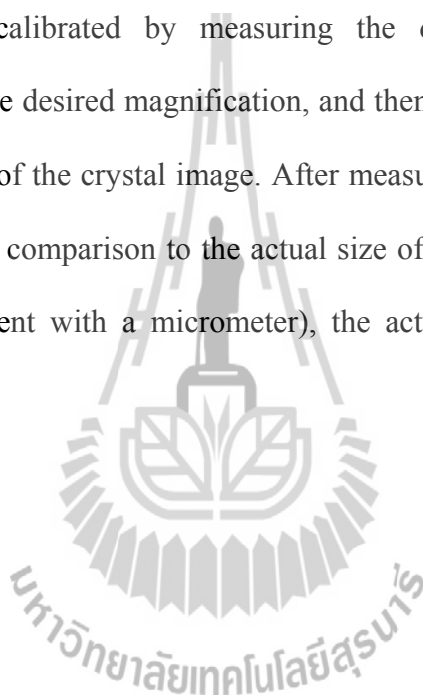


Figure 3.12 Photomicrographs of crystal growth of L-met·HCl single crystals in L-met·HCl solution ($\sigma = 0.005$) at 10°C, magnification 25x.

However, the growth of small crystals on the parent crystals in L-met·HCl supersaturated solutions was more orderly and resulted in more perfect shape than the growth in DL-met·HCl supersaturated solutions. The L-met·HCl small crystals in L-met·HCl supersaturated solution grow significantly in both visible directions (the width and the length) over time as shown in Figure 3.12, but the L-met·HCl small crystals in DL-met·HCl supersaturated solution grow significantly in the length direction only as shown in Figure 3.11. This may be due to the DL-met·HCl supersaturated solution has the D-met·HCl acting as a growth inhibitor of L-met·HCl. This modifies the growth behavior of the L-met·HCl crystals in the DL-met·HCl supersaturated solutions.

After recording all crystal growth data completely with the stereomicroscope; 9 L-met·HCl parent crystals grown in DL-met·HCl supersaturated solutions ($\sigma = 0.005$, $\sigma = 0.01$, $\sigma = 0.02$) at 10°C; 9 L-met·HCl parent crystals grown in L-met·HCl supersaturated solution ($\sigma = 0.005$, $\sigma = 0.01$, $\sigma = 0.02$) at 10°C, the crystal size was measured by comparison with a scale calibrated by a standard wire at various magnifications, e.g. 6.3x, 16x, 25x, and 40x, as shown in Figure 3.13. The standard wire was calibrated by measuring the diameter of the wire on a photomicrograph of the desired magnification, and then printing the photomicrograph at a size equal to that of the crystal image. After measurement of the size of standard wire using a ruler and comparison to the actual size of the standard wire (which was known via measurement with a micrometer), the actual dimensions of the crystal could be calculated.



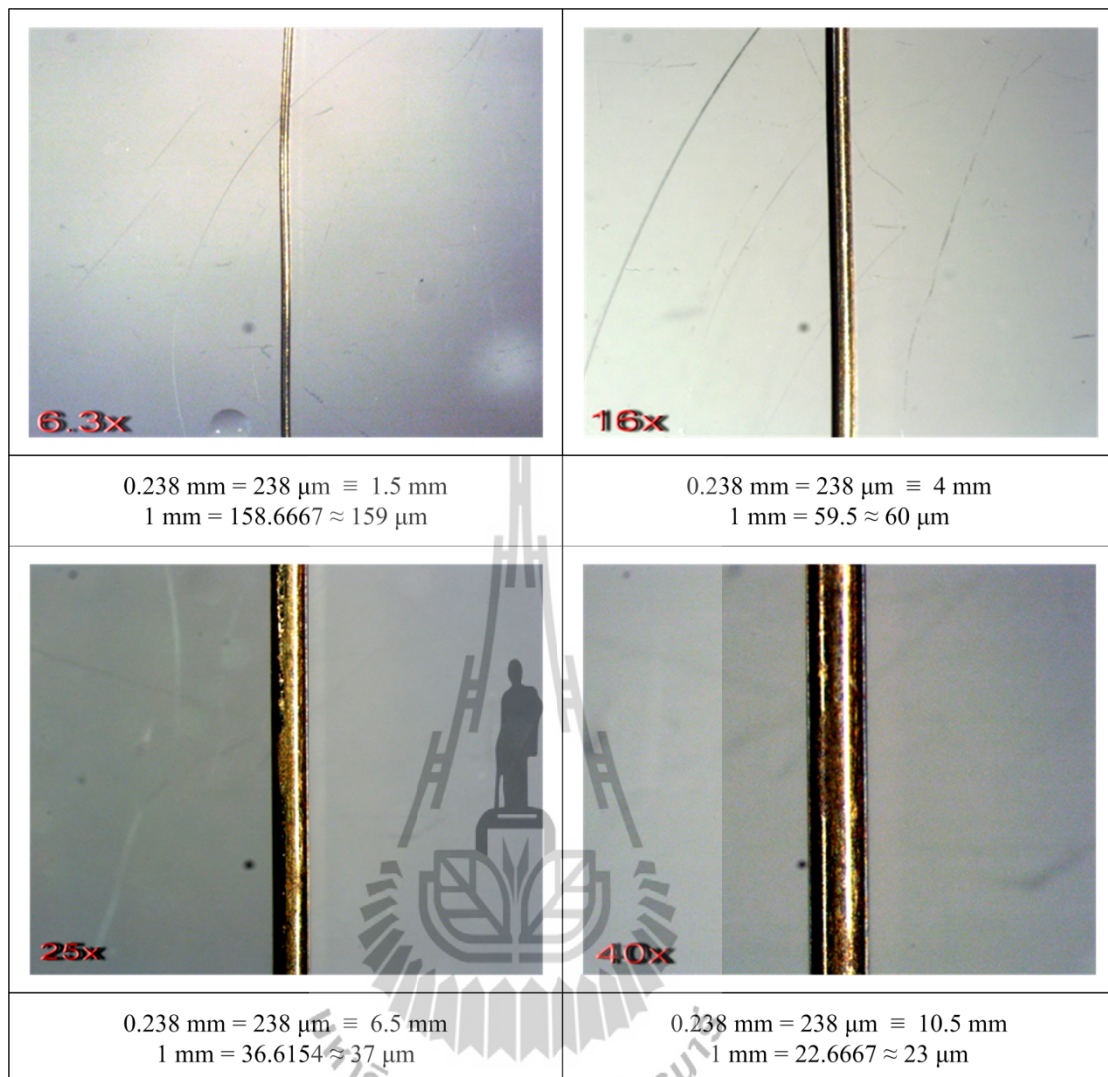


Figure 3.13 The photomicrographs and dimensions of the standard wire at four magnifications that were used to measure the size of crystals.

Figure 3.11 and Figure 3.12 show that the growth is not only of single crystals as expected, so that the small crystal particles growing on top of each parent crystals were also selected to determine the growth data, as shown in Figure 3.14. This shows a L-met·HCl parent crystal in L-met·HCl supersaturated solution ($\sigma = 0.005$) at 10°C using a magnification of 25x, with a sample time of 50 minutes. The 4

small crystal particles shown were selected to represent growth data of this condition by measurement of the growth only in the width direction of the crystals. The reason that only the growth of the width was chosen is that the length direction is out of the photomicrograph frame for some conditions. Thus, it was not possible to measure the growth of the length of the crystals continuously over time. The small crystals attached to each parent crystals were measured at various sampling times; examples are shown in Table 3.3. Data in Table 3.3 can plot the relationship between the sampling time (minutes) and the width of the crystals (μm) as shown in Figure 3.15. The graph shows the straight line of 4 small crystals in a period of 0–60 minute; where all data represents the growing constant of L-met·HCl parent crystal in L-met·HCl solution at 10°C . After this, the slope of each graph line can be determined which will give the crystal growth rate ($\mu\text{m}/\text{min}$) of the crystals shown in Table 3.4. There are 9 positions of the L-met·HCl parent crystals in each experimental conditions. There are 6 experimental conditions as mentioned above; the results are shown in Table 3.5 to Table 3.10.

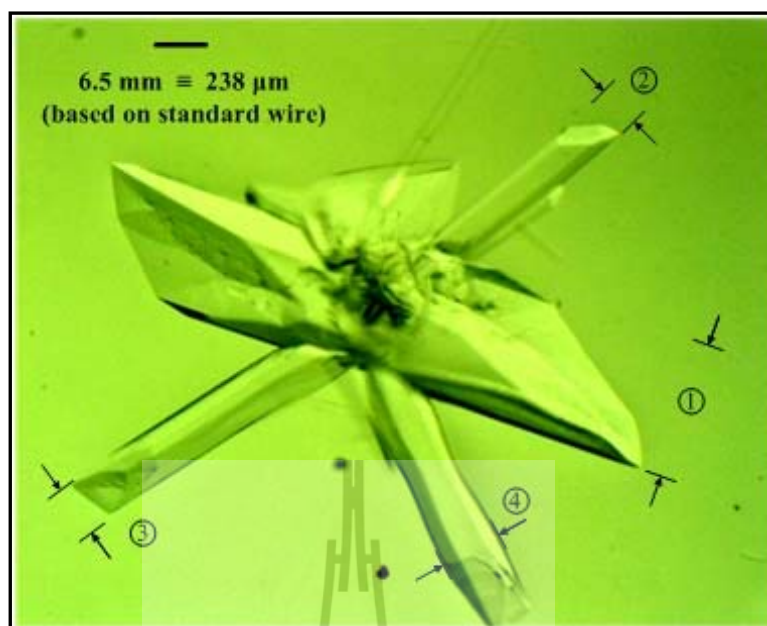


Figure 3.14 An example of measuring the size of L-met·HCl crystals in L-met·HCl solution ($\sigma = 0.005$) at 10°C, sample time 50 minutes, and magnification 25x.

Table 3.3 Experimental results of crystal growth of a L-met·HCl crystals in L-met·HCl supersaturated solution ($\sigma = 0.005$) at 10°C, magnification 25x.

(From Figure 3.14)

Time (minutes)	Width (μ m)			
	Crystal no. 1	Crystal no. 2	Crystal no. 3	Crystal no. 4
0	296.0	-	-	-
10	351.5	51.8	37.0	37.0
20	388.5	62.9	74.0	74.0
30	481.0	111.0	111.0	129.5
40	555.0	148.0	177.6	214.6
50	610.5	177.6	222.0	259.0

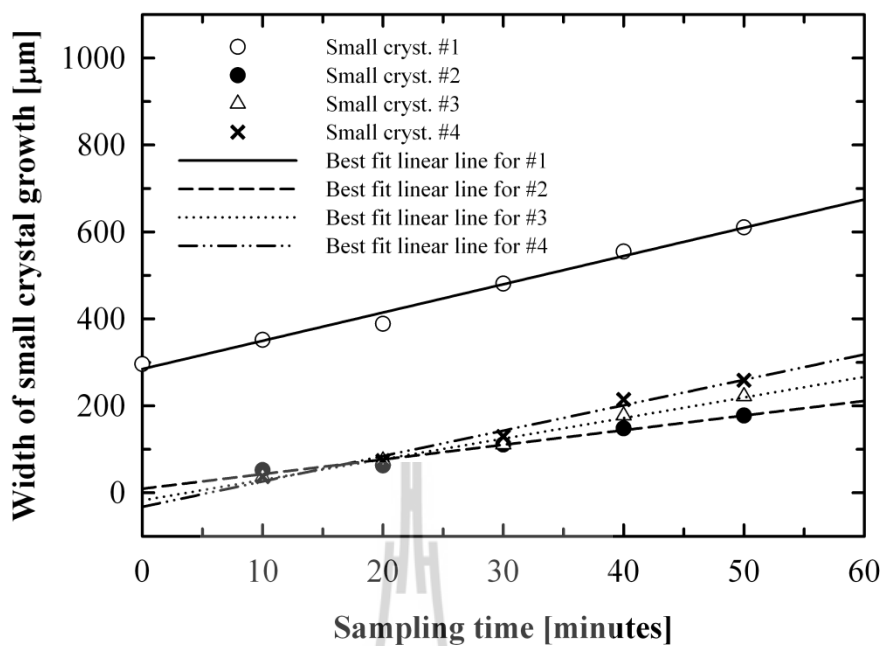


Figure 3.15 Crystal growth of L-met·HCl crystals in L-met·HCl supersaturated solution ($\sigma = 0.005$) at 10°C (plotted from Table 3.3).

Table 3.4 Crystal growth rates of L-met·HCl crystals in L-met·HCl supersaturated solution ($\sigma = 0.005$), 10°C , magnification 25x. (From Figure 3.15)

Small crystal (N, #)	Crystal growth rate, $\Delta\text{width}/\Delta t$; ($\mu\text{m}/\text{min}$)
1	6.501
2	3.367
3	4.736
4	5.846

Table 3.5 Results of crystal growth rate (G) of L-met·HCl crystals (total 45 crystal particles) in DL-met·HCl solution ($\sigma = 0.005$) at 10°C.

Small crystal (N, #) Position of parent crystal	1	2	3	4	5	6	7	8
1 st	G = 3.023*	2.185	1.725	1.150	4.025	-	-	-
2 nd	2.431	2.970	1.725	3.549	2.300	2.645	3.450	-
3 rd	2.431	2.530	1.725	-	-	-	-	-
4 th	2.924	1.412	3.335	-	-	-	-	-
5 th	2.399	2.694	4.025	-	-	-	-	-
6 th	2.563	1.840	1.955	-	-	-	-	-
7 th	2.661	1.587	1.541	2.070	2.070	2.875	1.702	-
8 th	4.107	1.955	1.679	2.093	2.438	1.909	2.139	1.725
9 th	2.497	3.864	2.583	2.267	1.495	5.405	-	-

Remark: * The crystal growth rate (G) is in the units of micrometer per minute ($\mu\text{m}/\text{min}$)

Table 3.6 Results of crystal growth rate (G) of L-met·HCl crystals (total 43 crystal particles) in DL-met·HCl solution ($\sigma = 0.01$) at 10°C.

Small crystal (N, #) Position of parent crystal	1	2	3	4	5	6	7	8
1 st	G = 3.119*	2.294	-	-	-	-	-	-
2 nd	2.400	1.221	2.257	2.109	-	-	-	-
3 rd	2.157	1.924	1.702	3.404	1.813	3.330	2.775	-
4 th	3.066	0.925	1.850	2.590	-	-	-	-
5 th	2.474	3.848	4.995	-	-	-	-	-
6 th	3.045	1.147	1.221	2.220	0.925	1.295	-	-
7 th	3.753	2.548	1.591	1.480	-	-	-	-
8 th	2.294	3.811	0.703	1.998	1.517	1.665	1.850	2.960
9 th	2.379	1.966	2.886	2.775	1.480	-	-	-

Remark: * The crystal growth rate (G) is in the units of micrometer per minute ($\mu\text{m}/\text{min}$)

Table 3.7 Results of crystal growth rate (G) of L-met·HCl crystals (total 60 crystal particles) in DL-met·HCl solution ($\sigma = 0.02$) at 10°C.

Small crystal (N, #) Position of parent crystal	1	2	3	4	5	6	7	8	9
1 st	G = 2.326*	3.774	3.700	2.442	2.775	-	-	-	-
2 nd	5.550	4.995	3.256	3.515	4.995	2.960	-	-	-
3 rd	3.145	3.219	3.700	2.960	2.220	2.331	-	-	-
4 th	2.854	3.478	2.479	2.590	-	-	-	-	-
5 th	2.220	3.478	3.108	2.035	1.665	2.479	3.404	2.035	-
6 th	2.347	3.293	2.849	1.591	1.961	2.220	1.628	3.663	2.035
7 th	2.537	2.294	3.885	3.330	3.700	4.625	-	-	-
8 th	2.569	3.219	3.219	3.367	2.442	1.961	4.921	-	-
9 th	3.700	4.773	3.071	3.330	4.625	3.811	2.405	3.256	4.033

Remark: * The crystal growth rate (G) is in the units of micrometer per minute ($\mu\text{m}/\text{min}$)

Table 3.8 Results of crystal growth rate (G) of L-met·HCl crystals (total 38 crystal particles) in L-met·HCl solution ($\sigma = 0.005$) at 10°C.

Small crystal (N, #) Position of parent crystal	1	2	3	4	5	6
1 st	G = 9.091*	2.273	3.023	3.515	-	-
2 nd	4.863	4.736	1.517	4.255	9.879	-
3 rd	6.628	4.773	2.960	2.072	-	-
4 th	6.523	3.256	6.179	-	-	-
5 th	6.142	4.958	2.590	3.330	-	-
6 th	6.713	6.845	8.177	8.547	2.775	-
7 th	6.131	4.107	7.030	6.882	8.436	7.363
8 th	10.920	4.292	3.663	-	-	-
9 th	6.501	3.367	4.736	5.846	-	-

Remark: * The crystal growth rate (G) is in the units of micrometer per minute ($\mu\text{m}/\text{min}$)

Table 3.9 Results of crystal growth rate (G) of L-met·HCl crystals (total 57 crystal particles) in L-met·HCl solution ($\sigma = 0.01$) at 10°C.

Small crystal (N, #) Position of parent crystal	1	2	3	4	5	6	7	8	9	10	11	12	13
1 st	G = 5.973*	4.625	4.181	4.218	3.330	-	-	-	-	-	-	-	-
2 nd	4.387	6.026	-	-	-	-	-	-	-	-	-	-	-
3 rd	4.704	3.700	4.625	7.215	1.850	3.885	5.994	2.960	4.107	7.733	5.476	1.665	1.369
4 th	3.737	3.256	2.960	2.442	-	-	-	-	-	-	-	-	-
5 th	3.911	4.625	11.100	7.400	3.145	6.845	4.070	4.255	-	-	-	-	-
6 th	5.201	2.960	1.406	2.775	-	-	-	-	-	-	-	-	-
7 th	2.886	1.813	2.997	2.553	3.071	3.552	4.699	1.517	8.325	2.035	-	-	-
8 th	5.339	1.332	6.882	2.405	1.628	-	-	-	-	-	-	-	-
9 th	4.017	4.176	7.918	3.922	4.625	1.850	-	-	-	-	-	-	-

Remark: * The crystal growth rate (G) is in the units of micrometer per minute ($\mu\text{m}/\text{min}$)

Table 3.10 Results of crystal growth rate (G) of L-met·HCl crystals (total 78 crystal particles) in L-met·HCl solution ($\sigma = 0.02$) at 10°C.

Small crystal (N, #) Position of parent crystal	1	2	3	4	5	6	7	8	9	10	11
1 st	G = 8.040*	25.680	19.680	19.200	11.400	18.600	15.000	-	-	-	-
2 nd	12.120	8.400	12.840	9.120	18.600	24.360	5.640	14.520	-	-	-
3 rd	21.360	9.840	14.040	20.160	10.560	13.560	15.960	14.760	-	-	-
4 th	6.840	17.640	17.520	14.400	17.280	10.920	26.400	29.400	-	-	-
5 th	14.160	20.760	13.920	12.600	12.720	7.080	12.600	12.000	-	-	-
6 th	18.000	10.320	8.640	22.200	27.000	11.400	13.800	5.400	16.680	9.000	15.000
7 th	3.902	3.634	3.180	3.809	5.469	5.792	5.137	5.671	4.089	3.372	-
8 th	12.325	22.227	12.114	5.663	5.542	6.293	7.666	3.824	-	-	-
9 th	17.665	15.533	18.810	11.156	13.451	12.002	16.536	22.578	12.720	18.762	-

Remark: * The crystal growth rate (G) is in the units of micrometer per minute ($\mu\text{m}/\text{min}$)

Table 3.5 to Table 3.10 show all the crystal growth rate results; there are 321 total data for the crystal growth rate, and these data represents 54 parent crystals at 6 experimental conditions. These data can be plotted to show the relationship between growth rate ($\mu\text{m}/\text{min}$) versus number of crystals (#), which represents the probability distribution of L-met·HCl single crystal growth rates in both DL- and L-met·HCl supersaturated solutions, as presented using the vertical bar charts in Figure 3.16 to Figure 3.21. This can also be plotted using the empirical representation of a growth rate data distribution, using a log-normal distribution. The log-normal growth rate distribution is simply a normal distribution in terms of $\log G$. Thus the log-normal distribution expressed as a density function is distributed about values of $\log G$ and is given as (Randolph and Larson, 1988):

$$f(\log G) = [(2\pi)^{1/2} \log \sigma']^{-1} \times \exp \left[- \left(\frac{\log G / \bar{G}'}{\sqrt{2} \log \sigma'} \right)^2 \right] \quad (3.4)$$

where G is the independent growth rate variable, \bar{G}' is the geometric mean growth rate, and σ' is the geometric standard deviation. Equation (3.4) can be transformed to equation (3.7), which is used to compare with equation (3.8) (the equation modeled in the SigmaPlot program) for fitting the growth rate data in Table 3.5 to Table 3.10 with the log-normal distribution using SigmaPlot[®] version 11.0.

$$f(\log G) = [(2\pi)^{1/2} \log \sigma']^{-1} \times \exp \left[- \left(\frac{\ln G / \bar{G}'}{(2.303)\sqrt{2} \log \sigma'} \right)^2 \right] \quad (3.5)$$

$$f(\log G) = [(2\pi)^{1/2} \log \sigma']^{-1} \times \exp \left[-\frac{1}{\sqrt{2} \times \sqrt{2}} \left(\frac{\ln G/\bar{G}'}{(2.303) \log \sigma'} \right)^2 \right] \quad (3.6)$$

$$f(\log G) = [(2\pi)^{1/2} \log \sigma']^{-1} \times \exp \left[-0.5 \left(\frac{\ln G/\bar{G}'}{(2.303) \log \sigma'} \right)^2 \right] \quad (3.7)$$

$$y = \frac{a}{x} \exp \left[-0.5 \left(\frac{\ln(x/x_0)}{b} \right)^2 \right] \quad (3.8)$$

where a/x represents the term $[(2\pi)^{1/2} \log \sigma']^{-1}$, and b represents the term $(2.303) \log \sigma'$, which can be plotted by the relationship between growth rate ($\mu\text{m}/\text{min}$) versus number of crystals (#) as in Figure 3.16 to Figure 3.21. These figures show a typical log-normal distribution of the growth rate data from a small-cell crystallizer run at 10°C plotted on a linear scale.

Figure 3.16 shows the growth rate distribution of L-met·HCl single crystals in DL-met·HCl supersaturated solution ($\sigma = 0.005$) in the growth rate range 1.0–5.5 $\mu\text{m}/\text{min}$. Most of the growth rate distribution is in the range of 1.5–2.5 $\mu\text{m}/\text{min}$, and the mean growth rate (\bar{G}) is 2.01 $\mu\text{m}/\text{min}$. Figure 3.17 shows the growth rate distribution of L-met·HCl single crystals in DL-met·HCl supersaturated solution ($\sigma = 0.01$) in the growth rate range 0.5–5.0 $\mu\text{m}/\text{min}$; most of the growth rate distribution is in the range of 1.5–2.0 $\mu\text{m}/\text{min}$, and mean growth rate (\bar{G}) is also 2.01 $\mu\text{m}/\text{min}$. Figure 3.18 shows the growth rate distribution of L-met·HCl single crystals in DL-met·HCl supersaturated solution ($\sigma = 0.02$) in the growth rate range 1.5–6.0 $\mu\text{m}/\text{min}$. Two peaks appear: the first one occurs at about 2.0–2.5 $\mu\text{m}/\text{min}$, whereas the

second peak is situated at approximately 3.0–3.5 $\mu\text{m}/\text{min}$; the mean growth rate (\bar{G}) is 2.73 $\mu\text{m}/\text{min}$. The growth rate distribution is wide for highly supersaturated solutions of DL-met·HCl, $\sigma = 0.02$ in this case. However the growth rate distribution of L-met·HCl single crystals in DL-met·HCl supersaturated solution at $\sigma = 0.005$ and $\sigma = 0.01$ were not much different, and also their mean growth rates were very similar. The DL-met·HCl concentration has constant value throughout the experiments since there is a very small mass of crystal in comparison to the mass of solution.

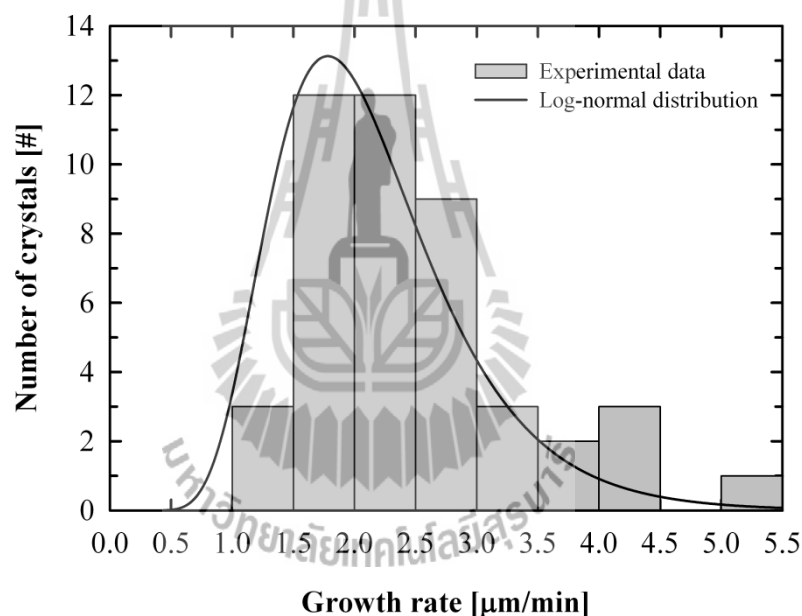


Figure 3.16 Growth rate distribution of L-met·HCl crystals in DL-met·HCl solution ($\sigma = 0.005$).

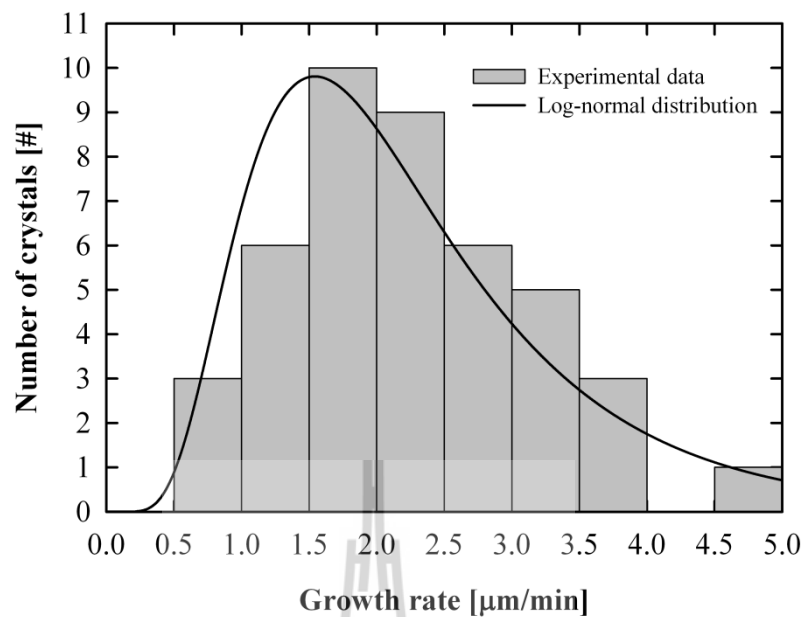


Figure 3.17 Growth rate distribution of L-met·HCl crystals in DL-met·HCl solution ($\sigma = 0.01$).

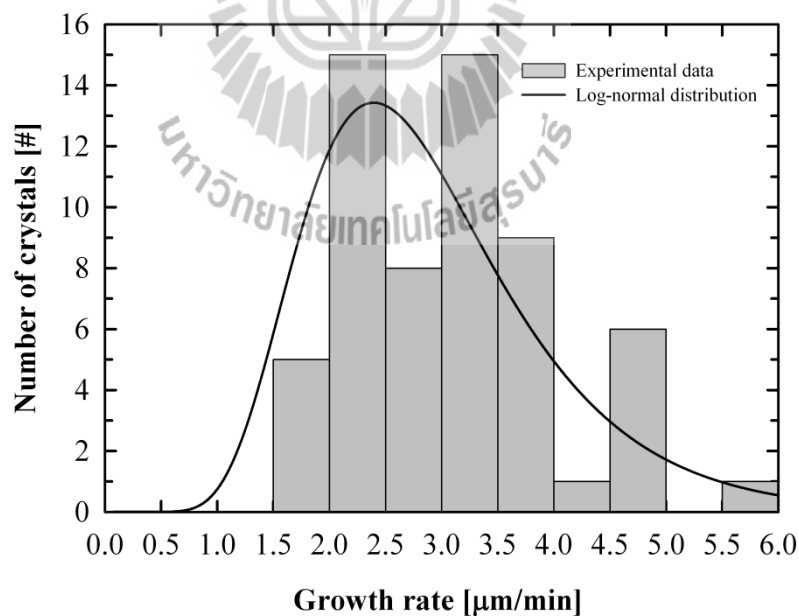


Figure 3.18 Growth rate distribution of L-met·HCl crystals in DL-met·HCl solution ($\sigma = 0.02$).

Figure 3.19 shows the growth rate distribution of L-met·HCl single crystals in L-met·HCl supersaturated solution ($\sigma = 0.005$) in the growth rate range 1–11 $\mu\text{m}/\text{min}$. Two peaks appear: the first one occurs at about 4–5 $\mu\text{m}/\text{min}$, whereas the second peak is situated at approximately 6–7 $\mu\text{m}/\text{min}$. The mean growth rate (\bar{G}) is 5.13 $\mu\text{m}/\text{min}$. Figure 3.20 shows growth rate distribution of L-met·HCl single crystals in L-met·HCl supersaturated solution ($\sigma = 0.01$) in the growth rate range 1–12 $\mu\text{m}/\text{min}$, with most of the growth rate distribution in the range of 4–5 $\mu\text{m}/\text{min}$, and also the mean growth rate (\bar{G}) is 3.58 $\mu\text{m}/\text{min}$. Figure 3.21 shows the growth rate distribution of L-met·HCl single crystals in L-met·HCl supersaturated solution ($\sigma = 0.02$) in the growth rate range 2–30 $\mu\text{m}/\text{min}$, and most of the growth rate distribution is in the range 12–14 $\mu\text{m}/\text{min}$, and the mean growth rate (\bar{G}) is 18.4 $\mu\text{m}/\text{min}$. These results show a wide range of growth rate distribution of L-met·HCl single crystals in L-met·HCl supersaturated solution. Moreover, L-met·HCl single crystals can be grown in the L-met·HCl supersaturated solution better than the growth in the DL-met·HCl supersaturated solution, which has the effect of D-met·HCl acting as a growth inhibitor of L-met·HCl. Hence, the growth rate distribution of L-met·HCl single crystals in L-met·HCl supersaturated solution have larger growth rates than the growth rate distribution of L-met·HCl single crystals in DL-met·HCl supersaturated solution. The mean growth rate (\bar{G}) is a function of the relative supersaturation (σ) value, nevertheless. The mean growth rate of L-met·HCl single crystals in both met·HCl supersaturated solution at $\sigma = 0.01$ were reduced from the expected values as shown in Figure 3.24. The L-met·HCl solution concentration has constant value throughout the experiments also.

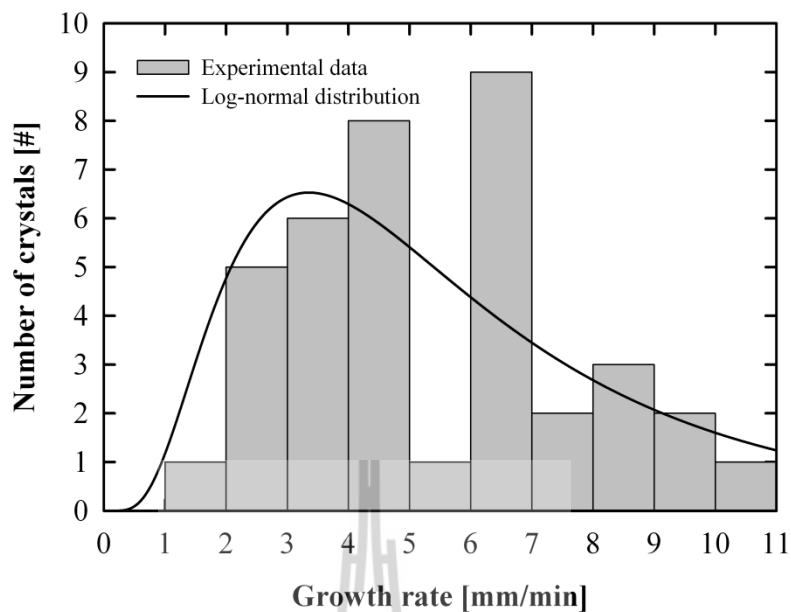


Figure 3.19 Growth rate distribution of L-met·HCl crystals in L-met·HCl solution ($\sigma = 0.005$).

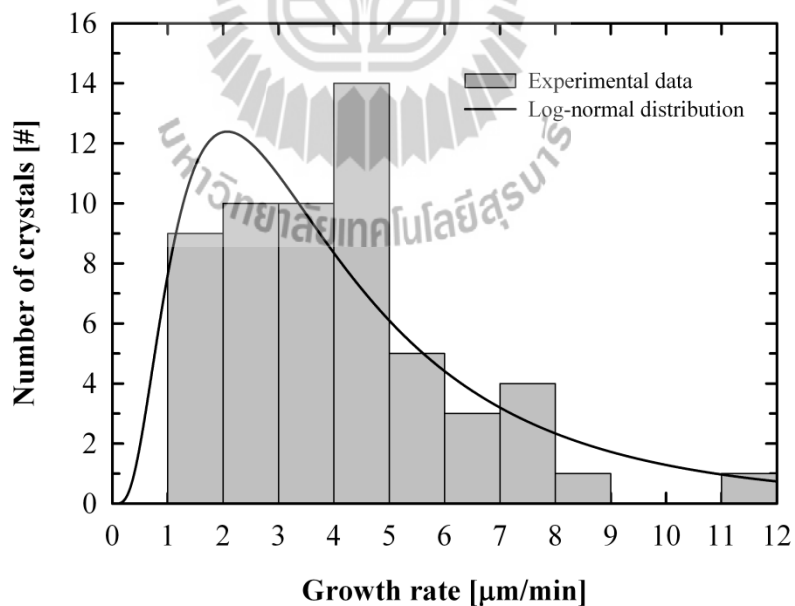


Figure 3.20 Growth rate distribution of L-met·HCl crystals in L-met·HCl solution ($\sigma = 0.01$).

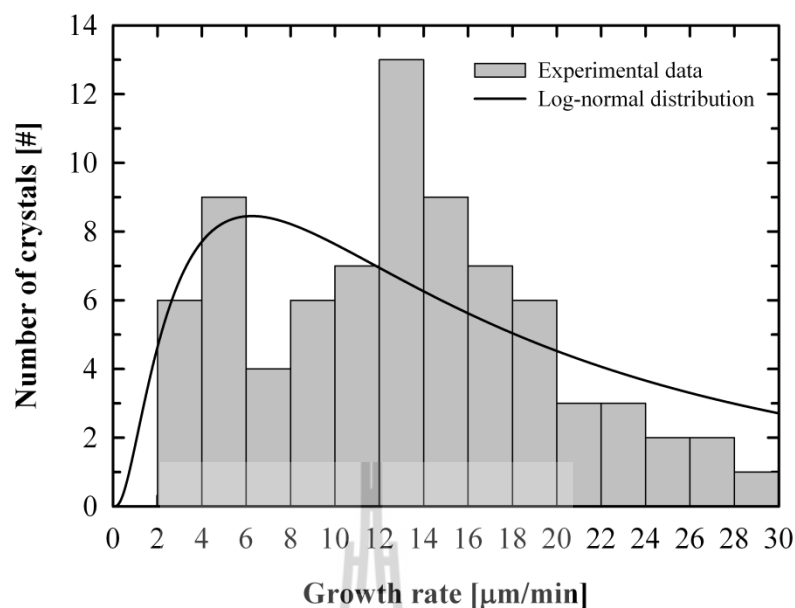


Figure 3.21 Growth rate distribution of L-met·HCl crystals in L-met·HCl solution ($\sigma = 0.02$).

3.5.3 Mean Growth Rates of L-met·HCl Single Crystals in DL- and L-met·HCl Supersaturated Solution

The predicted growth rate distributions were calculated using the crystal growth rate of each crystal. From the data analysis of SigmaPlot mathematical programming of the results in Figure 3.16 to Figure 3.21, the growth rate distributions of each experimental condition can be determined and compared as shown in Figure 3.22 and Figure 3.23, assuming log-normal distributions. This allows for analysis of the mean growth rate for each condition, shown in Table 3.11, and also the geometric standard deviation.

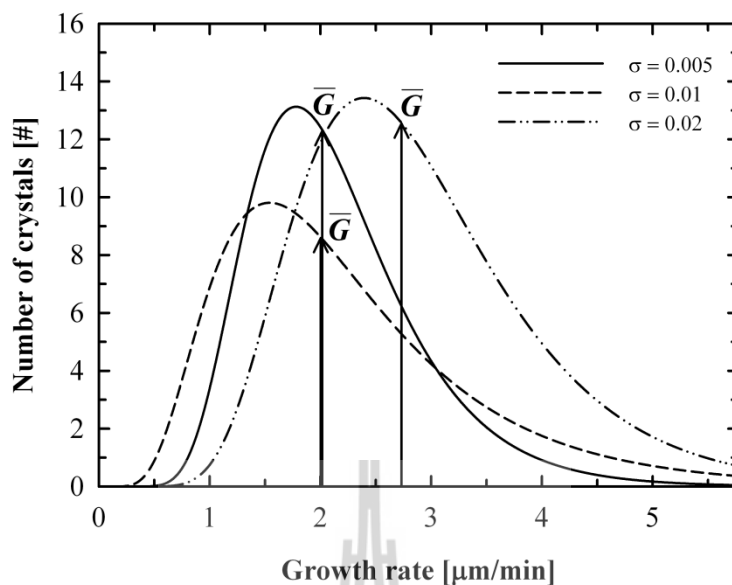


Figure 3.22 Mean growth rates of L-met·HCl crystals in DL-met·HCl supersaturated solution at 10°C with three relative supersaturations.

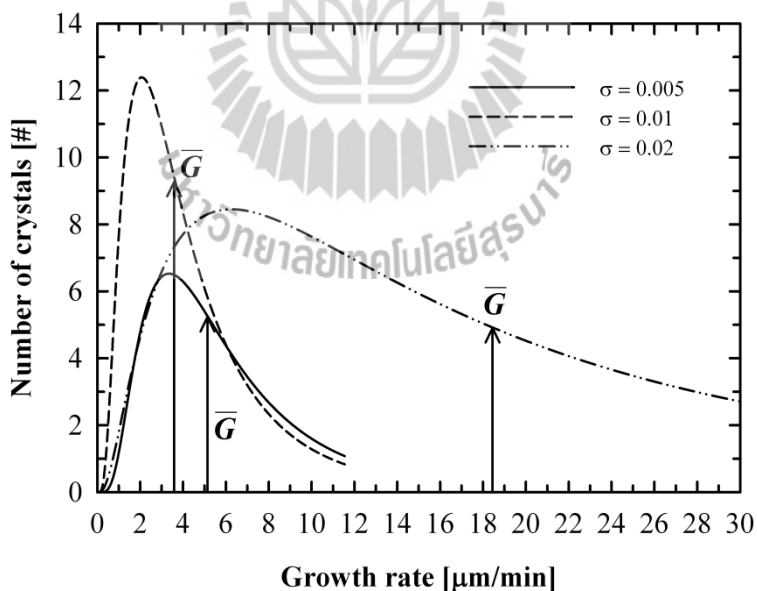


Figure 3.23 Mean growth rates of L-met·HCl crystals in L-met·HCl supersaturated solution at 10°C with three relative supersaturations.

Table 3.11 Mean and standard deviation (S.D.) of the crystal growth rate distributions of L-met·HCl crystals in DL- and L-met·HCl solutions at 10°C.

Number of growth rate data	Relative supersaturation (σ)	Mean growth rate \bar{G} ($\mu\text{m}/\text{min}$) \pm S.D.
Growth in DL-met·HCl solution		
45	0.005	2.01 \pm 0.13
43	0.01	2.01 \pm 0.14
60	0.02	2.73 \pm 0.12
Growth in L-met·HCl solution		
38	0.005	5.13 \pm 0.37
57	0.01	3.58 \pm 0.47
78	0.02	18.42 \pm 0.80

Figure 3.22 and Figure 3.23 show comparison of the growth rate distributions of L-met·HCl single crystals in DL- and L-met·HCl supersaturated solution using a linear scale. From Figure 3.22, it can be seen that the growth rate distribution of L-met·HCl single crystals in DL-met·HCl solution of three relative supersaturation were quite similar values, and also the mean growth rate did not differ much. Figure 3.23 shows the growth rate distribution in L-met·HCl supersaturated solutions, and it is seen that at $\sigma = 0.02$ the growth rate distribution was quite wide compared to solutions at $\sigma = 0.005$ and $\sigma = 0.01$. However, by comparison between growth rate distribution in DL-met·HCl supersaturated solution and growth rate distribution in L-met·HCl supersaturated solution, it was found that the width of the growth rate distribution of L-met·HCl crystals in L-met·HCl supersaturated solution is more than the width of the growth rate distribution of L-met·HCl crystals in DL-met·HCl supersaturated solution. The mean growth rates and the uncertainty limits of the mean

(represented by standard deviation, see Appendix A) of each relative supersaturations are shown in Table 3.11. Data from Table 3.11 can be plotted to show the relationship between relative supersaturation versus mean growth rate ($\mu\text{m}/\text{min}$) as shown in Figure 3.24. It can be seen that, at constant temperature, the mean growth rates increase with increasing relative supersaturation, and also growth rate of L-met·HCl single crystals in L-met·HCl supersaturated solution is faster than growth rate in DL-met·HCl supersaturated solution.

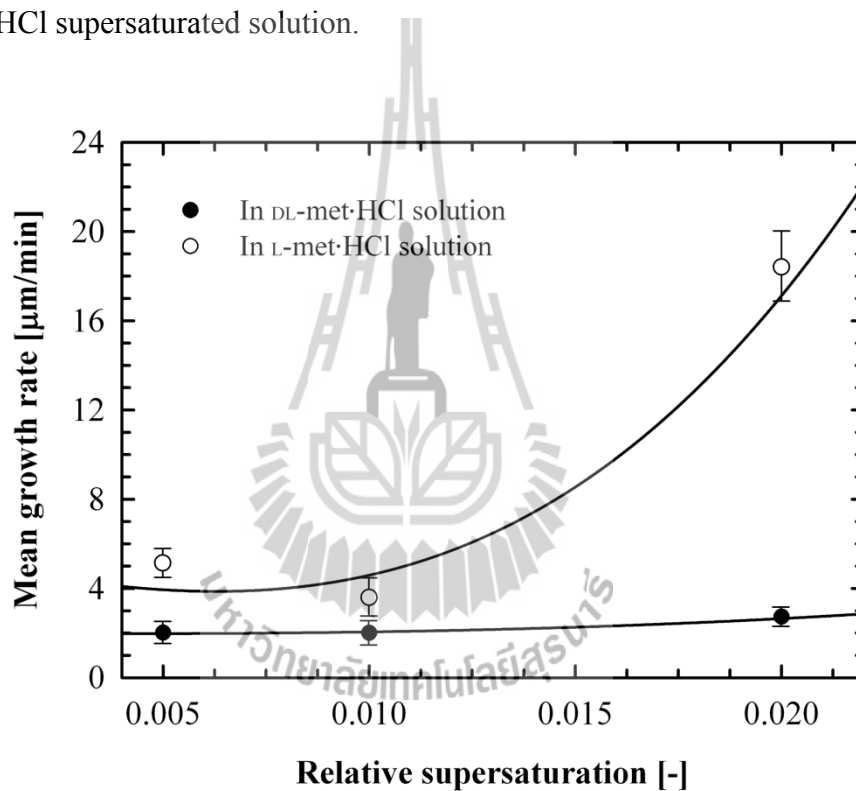


Figure 3.24 Mean growth rates for L-met·HCl crystals as a function of relative supersaturation of DL- and L-met·HCl supersaturated solution at 10°C .

3.6 Conclusions

The primary and secondary nucleation threshold measurements of DL-met·HCl solution were determined with a modified method using the relationship between induction time and supersaturation measurement at a constant temperature (10°C) in a glass batch crystallizer with a closed jacket system. There is simple method for measurement of the nucleation threshold by using observation of the change of the turbidity of the solutions with the naked eye, which allows measurements of the primary and secondary nucleation thresholds of DL-met·HCl solution. From the experimental results, the induction time dependence on the relative supersaturation for the primary and secondary nucleation thresholds can be determined. The induction time increases as the relative supersaturation of primary and secondary nucleation threshold decreases, and also the induction time of the secondary nucleation threshold is less than the induction time of the primary nucleation threshold because of the influence of L-met·HCl seed crystals. The rate of secondary nucleation is increased by the added seeds resulting in the nucleation threshold for secondary nucleation being smaller than that for primary nucleation.

The growth rate distribution and the mean growth rate of L-met·HCl crystals in met·HCl supersaturated solution were studied to optimize the operation of the preferential crystallization of DL-met·HCl. These data were determined in a small-cell crystallizer and the stereomicroscope with the digital camera at constant 10°C in a stagnant solution. From the experimental results, it is found that the parent crystals are not the single crystals due to the imperfection of the crystal surface. They have the small crystal particles attached on the surface of parent crystals at the initial time. They were grown mostly on sideways on the parent crystals, and were grown very

well in both directions (the width and the length) into the supersaturated solution with different relative supersaturation (σ). Nevertheless, the growth of L-met·HCl crystals in L-met·HCl supersaturated solution are grown orderly and perfect shape rather than the growth of L-met·HCl crystals in DL-met·HCl supersaturated solution. The latter grow in a disorganized way, like the group of small needle crystals grown from the surface of parent crystals. This is because of the growth in the DL-met·HCl supersaturated solution has the effect of D-met·HCl acting as a growth inhibitor of L-met·HCl, that makes the growth of L-met·HCl parent crystals in DL-met·HCl supersaturated solution produce worse shaped crystals, and the crystals were also grown more slowly than the growth in pure L-met·HCl supersaturated solution.

The crystal growth rate depends strongly on the relative supersaturation (especially from pure L-met·HCl supersaturated solutions), with the crystal growth rate at $\sigma = 0.02 > \sigma = 0.01 > \sigma = 0.005$. Also there is a wide crystal growth rate distribution from both types of supersaturated solution. Hence, the mean growth rate (\bar{G}) of L-met·HCl single crystals in L-met·HCl supersaturated solution is larger than the mean growth rate from DL-met·HCl supersaturated solution.

The results of primary and secondary nucleation threshold, and also the growth rate and growth rate distribution of L-met·HCl single crystals in met·HCl supersaturated solution can lead to the efficient operation of preferential crystallization experiments in the next chapter. We need to know the suitable resolution time on seeding, including L-met·HCl crystals growth behavior on preferential crystallization for high purity of the crystal (the desired crystal form) and cost effectiveness in manufacturing.

3.7 References

- Barrett, P., Smith, B., Worlitschek, J., Bracken, V., O'Sullivan, B., and O'Grady, D. (2005). A review of the use of process analytical technology for the understanding and optimization of production batch crystallization processes. **Organic Process Research & Development** 9(3): 348-355.
- Chattopadhyay, S., Erdemir, D., Evans, J. M. B., Ilavsky, J., Amenitsch, H., Segre, C. U., and Myerson, A. S. (2005). SAXS study of the nucleation of glycine crystals from a supersaturated solution. **Crystal Growth & Design** 5(2): 523-527.
- Crosio, M. P. and Jullien, M. (1992). Fluorescence study of precrystallization of ribonuclease A: Effect of salts. **Journal of Crystal Growth** 122: 66-70.
- Funakoshi, K. and Matsuoka, M. (2008). Primary nucleation of threonine crystals from ternary solutions. **Crystal Growth & Design** 8(5): 1754-1759.
- Garside, J. and Davey, R. J. (1980). Invited review secondary contact nucleation: Kinetics, growth and scale-up. **Chemical Engineering Communications** 4: 393-424.
- Garside, J. and Larson, M. A. (1978). Direct observation of secondary nuclei production. **Journal of Crystal Growth** 43: 694-704.
- Hu, H., Hale, T., Yang, X., and Wilson, L. J. (2001). A spectrophotometer-based method for crystallization induction time period measurement. **Journal of Crystal Growth** 232(1-4): 86-92.
- Jiang, S. and ter Horst, J. H. (2011). Crystal nucleation rates from probability distributions of induction times. **Crystal Growth & Design** 11: 256-261.

- Kobari, M., Kubota, N., and Hirasawa, I. (2010). Simulation of metastable zone width and induction time for a seeded aqueous solution of potassium sulfate. **Journal of Crystal Growth** 312: 2734-2739.
- Kozlovskii, M. I., Wakita, H., and Masuda, I. (1983). Analyses of precipitation process of BIS(dimethylglyoximate)Ni(II) and related complexes. **Journal of Crystal Growth** 61(2): 377-382.
- Kubota, N. (2008). A new interpretation of metastable zone widths measured for unseeded solutions. **Journal of Crystal Growth** 310: 629-634.
- Kubota, N. (2010). A unified interpretation of metastable zone widths and induction times measured for seeded solutions. **Journal of Crystal Growth** 312: 548-554.
- Kuldipkumar, A., Kwon, G. S., and Zhang, G. G. Z. (2007). Determining the growth mechanism of tolazamide by induction time measurement. **Crystal Growth & Design** 7(2): 234-242.
- Larson, M. A. (1981). Secondary nucleation: An analysis. **Chemical Engineering Communications** 12: 161-169.
- Lowe, J., Ogdena, M., McKinnon, A., and Parkinson, G. (2002). Crystal growth of sodium oxalate from aqueous solution. **Journal of Crystal Growth** 237-239: 408-413.
- Michinomae, M., Mochizuki, M., and Ataka, M. (1999). Electron microscope studies on the initial process of lysozyme crystal growth. **Journal of Crystal Growth** 122(1-4): 66-70.
- Mullin, J. W. (2001). **Crystallization**. Oxford: Butterworth-Heinemann.

- Myerson, A. S. and Ginde, R. (2002). Crystals, crystal growth, and nucleation. In A. S. Myerson (Ed.), **Handbook of industrial crystallization** (pp. 33-65). Boston: Butterworth-Heinemann.
- Phillips, V. R. and Epstein, N. (2004). Growth of nickel sulfate in a laboratory-scale fluidized-bed crystallizer. **AIChE Journal** 20(4): 678-687.
- Randolph, A. D. and Larson, M. A. (1988). **Theory of particulate processes: Analysis and techniques of continuous crystallization**. California: Academic Press.
- Rodríguez-Hornedo, N. and Murphy, D. (1999). Significance of controlling crystallization mechanisms and kinetics in pharmaceutical systems. **Journal of Pharmaceutical Sciences** 88(7): 651-660.
- Shimizu, K., Tsukamoto, K., Horita, J., and Tadaki, T. (1984). Origin of secondary nucleation as revealed by isotopic labelling. **Journal of Crystal Growth** 69: 623-626.
- Söhnel, O. and Mullin, J. W. (1978). A method for the determination of precipitation induction periods. **Journal of Crystal Growth** 44(4): 377-382.
- Srisa-nga, S., Flood, A. E., and White, E. T. (2006). The secondary nucleation threshold and crystal growth of α -glucose monohydrate in aqueous solution. **Crystal Growth & Design** 6(3): 795-801.

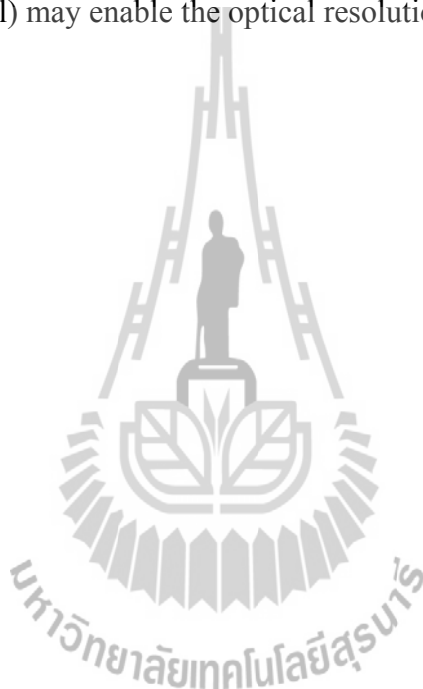
CHAPTER IV

**THE PURIFICATION OF L-METHIONINE
HYDROCHLORIDE VIA OPTICAL RESOLUTION
OF DL-METHIONINE HYDROCHLORIDE BY
PREFERENTIAL CRYSTALLIZATION**

4.1 Abstract

In order to design and efficiently operate the preferential crystallization the basic properties and parameters of the crystallization of methionine hydrochloride have been determined in previous chapters. These include solubility data, the ternary phase diagram of met·HCl (which is a conglomerate forming system), the primary and secondary nucleation threshold, mean growth rate, and growth rate distributions (GRD). This chapter deals with the resolution of DL-met·HCl using the preferential crystallization technique, that will be used to separate the desired enantiomer (L-met·HCl) from the racemic solution (DL-met·HCl). The study was also performed in an attempt to improve the efficiency and economics of the optical resolution of methionine. All experiments were operated in a batch crystallizer at low temperature and various relative supersaturations of L-met·HCl. L-met·HCl crystals were used as a homochiral seed to induce the desired enantiomer (L-met·HCl) from DL-met·HCl aqueous solution. The optical activity measurement via polarimetry was used to evaluate the percent purity of L-met·HCl crystal. The results reveal the purity of

L-met·HCl crystal decreased rapidly to the equilibrium value over time, due to the influence of the nucleation threshold of the counter enantiomer being small. Using preferential crystallization to separate the enantiomers of met·HCl from an aqueous solution to obtain a high purity product appears to be very difficult; this study cannot separate the desired enantiomer to close to 100% purity. A process in which a tailor-made additive agent is used to inhibit the primary nucleation of the undesired enantiomer (D-met·HCl) may enable the optical resolution from aqueous solution to be more effective.



4.2 Introduction

The chiral nature of drugs is a major concern in the pharmaceutical industry, since a pair of enantiomers has different pharmacological activity. Only one possible form of two enantiomers can be found in chiral drugs and other chiral molecules from natural sources, and also by semi-synthesis. A mixture of both enantiomers can be obtained from total synthesis mostly. The pure enantiomers of chiral molecules can be developed commercially by two alternative approaches, that are (i) enantioselective synthesis of the desired enantiomer, or (ii) separation of both isomers from a racemic mixture. The separation is focused on the target molecule or on one of its chemical precursors obtained from the ordinary synthetic procedures. Both operation methods have advantages and disadvantages. All separation techniques allowing a certain amount of the pure enantiomer of a product can be qualified as being preparative. In contrast, analytical techniques are devoted to detect the presences in a sample and/or quantify them (Franco and Minguillón, 2001). Nowadays, the separation of racemates via the crystallization is a useful key technology for preparing the optically active compounds in an industrial scale production (Nohira and Sakai, 2004). Crystallization is basically a separation technique that is used to separate the desirable substances from impurities or from by-products that come from secondary reactions in their synthesis. Crystallization can also separate the pure enantiomers from a racemate or an enantiomerically enriched sample (Jacques, Collet, and Wilen, 1981; Bayley and Vaidya, 1992; Wood, 1997).

Resolution by crystallization includes direct crystallization (preferential crystallization or spontaneous resolution) (Coquerel, 2007) and diastereomeric crystallization (classical resolution) (Kozma, 2001). Preferential crystallization (or

resolution by entrainment) is an attractive technology to separate racemic mixtures of the group of conglomerate forming systems into their pure enantiomers, due to the advantages of obtaining directly a solid product and economic considerations. It is an effective and comparatively cheap technology for the production of pure enantiomers at different scale. However, the direct crystallization of pure enantiomers from racemic solutions is limited to conglomerates (5–10% of all chiral systems). Unfortunately, the major part of the chiral substances belongs to the racemic compound forming systems (Lorenz, Polenske, and Seidel-Morgenstern, 2006). Preferential crystallization is based on the selective crystallization of one species out of a slightly supersaturated solution of a racemic mixture. The supersaturated binary mixture is induced with pure crystals of one of the enantiomers, and only the crystals of the same kind of enantiomer are allowed to grow selectively for a certain period of time before the counter species nucleates (Nohira and Sakai, 2004; Polenske, Lorenz, and Seidel-Morgenstern, 2009). Moreover, crystallization is often used in combination with other enantioselective techniques, such as enantioselective synthesis, enzymatic kinetic resolution or simulated moving bed (SMB) chromatography (Collins, Sheldrake, and Crosby, 1997; Blehaut and Nicoud, 1998; Seebach, Hoffmann, Sting, Kinkel, Schulte, and Küsters, 1998).

This work aims to study the optimum mechanism of preferential crystallization to separate the pure enantiomer of L-met·HCl from a racemic solution of DL-met·HCl to gain the maximum percentage purity of the product crystals from the enriched solution. There is also a study of the viability of the preferential crystallization of L-met·HCl in aqueous solution of DL-met·HCl at various relative supersaturations. The process design is based on the knowledge of solid-liquid

equilibrium (SLE), nucleation and growth rate kinetics to define the optimum operating parameters, such as crystallization temperature, resolution time, and initial supersaturation. Moreover, the study was performed in an attempt to improve the efficiency and economics of the optical resolution of methionine. In the following section the liquid phase and product crystal analysis using polarimetry and refractometry is described.



4.3 Theory

4.3.1 Principle of Preferential Crystallization

Preferential crystallization is one of the most successful processes to resolve many racemates in conglomerate forming systems into the pure enantiomers (Gou, Lorenz, and Seidel-Morgenstern, 2011). Enantiomers are substances with identical physical and chemical properties, but different metabolic effects. The principle of a kinetically controlled preferential crystallization process can be illustrated in a ternary phase diagram as shown in Figure 4.1. The corners of the diagram represent the pure solvent and two pure enantiomers (D-enantiomer and L-enantiomer). The crystallization starts from a saturated solution at temperature $T_{\text{cryst}} + \Delta T$. It is rapidly cooled down to the crystallization temperature T_{cryst} within the metastable zone. The solution becomes supersaturated but nuclei do not appear in the solution (as no spontaneous primary nucleation will occur). Point A represents the initial mixture of two enantiomers and a solvent. The separation process can be well processed using an enantiomeric excess, but it is not strictly necessary. If the crystallizer is seeded with seeds of both enantiomers (D-enantiomer and L-enantiomer) at point A, the two types of crystal will start to grow and also induce the secondary nucleation, as the two enantiomers are being produced simultaneously. The process will eventually end at point E, which represents the equilibrium point for the temperature T_{cryst} . In the equilibrium state, the liquid phase will have a racemic composition (point E) and the solid phase will consist of a mixture of crystals of both enantiomers (Elsner, Menéndez, Muslera, and Seidel-Morgenstern, 2005). However, the aforementioned process is not an example of enantioselective preferential crystallization.

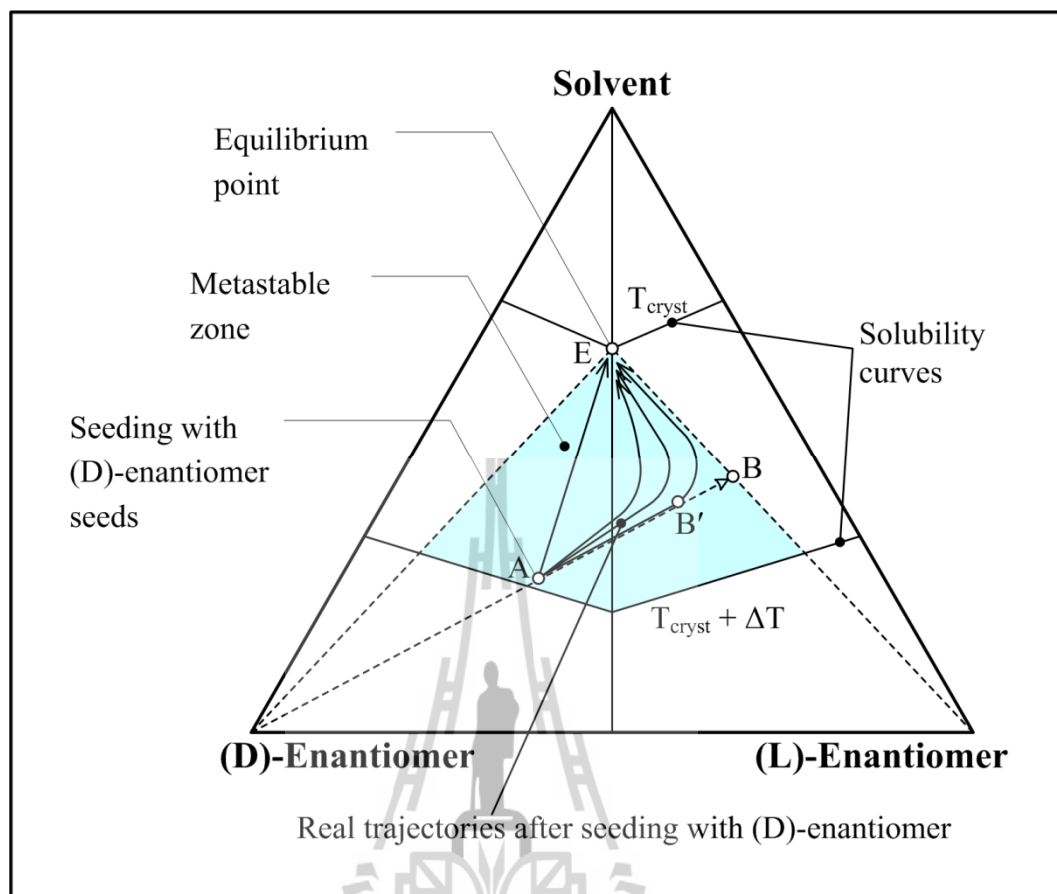


Figure 4.1 Illustration of the principle of preferential crystallization for conglomerate forming system in ternary phase diagram (Qamar, Angelov, Elsner, Ashfaq, Seidel-Morgenstern, and Warnecke, 2009).

In other cases, the composition in liquid phase does not move directly to point E when the crystallizer is seeded with the seeds of pure enantiomer only (in this case the D-enantiomer) at point A. The D-enantiomer at point A begins to crystallize and also the liquid phase composition tends towards point B which is due to the increased mass of D-enantiomer crystal reducing the concentration of the D-enantiomer in solution. This methodology can be used to produce the crystals of just one of the enantiomers by preferential crystallization. However, the spontaneous

crystallization of unseeded L-enantiomer is observed after going through a certain period of the experiment. Eventually, the crystallization process is operated along a new trajectory and also reaches to the equilibrium at point E. Therefore, the designed preferential crystallization process must be stopped at point B' (as an example) before significant nucleation of the unseeded L-enantiomer occurs (Angelov, Raisch, Elsner, and Seidel-Morgenstern, 2008).

4.3.2 Optical Activity Measurement

Polarimetry is one technique in the chiroptical methods that are used in the analysis of optically active compounds, which also include optical rotator dispersion (ORD) and circular dichroism (CD); these are the traditional optical activity measurement techniques (Spencer, Edmonds, Rauh, and Carrabba, 1994; Schreier, Bernreuther, and Huffer, 1995). Optical activity is the ability of a chiral molecule to rotate the plane of polarization of plane-polarized light. When plane-polarized light is passed through a sample containing one enantiomer of a chiral compound, the plane of polarization of the light is rotated. The samples that rotate plane-polarized light are said to be optically active. Therefore, optical activity is the ability of a chiral molecule to rotate the plane of plane-polarized light. It is measured using a polarimeter, which consists of a light source, polarizing lens, sample tube and analyzing lens. The diagram of the plane of polarization on a polarimeter, using which the optically activity of chiral compounds are studied, is shown in Figure 4.2 (Brown, 2000; Hornback, 2005). The light source emits light moving in all planes. When the light passes through the first polarizing filter (polarizer), only one plane emerges. The plane-polarized beam enters the sample compartment, which contains a solution enriched in one of enantiomers of a chiral substance. The plane of polarization is

rotated as it passes through a solution of a chiral compound, and the light emerges with its plane of polarization changed. Thus, a chiral compound rotates the plane of polarization. The magnitude of the optical rotation (observed rotation; α) in degrees, is measured by a second polarizing filter (called the analyzing polarizer). If the beam has been rotated in a clockwise direction it is called dextrorotatory, (*d*), and the optical rotation is assigned a positive value (+). Conversely, if the beam has been rotated in a counterclockwise direction it is called levorotatory, (*l*), and the optical rotation is assigned a negative value (–) (Carey, 2003; Bruice, 2004). This gives the sign of the optical rotation (α) of the solution.

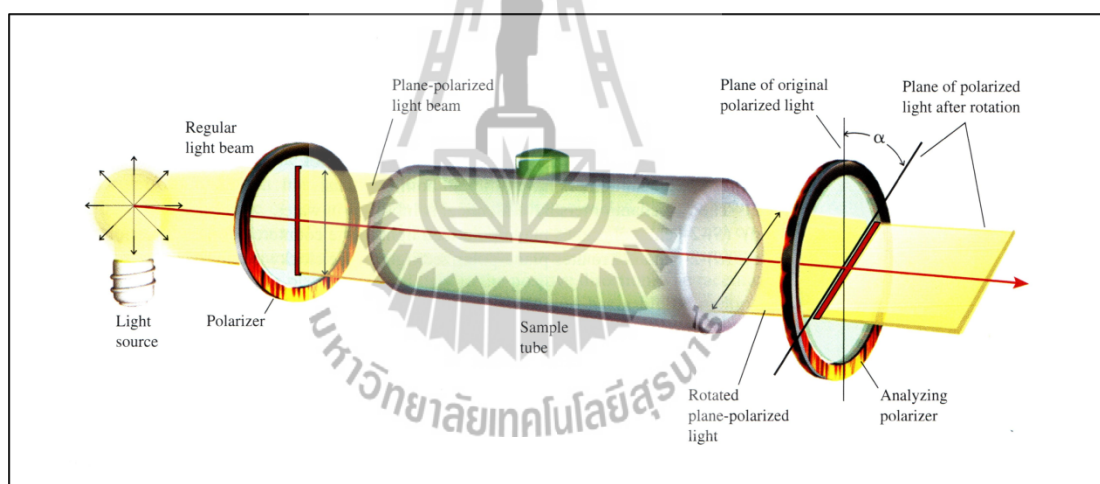


Figure 4.2 Schematic diagram of a polarimeter (Hornback, 2005).

The nature of a solution of optically active compound was described by introducing the specific rotation of substance. Specific rotation is a physical property of a substance, just like its melting point, boiling point, density, and solubility. The specific rotation is the number of degrees of rotation of the polarized

light caused by a solution of 1.0 g of compound/ml of solution in a polarimeter tube 1.0 dm long at specified temperature and wavelength (Bruice, 2004).

A recording the specific rotation must be identified with the temperature and wavelength, since the specific rotation depends on the temperature and wavelength also. The most important factor is that two enantiomers will have the same magnitude of specific rotation but rotate the light in opposite directions. Each optically active compound has a constant characteristic specific rotation that can be calculated from the observed rotation (optical rotation) obtained in the laboratory by the Biot's law which is given as (Carey, 2003):

$$[\alpha]_{\lambda}^T = \frac{100 \times \alpha}{c \times l} \quad (4.1)$$

where $[\alpha]_{\lambda}^T$ is the specific rotation. The conventional unit of specific rotation is degree milliliters per decimeter gram $[(^{\circ}) \cdot \text{ml} \cdot \text{dm}^{-1} \cdot \text{g}^{-1}]$ but scientific literature uses just degrees ($^{\circ}$) (Mohrig, Hammond, and Schatz, 2010). T is temperature in degrees Celsius ($^{\circ}\text{C}$) and λ is the wavelength of the incident light (when the sodium D-line is commonly used for this purpose, $\lambda = 589 \text{ nm}$, λ is indicated as D), respectively, as superscript and subscript. c is the concentration of the sample in grams per 100 ml of solution, and l is the length of the polarimeter tube in decimeters (dm). α is an optical rotation (observed rotation) of chiral compound in degrees.

4.4 Experimental Procedure

4.4.1 Materials

DL- and L-met·HCl compounds were prepared similarly to the method in section 2.4.1, Chapter II. Approximately 40 g of total supersaturated solution of DL-met·HCl in water for one sample was prepared at 0.005 and 0.01 relative supersaturation (σ) based on the equilibrium concentration of DL-met·HCl at 10°C. These were prepared by dissolving DL-met·HCl in a heating bath at 40°C until the solution is homogeneous and no nuclei remained. All supersaturated solutions were prepared in 100 ml laboratory glass bottles with screw caps (Schott Duran, Germany), and were maintained at 40°C in a heating bath before starting the experiment. The preferential crystallization temperature is 10°C with temperature control to within $\pm 0.5^\circ\text{C}$. L-met·HCl crystals were prepared as seed crystals for use to induce the desired product form in the preferential crystallization of DL-met·HCl aqueous solution. Seed crystals were not sieved in this experiment.

4.4.2 Preferential Crystallization of DL-met·HCl Aqueous Solution

In this experiment, a 100 ml beaker (Schott Duran, Germany) was used as a seeded batch crystallizer for preferential crystallization of DL-met·HCl aqueous solution. An experimental setup schematic for the preferential crystallization of DL-met·HCl is shown in Figure 4.3. Supersaturated solutions of DL-met·HCl in water were prepared by dissolution at 40°C until the solution is homogeneous, then the solution was quickly cooled down to 10°C in less than 3 minutes by another cooling bath, to avoid the secondary nucleation in the solution. The DL-met·HCl aqueous solution was maintained at the crystallization temperature within $\pm 0.5^\circ\text{C}$, which was

checked using a mercury thermometer. At the same time, the initial solution concentration at $10\pm 0.5^\circ\text{C}$ was measured to verify the accuracy of the concentration before the start of the experiment using an automatic digital refractometer (Model RFM340, Bellingham and Stanley Ltd.). Approximately 1.00 g of L-met·HCl seed crystals was added to the DL-met·HCl aqueous solution at the start of the experiment for inducing the crystallization, with experimental resolution times of 2, 5, 8, and 10 minutes. The suspension in the seeded batch crystallizer was agitated by a centrally located, four-blade impeller driven by an overhead stirrer. A constant crystallization temperature was maintained by placing the crystallizer inside a constant temperature water bath.



Figure 4.3 Experimental setup for preferential crystallization of DL-met·HCl aqueous solution.

After the resolution time is reached, at least 4 ml of the suspension was sampled at 10°C and was filtered rapidly through a 61 μm wire mesh sieve for the 2 minute resolution time, and a 104 μm wire mesh sieve for 5, 8, and 10 minute resolution time for separating the solids (the desired product) from the liquid (the undesired product), using a 250 ml filter holder with receiver (Nalgene Labware, USA) connected to an aspirator (Eyela model A-3S, Tokyo): the solution could be filtered within a few minutes at lower than 20°C controlled room temperature. Both solid and liquid contents were weighed on an electronic balance (Sartorius model BP221S, USA) to determine the suspension density of DL-met·HCl. Simultaneously, the concentration of the liquid product was measured for monitoring changes in the concentration using a RFM340 automatic digital refractometer. The solid product was dried in a desiccator over silica gel for 2 or 3 weeks before the measurement of the optical rotation.

4.4.3 Optical Activity of L-met·HCl by Polarimetry

For the preferential crystallization step, the experimental products are the solid content (desired product) and the liquid content after the filtration is complete. The solid product was dried in a desiccator over silica gel for 2 to 3 weeks, and was weighed everyday on an electronic balance, to measure the changes of solid weight until the weight of solid was relatively stable. Between 2.00 g to 5.00 g of solid content was dissolved into distilled water at room temperature to obtain 15.0 ml or 20.0 ml of total aqueous solution; solutions were prepared in a graduated cylinder so that the concentration of the samples was exactly known. All solid solutions were stored in 50 ml laboratory glass bottles and screw caps, which were kept at constant temperature (25°C) in a water bath for one hour. For accurate concentration

determination, the solution concentration was measured by a refractive index method using a RFM340 automatic digital refractometer before starting the optical activity. The optical rotations of solid solutions at various the resolution times were determined by polarimetry in a polarimeter (Model P20, Bellingham and Stanley Ltd.) at room temperature (controlled to approximately 25°C by an air conditioner). An illustration of the P20 polarimeter was used to record the optical rotation of chiral compounds is shown in Figure 4.4.

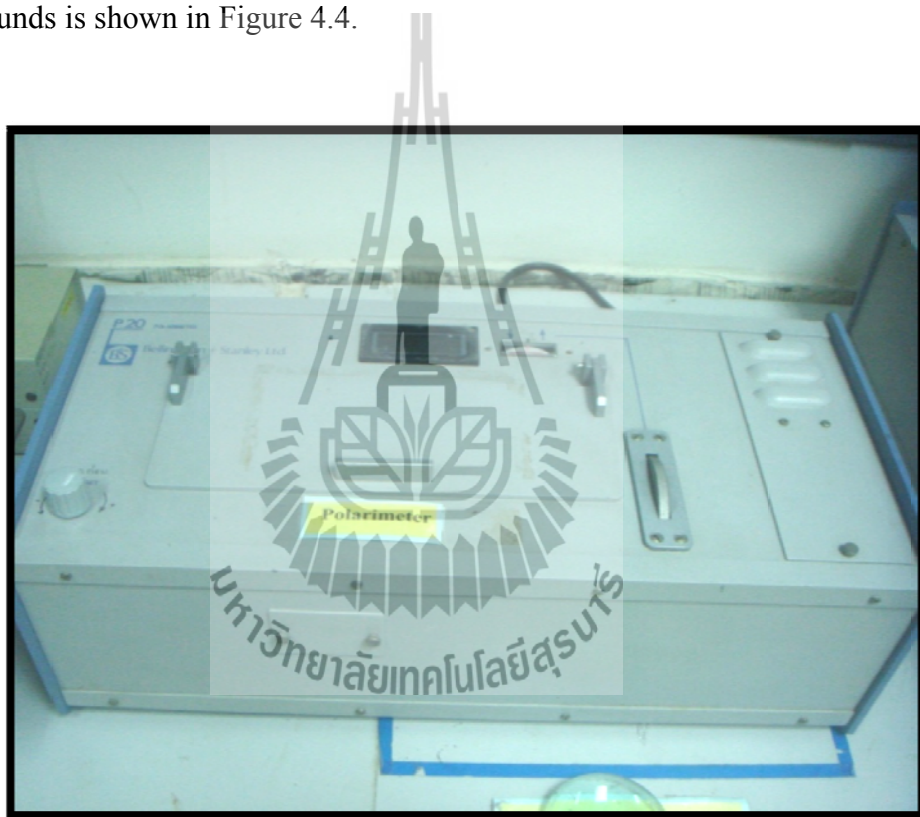
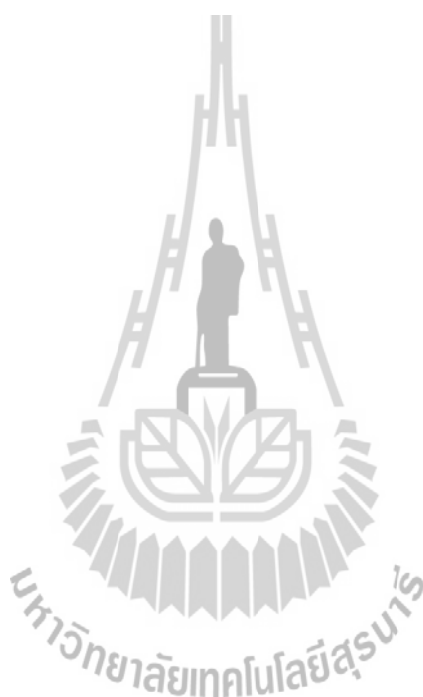


Figure 4.4 The P20 polarimeter used to measure the optical rotation of chiral compound solution.

The optical rotations (observed rotation) of solutions containing the solids were used to calculate the specific rotation $[\alpha]_D^{25}$ of the met·HCl sample, to analyze the percent purity of L-met·HCl in the met·HCl sample after the preferential

crystallization is completed. The magnitude of the observed rotation for a particular compound depends on its concentration, the length of the sample tube, the temperature, the solvent, and the wavelength of the light used (Brown, 2000).



4.5 Results and Discussion

4.5.1 The Suspension Density of DL-met·HCl Aqueous Solution on Preferential Crystallization

The preferential crystallization experiments were performed in an isothermal batch process, called seeded isothermal preferential crystallization (SIPC). The experimental results of preferential crystallization of DL-met·HCl aqueous solution at 10°C in two relative supersaturation values ($\sigma = 0.005$ and $\sigma = 0.01$) and four resolution times ($t = 2, 5, 8,$ and 10 minutes) are shown in Table 4.1 and Table 4.2. The preferential crystallization experiments were repeated at each experimental condition at least 4 times to confirm the experimental results were reproducible.

These tables show the actual amount of DL-met·HCl used, which is based on the solubility data of DL-met·HCl at 10°C, and also the total amount of DL-met·HCl solution used in each batch experiment. The DL-met·HCl solution concentration was measured to check the stability of the solution concentration throughout the experiment in both the initial time and the end time of the crystallization cycle, which was measured by the refractive index method at 25°C using an automatic digital refractometer. When the preferential crystallization was completed, the solid product and the liquid product were separated by filtration and weighed to determine the suspension density (M_T) according to equation (4.2).

$$\text{Suspension density} = M_T = \frac{\text{g of crystal}}{\text{g of crystal} + \text{g of liquid}} \quad (4.2)$$

The suspension density is the primary parameter that indicates the tendency of the quantity of crystal growth in a crystallization process. The amount of solid, amount of liquid and suspension density are shown in Table 4.3 and Table 4.4.



Table 4.1 The experimental conditions and results of the preferential crystallization of DL-met·HCl aqueous solution at 10°C ($\sigma = 0.005$).

Resolution time (minutes) / Batch		Total weight of solution (g)	Amount of DL-met·HCl (g)	Amount of solid product (g)	Amount of liquid product (g)	C (t = 0) (g DL-met·HCl/g solution)	C (t = t _{cryst.}) (g DL-met·HCl/g solution)
2	1 st	40	29.7480	1.1209	16.7102	0.7374	0.7330
	2 nd	40	29.7481	1.1108	33.9302	0.7416	0.7329
	3 rd	40	29.7480	1.1364	31.9103	0.7411	0.7387
	4 th	40	29.7480	1.1575	33.5908	0.7419	0.7389
5	1 st	67	49.8278	3.5417	47.6835	0.7400	0.7384
	2 nd	40	29.7480	2.8853	67.4238	0.7419	0.7341
	3 rd	40	29.7481	3.2256	68.2130	0.7428	0.7359
	4 th	40	29.7480	3.4186	69.2537	0.7409	0.7370
8	1 st	67	49.8280	4.8210	49.1168	0.7380	0.7212
	2 nd	40	29.7481	3.5719	74.8366	0.7405	0.7370
	3 rd	40	29.7481	3.1964	76.3168	0.7407	0.7369
	4 th	40	29.7480	3.2063	73.1130	0.7415	0.7346
10	1 st	40	29.7481	1.6206	4.3386	0.7367	0.7191
	2 nd	40	29.7480	1.2794	19.3164	0.7402	0.7303
	3 rd	40	29.7480	2.3601	38.9732	0.7403	0.7308
	4 th	40	29.7480	1.8492	28.5831	0.7417	0.7370

Table 4.2 The experimental conditions and results of the preferential crystallization of DL-met·HCl aqueous solution at 10°C ($\sigma = 0.01$).

Resolution time (minutes) / Batch		Total weight of solution (g)	Amount of DL-met·HCl (g)	Amount of solid product (g)	Amount of liquid product (g)	C (t = 0) (g DL-met·HCl/g solution)	C (t = t _{cryst.}) (g DL-met·HCl/g solution)
2	1 st	40	29.8960	1.4168	21.4537	0.7378	0.7320
	2 nd	40	29.8960	1.3861	39.8816	0.7449	0.7364
	3 rd	40	29.8961	1.1482	34.8264	0.7426	0.7376
	4 th	40	29.8961	1.4280	37.5029	0.7442	0.7386
5	1 st	67	50.0757	6.3969	46.7863	0.7444	0.7323
	2 nd	40	29.8960	3.6081	74.2131	0.7423	0.7329
	3 rd	40	29.8960	2.7380	52.3722	0.7439	0.7356
	4 th	40	29.8960	2.6264	53.9530	0.7438	0.7362
8	1 st	40	29.8961	2.5757	9.5702	0.7439	0.7184
	2 nd	40	29.8961	2.4356	37.3082	0.7434	0.7225
	3 rd	40	29.8960	2.5811	38.0526	0.7438	0.7268
	4 th	40	29.8961	2.2743	36.5580	0.7421	0.7297
10	1 st	67	50.0758	10.7359	37.0586	0.7467	0.7246
	2 nd	40	29.8960	4.1229	17.5055	0.7433	0.7142
	3 rd	40	29.8960	3.8543	41.8301	0.7458	0.7252
	4 th	40	29.8960	3.5162	39.8051	0.7429	0.7174
	5 th	40	29.8960	3.4201	37.6017	0.7426	0.7270

Table 4.3 Suspension density results for preferential crystallizationof DL-met·HCl aqueous solution at 10°C ($\sigma = 0.005$).

Resolution time (minutes) / Batch***		Amount of solid content (g)	Amount of liquid content (g)	Suspension density; M_T (g crystal/g suspension)
At initial (t = 0)		1.0000*	40.00**	0.0244
2	1 st	1.1209	16.7102	0.0629
	2 nd	1.1108	33.9302	0.0317
	3 rd	1.1364	31.9103	0.0344
	4 th	1.1575	33.5908	0.0333
5	1 st	3.5417	47.6835	0.0691
	2 nd	2.8853	67.4238	0.0410
	3 rd	3.2256	68.2130	0.0452
	4 th	3.4186	69.2537	0.0470
8	1 st	4.8210	49.1168	0.0894
	2 nd	3.5719	74.8366	0.0456
	3 rd	3.1964	76.3168	0.0402
	4 th	3.2063	73.1130	0.0420
10	1 st	1.6206	4.3386	0.2719
	2 nd	1.2794	19.3164	0.0621
	3 rd	2.3601	38.9732	0.0571
	4 th	1.8492	28.5831	0.0608
At equilibrium (t = ∞)		1.5749	39.4251	0.0380

Remark : * Amount of L-met·HCl as seed crystal.

** Total DL-met·HCl aqueous solution.

*** The 1st run of the experimental data in each crystallization cycle times were neglected and was not plotted with other run data, because this data point has a larger relative error.

Table 4.4 Suspension density results for preferential crystallizationof DL-met·HCl aqueous solution at 10°C ($\sigma = 0.01$).

Resolution time (minutes) / Batch***		Amount of solid content (g)	Amount of liquid content (g)	Suspension density; M_T (g crystal/g suspension)
At initial (t = 0)		1.0000*	40.00**	0.0244
2	1 st	1.4168	21.4537	0.0619
	2 nd	1.3861	39.8816	0.0336
	3 rd	1.1482	34.8264	0.0319
	4 th	1.4280	37.5029	0.0367
5	1 st	6.3969	46.7863	0.1203
	2 nd	3.6081	74.2131	0.0464
	3 rd	2.7380	52.3722	0.0497
	4 th	2.6264	53.9530	0.0464
8	1 st	2.5757	9.5702	0.2121
	2 nd	2.4356	37.3082	0.0613
	3 rd	2.5811	38.0526	0.0635
	4 th	2.2743	36.5580	0.0586
10	1 st	10.7359	37.0586	0.2246
	2 nd	4.1229	17.5055	0.1906
	3 rd	3.8543	41.8301	0.0844
	4 th	3.5162	39.8051	0.0812
	5 th	3.4201	37.6017	0.0834
At equilibrium (t = ∞)		2.1498	38.8502	0.0516

Remark : * Amount of L-met·HCl as seed crystal.

** Total DL-met·HCl aqueous solution.

*** The 1st run (and 2nd run at 10 minutes only) of the experimental data in each crystallization cycle times were neglected and was not plotted with other run data, because this data point has a larger relative error.

Table 4.3 and Table 4.4 show the calculated results of the suspension density of the preferential crystallization of DL-met-HCl aqueous solution at 10°C. These tables also show the suspension density at the equilibrium state, from which it can be seen that both results at $\sigma = 0.005$ and $\sigma = 0.01$ are less than the suspension density at 5, 8, and 10 minutes of resolution time for $\sigma = 0.005$, and less than the suspension density at 8 and 10 minutes of resolution time for $\sigma = 0.01$. This is because the efficiency in separating the solids and liquids is not good enough, which made these suspension density values appear larger than the suspension density at the equilibrium state. Both suspension densities at equilibrium were obtained from the material balance calculation in Appendix C. The results from Table 4.3 and Table 4.4 are plotted for the suspension density (g crystal/g solution) versus resolution time (minutes) as shown in Figure 4.5 and Figure 4.6.

The suspension density data were plotted using a scatter plot with multiple error bars (2 standard deviations) and the suspension density curves were fitted using an exponential rise to maximum, 3 parameters, fitted by SigmaPlot[®] version 11.0, with the results shown in equation (4.3) and equation (4.4), where M_T represents the suspension density in g crystal/g solution and t represents the resolution time in minutes.

For $\sigma = 0.005$:

$$M_T = 0.0265 + (56.0365)(1 - \exp(-5.2309 \times 10^{-5} t)) \quad ; r^2 = 0.8054 \quad (4.3)$$

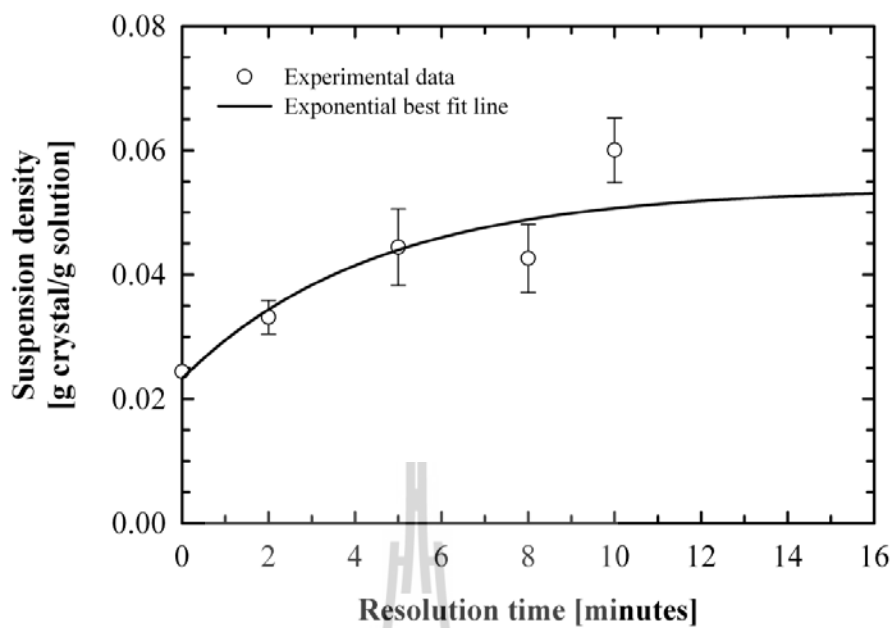


Figure 4.5 Suspension density results for preferential crystallization of DL-met·HCl ($\sigma = 0.005$).

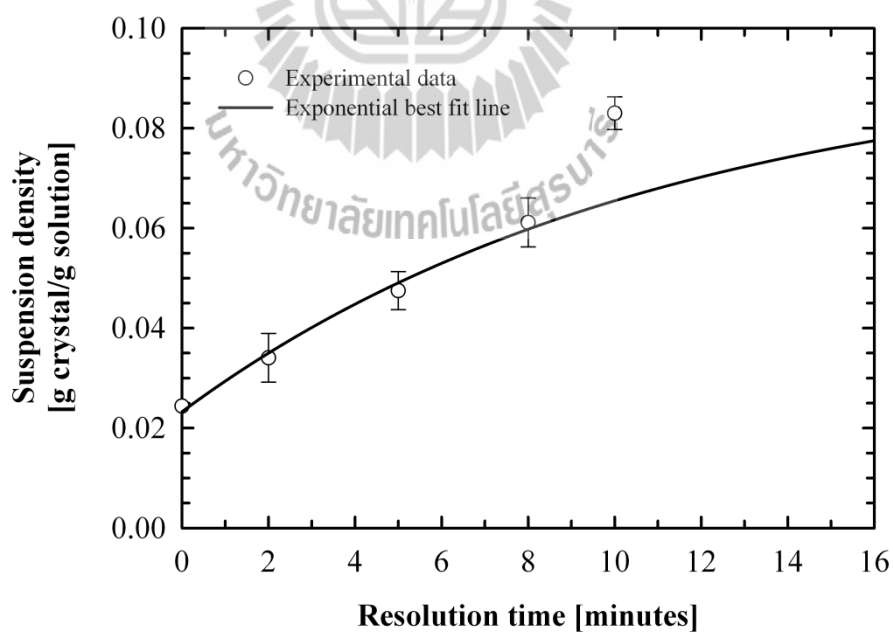


Figure 4.6 Suspension density results for preferential crystallization of DL-met·HCl ($\sigma = 0.01$).

For $\sigma = 0.01$:

$$M_T = 0.0214 + (235.1281)(1 - \exp(-2.4042 \times 10^{-5} t)) \quad ; \quad r^2 = 0.9526 \quad (4.4)$$

These graphs show the tendency of the crystal growth during the preferential crystallization of DL-met·HCl aqueous solution, where the suspension density increases with increasing crystallization cycle time (or resolution time), which indicates the birth of new nuclei and growth of crystals at all times. The suspension density will be taken to the equilibrium condition over time.

4.5.2 Determination of the Percent Purity of L-met·HCl Crystals

The measured rotation (in degrees) is the optical rotation (α) of the sample, which is shown in Table 4.5 and Table 4.6. These tables show all experimental results; the actual solution concentration in g crystal/ml solution after dissolving the crystal sample into the solvent, the measured solution concentration (in the same units), which were measured by automatic digital refractometer (Model RFM340, Bellingham and Stanley Ltd.). The optical rotation is shown in degrees ($^\circ$) or angular (\AA) unit that could be identified in 2 values; if it is a positive value it indicates the L-enantiomer of met·HCl is in excess, and if it is a negative value it indicates the D-enantiomer of met·HCl is in excess. The specific rotation is calculated from the optical rotation according to equation (4.1), which shows all positive values.

The specific rotation, $[\alpha]_D^T$, can be used to calculate the percent purity of L-met·HCl crystal in mother liquor of DL-met·HCl using the correlation shown in equation (4.9). This equation can be described by the mathematical relationships below and Figure 4.7, which indicates the relationship between the specific rotation at

25°C, sodium D-line wavelength, $[\alpha]_D^{25}$, and the percent purity of L-crystal (%L-crystal). Figure 4.7 can be plotted with a linear equation, using SigmaPlot® version 11.0. This graph was used to describe the relationship of the specific rotation of L-met·HCl crystal and the percent purity of L-met·HCl crystal during the preferential crystallization process.



Table 4.5 The optical activity results of preferential crystallization of DL-met·HCl aqueous solution at 10°C ($\sigma = 0.005$).

Resolution Time (minutes) / Batch		$C_{\text{crystal,initial}}$ (g met·HCl / 100 ml solution)	$C_{\text{crystal,measured}}$ (g met·HCl / 100 ml solution)	Optical rotation (α ; degrees)	Specific rotation ($[\alpha]_D^{25}$, degrees)	% Purity of L-crystal
2	1 st	7.0427	6.6376	(+) 01.56°	(+) 11.7512°	82.1774
	2 nd	6.9880	6.5564	(+) 01.64°	(+) 12.5069°	84.2467
	3 rd	7.0073	6.6376	(+) 01.49°	(+) 11.2239°	80.7336
	4 th	7.1233	6.7182	(+) 01.58°	(+) 11.7591°	82.1991
5	1 st	20.0200	17.8452	(+) 03.19°	(+) 8.9380°	74.4743
	2 nd	16.2007	15.0196	(+) 02.86°	(+) 9.5209°	76.0704
	3 rd	19.0780	18.5170	(+) 03.51°	(+) 9.4778°	75.9524
	4 th	20.0080	17.8452	(+) 03.25°	(+) 9.1061°	74.9346
8	1 st	20.0180	17.5574	(+) 01.23°	(+) 3.5028°	59.5915
	2 nd	18.9560	17.3692	(+) 01.33°	(+) 3.8286°	60.4836
	3 rd	17.8027	17.0838	(+) 01.61°	(+) 4.7121°	62.9028
	4 th	17.2200	17.1741	(+) 01.18°	(+) 3.4354°	59.4069
10	1 st	10.0040	8.4688	(+) 00.47°	(+) 2.7749°	57.5983
	2 nd	7.8847	7.7134	(+) 00.44°	(+) 2.8522°	57.8100
	3 rd	14.8493	14.7430	(+) 00.65°	(+) 2.2044°	56.0361
	4 th	10.2540	8.6377	(+) 00.53°	(+) 3.0679°	58.4006
Pure L-met·HClcrystal		25.0030	24.8532	(+) 09.13°	(+) 18.2578°	100

Table 4.6 The optical activity results of preferential crystallization of DL-met·HCl aqueous solution at 10°C ($\sigma = 0.01$).

Resolution Time (minutes) / Batch		$C_{\text{crystal,initial}}$ (g met·HCl / 100 ml solution)	$C_{\text{crystal,measured}}$ (g met·HCl / 100 ml solution)	Optical rotation (α ; degrees)	Specific rotation ($[\alpha]_D^{25}$, degrees)	% Purity of L-crystal
2	1 st	8.6333	8.2182	(+) 01.97°	(+) 11.9856°	82.8193
	2 nd	8.7013	8.3002	(+) 01.94°	(+) 11.6865°	82.0003
	3 rd	7.2467	7.1339	(+) 01.73°	(+) 12.1252°	83.2015
	4 th	8.9840	8.4688	(+) 02.04°	(+) 12.0442°	82.9797
5	1 st	25.0110	22.8924	(+) 02.38°	(+) 5.1982°	64.2338
	2 nd	16.1260	15.2055	(+) 01.91°	(+)6.2806°	67.1977
	3 rd	13.4440	12.5591	(+) 01.88°	(+)7.4846°	70.4945
	4 th	17.2013	17.0838	(+) 02.41°	(+)7.0535°	69.3141
8	1 st	16.3227	15.0196	(+) 01.37°	(+)4.5607°	62.4882
	2 nd	15.5907	15.2965	(+) 01.38°	(+)4.5108°	62.3516
	3 rd	16.4760	15.5739	(+) 01.17°	(+)3.7563°	60.2856
	4 th	14.5373	13.9145	(+) 01.31°	(+)4.7073°	62.8896
10	1 st	25.013	21.5783	(+) 00.96°	(+) 2.2245°	56.0912
	2 nd	19.8785	17.1741	(+) 01.05°	(+)3.0569°	58.3705
	3 rd	18.4025	17.7474	(+) 01.11°	(+)3.1272°	58.5630
	4 th	17.3520	16.9864	(+) 00.98°	(+)2.8847°	57.8990
	5 th	16.5910	15.9484	(+) 00.84°	(+)2.6335°	57.2111

From the linear equation, comparing all variables in equation (4.5) with Figure 4.7:

$$y = mx + c \quad (4.5)$$

where x-axis : %Purity of L-crystal

y-axis : Specific Rotation, $[\alpha]_D^{25}$

y-intercept : $[\alpha]_D^{25}$ of pure L-met-HCl crystal (see Table 4.5)

$$= -(+18.26^\circ)$$

$$m = \text{slope} = \frac{\Delta y}{\Delta x} = \frac{([\alpha]_D^{25})_2 - ([\alpha]_D^{25})_1}{(\%L)_2 - (\%L)_1}$$

Substituting all symbols and values in the linear equation,

$$[\alpha]_D^{25} = \left[\left(\frac{([\alpha]_D^{25})_2 - ([\alpha]_D^{25})_1}{(\%L)_2 - (\%L)_1} \right) \times (\% \text{Purity of L-crystal}) \right] + (-18.26^\circ) \quad (4.6)$$

$$[\alpha]_D^{25} = \left[\left(\frac{(18.26^\circ)_2 - (-18.26^\circ)_1}{(100)_2 - (0)_1} \right) \times (\% \text{Purity of L-crystal}) \right] + (-18.26^\circ) \quad (4.7)$$

Rearranged the equation (4.7) becomes,

$$[\alpha]_D^{25} = \left[\left(\frac{(2) \times (18.26^\circ)}{(100-0)} \right) \times (\% \text{Purity of L-crystal}) \right] - (18.26^\circ) \quad (4.8)$$

The percent purity of L-met·HCl in crystals can be calculated from equation (4.9) and also as shown the example of percent purity of L-crystal calculation in Appendix E.

$$\% \text{Purity of L-crystal} = \left[[\alpha]_D^{25} + (18.26^\circ) \right] \times \left[\frac{(100-0)}{(2) \times (18.26^\circ)} \right] \quad (4.9)$$

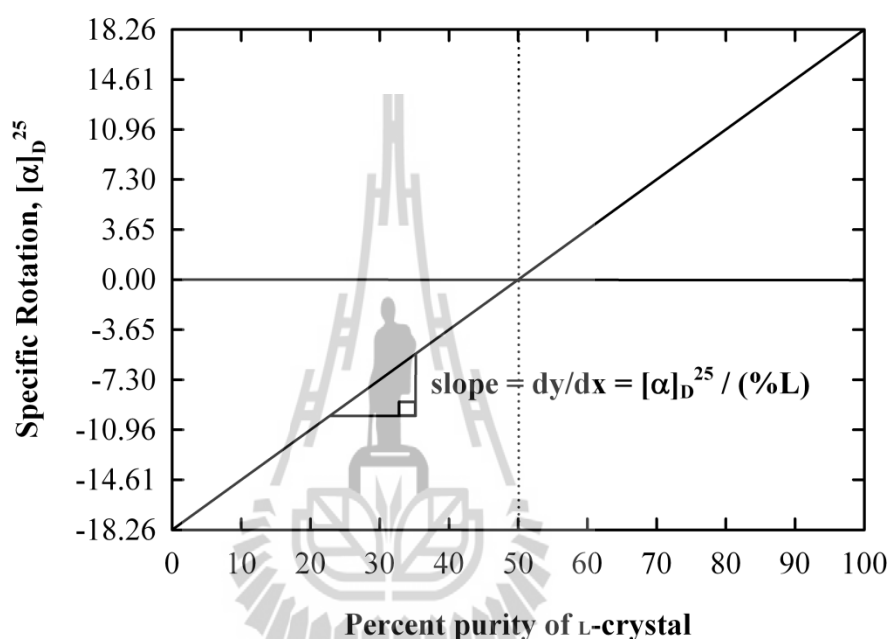


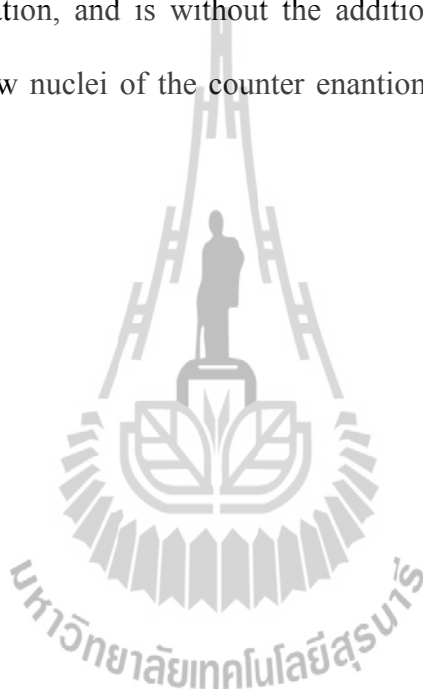
Figure 4.7 The relationship between specific rotation and amount of L-met·HCl in mixtures of D- and L-met·HCl.

This calculation method uses the principle that two enantiomers (*d,l* or *R,S* or *+/-*) have the same magnitude of specific rotation but that one will have a positive value, and the other will have a negative value. The enantiomer that rotates plane-polarized light to the right will be assigned to the symbol *d* or (+), and the other one is assigned to the symbol *l* or (-). Racemic solutions bend plane-polarized light in both directions, but with equal magnitude and so the specific rotation is zero.

The racemic solution of DL-met·HCl had caused some reduction in purity of the L-met·HCl seed crystals while the preferential crystallization process was operated. The preferential crystallization was started with 100% pure L-met·HCl as seed crystals, with the specific rotation of pure L-met·HCl solution at 25°C is $[\alpha]_D^{25} = +18.26^\circ$, as shown in Table 4.5 and Figure 4.7. The 100% pure L-met·HCl seed crystals decreased in percent purity over time until the purity of L-met·HCl will be 50% purity. At the same time the percent purity of L-met·HCl decreased, the nuclei of the unseeded (counter) enantiomer (D-met·HCl) were occurring and growing that made the percent purity of D-met·HCl increased to 50% purity. In this state, is called the racemic mixture (50% D-met·HCl and 50% L-met·HCl). Similarly, the specific rotation of L-met·HCl crystal will be decreased over time during the preferential crystallization process was operating, until the specific rotation of met·HCl is equal to $[\alpha]_D^{25} = \pm 00.00^\circ$ that is conglomerate DL-met·HCl crystal as Figure 4.7.

The data on Table 4.5 and Table 4.6 can be plotted for the relationship between the percent purity of L-met·HCl in crystals and resolution time (or crystallization cycle time) (min) and these plots are shown in Figure 4.8 and Figure 4.9, and the uncertainty in the graph is represented by 2 standard deviations of the mean (see Appendix A). These graphs show the experimental results do not much differ at $\sigma = 0.005$ and $\sigma = 0.01$, which shows the percent purity of the L-met·HCl crystal decreased rapidly from 100% pure L-met·HCl crystal to the equilibrium state (around 60% to 55% purity) over time. The percent purity of L-met·HCl decreases rapidly at the initial time, with no plateau at the 100% purity state, as shown in the research of Doki et al. The enantiomer ratio of solution is always 1:1 or a racemic mixture when no additive or no seed crystal was added. It indicates that D-enantiomer

and L-enantiomer have nucleated simultaneously at all times (Doki, Yokota, Sasaki, and Kubota, 2004), that made the percent purity of L-met·HCl crystal is decreased rapidly at the initial state, and also can be explained by the very short induction time for secondary nucleation threshold in these solutions, which maybe a result of the seed crystals (see section 3.5.1, Chapter III). This research only focuses on the study of the purity drop of L-met·HCl seed crystal in mother liquor of DL-met·HCl via the preferential crystallization, and is without the addition of another D-amino acid to inhibit the birth of new nuclei of the counter enantiomer (D-met·HCl) in the mother liquor.



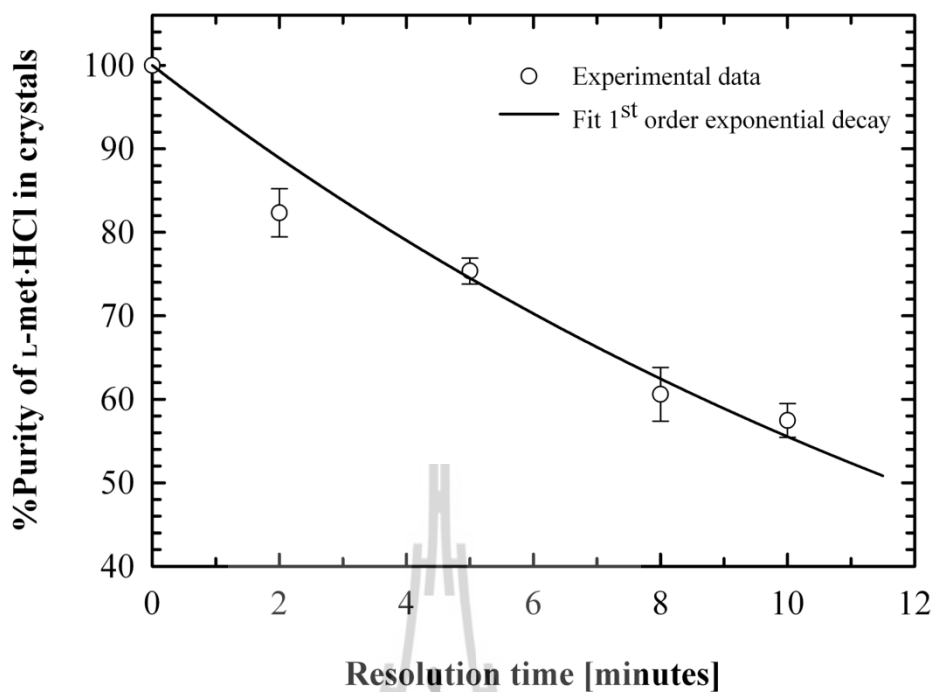


Figure 4.8 Optical purity of the produced L-met·HCl crystal during resolution by preferential crystallization from DL-met·HCl aqueous solution ($\sigma = 0.005$); Total solution: 40 g, Solvent: 10.45 cm³ of distilled water, Seed crystals: 1.000 g of L-met·HCl, Crystallization temperature: 10±0.5°C.

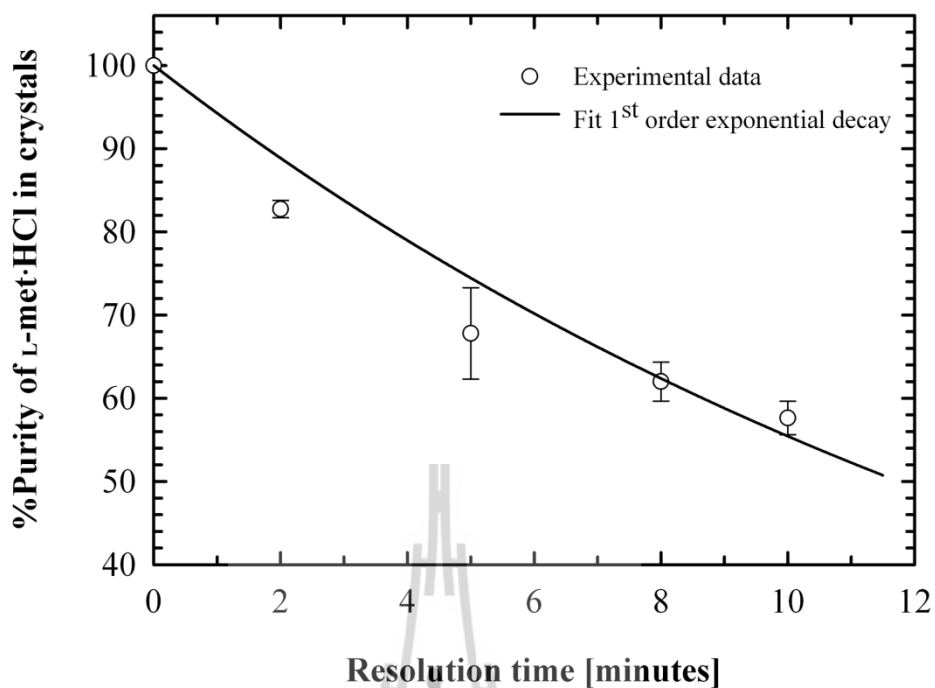


Figure 4.9 Optical purity of the produced L-met·HCl crystal during resolution by preferential crystallization from DL-met·HCl aqueous solution ($\sigma = 0.01$); Total solution: 40 g, Solvent: 10.30 cm³ of distilled water, Seed crystals: 1.000 g of L-met·HCl, Crystallization temperature: 10±0.5°C.

4.6 Conclusions

The last experiments studied the mechanisms and results of the preferential crystallization of DL-met·HCl, and analyzed the percent purity and purity drop of L-met·HCl in the crystal product by optical resolution using polarimetry. The seeded isothermal preferential crystallization (SIPC) was used in this experiment. The racemic mixture of DL-met·HCl and L-met·HCl crystal are the main chemical that were used in the experiment. DL-met·HCl supersaturated solutions ($\sigma = 0.005$ and $\sigma = 0.01$) were prepared at 10°C that corresponds to the solubility data of DL-met·HCl at 10°C. About 1.0000 g of L-met·HCl was seeded to the supersaturated solution of DL-met·HCl in preferential crystallization process to induce the L-enantiomer of met·HCl (desired product) in the saturated solution. The resolution time or crystallization cycle time for study the preferential crystallization is 2, 5, 8, and 10 minutes, because of the preferential crystallization period of DL-met·HCl is very short due to the effect of the primary and secondary nucleation threshold measured in the previous chapter.

The suspension density (M_T) during the preferential crystallization of DL-met·HCl aqueous solution increased rapidly with increasing crystallization cycle time in the current experiments partly due to the relatively large growth rates and also due to the large amount of seed crystal, which indicates the birth of new nuclei and growth of crystals all the time during the experiment. Finally, the system will be taken to the equilibrium state (about 0.0380 g crystal/g solution for $\sigma = 0.005$, and about 0.0516 g crystal/g solution for $\sigma = 0.01$) over time. The solid phase and liquid phase are at the equilibrium condition, which indicates no growth and no dissolution of the crystals anymore. The suspension density was used to indicate the tendency of quantity of crystal growth during the preferential crystallization process, and also to

know the total mass of new crystal at any time. Moreover, the suspension density can also be used to know the optimum cycle period for operating the preferential crystallization also. The purity drop and percent purity of L-met·HCl were studied by mathematical calculation of the specific rotation, that reveals the purity of the L-met·HCl crystal decreased rapidly to the equilibrium state (60% to 55% purity) over time, with almost no plateau at 100% purity at initial state. The equilibrium purity is larger than 50% due to the small amount of L-met·HCl seed crystals added at the start of the batch. The quick decrease in purity can be explained by the very short induction time for secondary nucleation in these solutions, which is a result of seed crystals.

This is the first project to develop and improve the chiral resolution (especially the preferential crystallization) technology, which only focuses on the mechanisms and effect of seed crystal to induce the desired form of enantiomer of chiral compounds. It cannot analyze or separate the desired enantiomer to 100% purity. It still needs to use another step to separate the desired enantiomer, such as “tailor-made” additives to inhibit the primary nucleation of the undesired enantiomer, or using a process where one enantiomer (the undesired form) of a compound converts to the other enantiomer (the desired form) by reacting with other compounds, a process called “racemization”.

4.7 References

- Angelov, I., Raisch, J., Elsner, M. P., and Seidel-Morgenstern, A. (2008). Optimal operation of enantioseparation by batch-wise preferential crystallization. **Chemical Engineering Science** 63: 1282-1292.
- Bayley, C. R. and Vaidya, N. A. (1992). Resolution of racemates by diastereomeric salt formation. In A. N. Collins, G. Sheldrake, and J. Crosby (Eds.). **Chirality in industry: The commercial manufacture and applications of optically active compounds** (pp. 69-77). Chichester: John Wiley & Sons.
- Blehaut, J. and Nicoud, R. M. (1998). Recent aspects in simulated moving bed. **Analysis Magazine** 26: M60-M70.
- Brown, W. H. (2000). **Introduction to organic chemistry**. Fort Worth, Texas: Saunders College Publishing.
- Bruice, P. Y. (2004). **Organic chemistry**. Upper Saddle River, New Jersey: Pearson Education.
- Carey, F. A. (2003). **Organic chemistry**. Boston: McGraw-Hill.
- Collins, A. N., Sheldrake, G. N., and Crosby, J. (1997). **Chirality in industry II: Developments in the manufacture and applications of optically active compounds**. Chichester: John Wiley & Sons.
- Coquerel, G. (2007). Preferential crystallization. In K. Sakai, N. Hirayama, and R. Tamura (Eds.). **Novel optical resolution technologies topics in current chemistry** (vol. 269, pp. 1-51). Berlin Heidelberg: Springer-Verlag.

- Doki, N., Yokota, M., Sasaki, S., and Kubota, N. (2004). Simultaneous crystallization of D- and L-asparagines in the presence of a tailor-made additive by natural cooling combined with pulse heating. **Crystal Growth & Design** 4(6): 1359-1363.
- Elsner, M. P., Menéndez, D. F., Muslera, E. A., and Seidel-Morgenstern, A. (2005). Experimental study and simplified mathematical description of preferential crystallization. **Chirality** 17: S183-S195.
- Franco, P. and Minguillón, C. (2001). Techniques in preparative chiral separations. In G. Subramanian (Ed.). **Chiral separation techniques: A practical approach** (pp. 1-23). Weinheim, Germany: Wiley-VCH.
- Gou, L., Lorenz, H., and Seidel-Morgenstern, A. (2011). Rational design of preferential crystallization. In **Poster of the 18th International Symposium on Industrial Crystallization** (poster no. 148). Zurich, Switzerland.
- Hornback, J. M. (2005). **Organic chemistry**. New York: W. W. Norton & Company.
- Jacques, J., Collet, A., and Wilen, S. H. (1981). **Enantiomers, racemates, and resolutions**. New York: John Wiley & Sons.
- Kozma, D. (2001). **CRC Handbook of optical resolutions via diastereomeric salt formation**. Boca Raton, Florida: CRC Press.
- Lorenz, H., Polenske, D., and Seidel-Morgenstern, A. (2006). Application of preferential crystallization to resolve racemic compounds in a hybrid process. **Chirality** 18: 828-840.
- Mohrig, J. R., Hammond, C. N., and Schatz, P. F. (2010). **Techniques in organic chemistry**. New York: W. H. Freeman & Company.

- Nohira, H. and Sakai, K. (2004). Optical resolution by means of crystallization. In F. Toda (Ed.). **Enantiomer separation: Fundamentals and practical methods** (pp. 165-191). Dordrecht, the Netherlands: Kluwer Academic Publishers.
- Polenske, D., Lorenz, H., and Seidel-Morgenstern, A. (2009). Potential of different techniques of preferential crystallization for enantioseparation of racemic compound forming system. **Chirality** 21: 728-737.
- Qamar, S., Angelov, I., Elsner, M. P., Ashfaq, A., Seidel-Morgenstern, A., and Warnecke, G. (2009). Numerical approximations of a population balance model for couple batch preferential crystallizers. **Applied Numerical Mathematics** 59: 739-753.
- Schreier, P., Bernreuther, A., and Huffer, M. (1995). **Analysis of chiral organic molecules: Methodology and applications**. Berlin: Walter de Gruyter & Company.
- Seebach, D., Hoffmann, M., Sting, A. R., Kinkel, J. N., Schulte, M., and Küsters, E. (1998). Chromatographic resolution of synthetically useful chiral glycine derivatives by high-performance liquid chromatography. **Journal of Chromatography A** 796: 299-307.
- Spencer, K. M., Edmonds, R. B., Rauh, R. D., and Carrabba, M. M. (1994). Analytical determination of enantiomeric purity using raman optical activity. **Analytical Chemistry** 66(8): 1269-1273.
- Vollhardt, K. P. C. and Schore, N. E. (2002). **Organic chemistry: Structure and function**. New York: W. H. Freeman & Company.

Wood, W. M. L. (1997). Crystal science techniques in the manufacture of chiral compounds. In A. N. Collins, G. Sheldrake, and J. Crosby (Eds.). **Chirality in industry II: Developments in the manufacture and applications of optically active compounds** (pp. 119-156). Chichester: John Wiley & Sons.



CHAPTER V

CONCLUSIONS AND RECOMMENDATIONS

5.1 Conclusions

This research aims to improve the knowledge of and develop the chiral resolution technology via the preferential crystallization process for selective enantioseparation of methionine and other amino acids. Methionine (met) is an essential amino acid that is important in human and animal metabolism, and cannot be synthesized by the human body. Only the L-form of methionine is required in the human body. L-methionine (L-met) is ingredient necessary in animal foods, an additive ingredient in the pharmaceutical industry, and is also used in cosmetic and agricultural industries. Preferential crystallization is a direct resolution technique for separating the desired form of a chiral molecule from the undesired form, and is also an effective and cheap technique. The thermodynamic and kinetic parameters involved in the preferential crystallization process of methionine, and nucleation and growth kinetics is still extremely important, but these are quite limited in the scientific literature.

This research aims to extend the understanding of preferential crystallization, both in aspects of thermodynamics and kinetics, for determination of ways to separate the pure L-enantiomer of methionine from racemic mixtures. The use of operating parameters of the crystallization allows considerable manipulation of preferential crystallization behavior. In order to achieve the research goal it is necessary to

investigate the thermodynamic parameters of methionine hydrochloride (met·HCl) and the effect of kinetic parameters on the percent purity of L-crystal of met·HCl. Properties of met·HCl have been determined in both pure enantiomer and racemic mixture in aqueous solution systems. The nucleation threshold and growth rates can be used to optimize the crystallization process through the use of models. Solubility data was used to investigate the ternary phase diagram of met·HCl : water which can define the phase region and state of species to determine the optimum pathway of preferential crystallization.

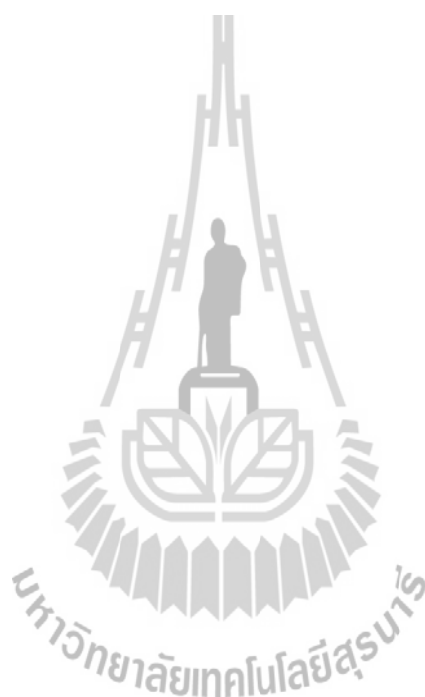
Thermodynamic properties of L- and DL-met·HCl in water are required to be investigated to better understand crystallization behavior as a function of temperature. The refractive index method is a convenient and simple measurement of solid content in liquids. The refractive index can well determine the solubility values. The solubility of three fixed enantiomeric mixtures in water (pure enantiomer, racemic conglomerate, and 75% L- and 25% D-met·HCl mixture) are strongly dependent on the temperature and solubility increased with increasing temperature. More specifically, it has been found that, when DL-met is converted into crystals of DL-met·HCl the resulting species has a much higher solubility in water than the free form (see Figure 2.9). On the other hand, the L-form or D-form of met·HCl has a lower solubility in water than conglomerate DL-met·HCl (see Figure 2.9). Thus, it becomes possible to separate crystals of the L-form or D-form of met·HCl from DL-met·HCl using the preferential crystallization process. The ternary solubility diagram of L-met·HCl + D-met·HCl + water is in accordance with the typical ternary phase diagram for a conglomerate type compound. The solubility equilibrium points on the ternary phase

diagram can define the phase regions on the phase diagram; hence the state condition of the substance can be determined.

The general kinetic properties of L- and DL-met·HCl in water are required to better understand the chiral resolution by preferential crystallization. Experimentally, the results reveal the primary and secondary nucleation threshold of DL-met·HCl solution. These results indicate the induction time dependence of the relative supersaturation of the primary and secondary nucleation thresholds. The induction time increases as the relative supersaturation of the primary and secondary nucleation threshold decreases, and also the induction time of the secondary nucleation threshold is smaller than the induction time of primary nucleation threshold because of the influence of L-met·HCl seed crystals. This is because the secondary nucleation was induced by the addition of seeds into the supersaturated solution.

Furthermore, the crystal growth rate of L-met·HCl depends strongly on the relative supersaturation from supersaturated solutions of pure L-met·HCl but not from racemic solutions. The mean growth rate of L-met·HCl seed crystals is significantly larger from pure L-met·HCl supersaturated solutions than from racemic solutions, and there is a large degree of growth rate dispersion in both systems. The suspension density (M_T) during the preferential crystallization of DL-met·HCl aqueous solution increases rapidly with resolution time in the current experiments partly due to the relatively large growth rates and also due to the large amount of seed crystal. The purity of the L-met·HCl crystal decreased rapidly to the equilibrium value over time, due to the influence of the nucleation threshold of the counter enantiomer being small. Using preferential crystallization to separate the enantiomers of met·HCl from an

aqueous solution to obtain a high purity product appears to be very difficult; this study cannot separate the desired enantiomer to close to 100% purity.



5.2 Recommendations

The current solubility data of DL- and L-met-HCl compounds are quite well in accordance with the solubility data of threonine in water, with both racemic and conglomerate forms (Flood, 2008), but it used the met-HCl compounds which are highly soluble in water. This causes significant wastage of met-HCl compounds in the solubility experiment. There are several ways to perform solubility experiments and save the chemicals used. To change the solvent is one way to reduce the solubility of met-HCl compounds from water solvent to solvent mixtures, such as a mixture of ethanol and hydrochloric acid etc. They can help to reduce the amount of met-HCl compounds required for the solubility experiment.

If changes in the solvent in solubility experiment make the met-HCl solution less viscous then the result of solubility condition of met-HCl solution is less viscous. Then the primary and secondary nucleation threshold of met-HCl solution by induction time method can be measured with a turbidity device which detects the value with light scattering connected with computer program recorder. They can give more accurate value than observation of the phase transition by eye.

Finally, this project is studied for develop and improve the preferential crystallization technology, which only focuses on the mechanisms and effect of seed crystal to induce the desired form of enantiomer of chiral compounds. It also cannot analyze or separate the desire enantiomer to be 100% purity. It still needs to use another processes to separate the desired enantiomer, such as where a tailor-made additive is used to inhibit the primary nucleation of the undesired enantiomer, or a process where one enantiomer (the undesired form) of a compound converts to the other enantiomer (the desired form) by reacting with other compounds, which is

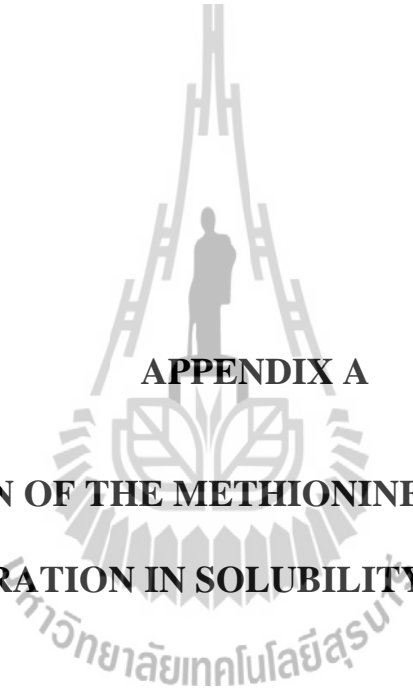
called the racemization process. This may enable the optical resolution from aqueous solution to be more effective.



5.3 Reference

Flood, A. E. (2008). Recent patents on the optical resolution of amino acid enantiomers by crystallization from solution. **Recent Patents on Materials Sciences** 1: 98-115.





APPENDIX A

**CALCULATION OF THE METHIONINE HYDROCHLORIDE
CONCENTRATION IN SOLUBILITY EXPERIMENTS**

The solubility experiment of methionine hydrochloride in pure water, a racemic conglomerate (DL-met·HCl), the pure enantiomer (L-met·HCl), and an intermediate mixture compositions (75% L-met·HCl : 25% D-met·HCl) have been measured at 5°C, 10°C, 25°C, and 40°C. All experimental conditions of three met·HCl forms can use a similar method to calculate the solubility results. All solubility results can be shown by an example of the calculation of the DL-met·HCl solubility at 5°C as following:

Mass ratio of dilution between DL-met·HCl and distilled water is set equal to 1 : 4.

Weight of DL-met·HCl = 0.5085 g
 Weight of distilled water = 2.0020 g } (obtained from the experiment)

The % Brix value of the diluted DL-met·HCl aqueous solution can be measured by refractometer at 25°C.

% Brix = 18.8

The % Brix can be converted to refractive index (RI) by using the conversion factor for Brix scale (sucrose) as shown Table A.1.

Refractive index (RI) = 1.3619

Table A.1 Conversion factor for brix scale (sucrose).

% Brix	RI	% Brix	RI
0.0	1.3330	45.0	1.4096
5.0	1.3403	50.0	1.4200
10.0	1.3479	55.0	1.4307
15.0	1.3557	60.0	1.4418
20.0	1.3639	65.0	1.4532
25.0	1.3723	70.0	1.4651
30.0	1.3811	75.0	1.4774
35.0	1.3902	80.0	1.4901
40.0	1.3997	85.0	1.5003

Source: OAKTON® TECH TIPS, Conversion Factors #30 ©2000,
[on-line] http://www.4oakton.com/TechTips/OAK_TT30.pdf

The calibrated concentration ($C_{\text{calibrated}}^*$) of DL-met·HCl can be calculated from the equation of met·HCl concentration calibration curve at 25°C in Chapter II, equation (2.1) as the following:

$$RI = (1.925 \times 10^{-3})C_{\text{calibrated}}^* + 1.3330$$

Thus, the calibrated concentration of DL-met·HCl at 25°C:

$$C_{\text{calibrated}}^* = \frac{(1.3619 - 1.3330)}{1.925 \times 10^{-3}}$$

$$C_{\text{calibrated}}^* = 15.0130 \text{ g DL-met·HCl/100 g solution}$$

$$\therefore C_{\text{calibrated}}^* = 0.150130 \text{ g DL-met·HCl/100 g solution}$$

$$\begin{aligned}
 \text{Mass ratio of DL-met}\cdot\text{HCl} : \text{distilled water} &= 0.5085 : 2.0020 \\
 &= \frac{0.5085}{0.5085} : \frac{2.0020}{0.5085} \\
 &= 1.0000 : 3.9371
 \end{aligned}$$

$$\text{Total mass of solution} = 1 + 3.9371 = 4.9371 \quad (-)$$

$$\begin{aligned}
 C_{\text{actual}}^* &= \text{Total mass of solution} \times C_{\text{calibrated}}^* \\
 &= 4.9371 \times 0.150130 \quad \text{g DL-met}\cdot\text{HCl/g solution} \\
 \therefore C_{\text{actual}}^* &= 0.7412 \quad \text{g DL-met}\cdot\text{HCl/g solution}
 \end{aligned}$$

Hence, the DL-met·HCl concentration at 5°C is 0.7412 g DL-met·HCl/g solution

Table A.2 to Table A.13 show all the raw data of solubility measurements in water of DL-met·HCl, L-met·HCl, and 75% L-met·HCl : 25% D-met·HCl at 5°C, 10°C, 25°C, and 40°C, respectively. All experiments were duplicated to check reproducibility.

Table A.2 Raw data of solubility measurement of DL-met·HCl aqueous solution at 5°C.

Batch	Set	% Brix	RI	g DL-met·HCl/100 g solution ($C_{\text{calibrated}}^*$)	g DL-met·HCl/g solution (C_{actual}^*)
1	1	18.8	1.3619	15.0130	0.7412
	2	18.9	1.3621	15.1169	0.7410
	3	18.6	1.3616	14.8571	0.7415
	4	18.3	1.3611	14.5974	0.7315
Average					0.7388
2	1	17.9	1.3605	14.2857	0.7135
	2	17.8	1.3603	14.1818	0.7105
	3	18.0	1.3606	14.3377	0.7180
	4	17.9	1.3605	14.2857	0.7133
	5	17.8	1.3603	14.1818	0.7113
	6	17.9	1.3605	14.2857	0.7140
	7	17.8	1.3603	14.1818	0.7109
	8	17.8	1.3603	14.1818	0.7118
Average					0.7129
3	1	17.7	1.3601	14.0779	0.7067
	2	17.7	1.3601	14.0779	0.7041
	3	17.8	1.3603	14.1818	0.7085
	4	17.8	1.3603	14.1818	0.7084
	5	17.8	1.3603	14.1818	0.7097
	6	17.8	1.3603	14.1818	0.7102
	7	17.8	1.3603	14.1818	0.7076
	8	17.7	1.3601	14.0779	0.7055
	9	17.7	1.3601	14.0779	0.7066
	10	17.9	1.3605	14.2857	0.7136
Average					0.7081

Table A.3 Raw data of solubility measurement of DL-met·HCl aqueous solution
at 10°C.

Batch	Set	% Brix	RI	g DL-met·HCl/100 g solution ($C_{\text{calibrated}}^*$)	g DL-met·HCl/g solution (C_{actual}^*)
1	1	18.8	1.3619	15.0130	0.7391
	2	19.0	1.3623	15.2208	0.7442
	3	18.7	1.3618	14.9610	0.7440
	4	18.8	1.3619	15.0130	0.7381
Average					0.7414
2	1	18.6	1.3616	14.8571	0.7430
	2	18.6	1.3616	14.8571	0.7438
	3	18.4	1.3613	14.7013	0.7449
	4	18.4	1.3613	14.7013	0.7425
Average					0.7436
3	1	18.0	1.3606	14.3377	0.7167
	2	18.0	1.3606	14.3377	0.7159
	3	18.0	1.3606	14.3377	0.7163
	4	18.0	1.3606	14.3377	0.7181
	5	18.1	1.3608	14.4416	0.7231
	6	18.0	1.3606	14.3377	0.7193
	7	18.1	1.3608	14.4416	0.7240
	8	18.2	1.3609	14.4935	0.7245
	9	18.1	1.3608	14.4416	0.7251
Average					0.7203

Table A.4 Raw data of solubility measurement of DL-met·HCl aqueous solution
at 25°C.

Batch	Set	% Brix	RI	g DL-met·HCl/100 g solution ($C_{\text{calibrated}}^*$)	g DL-met·HCl/g solution (C_{actual}^*)
1	1	19.2	1.3626	15.3766	0.7497
	2	18.9	1.3621	15.1169	0.7504
	3	18.8	1.3619	15.0130	0.7442
	4	18.8	1.3619	15.0130	0.7501
Average					0.7486
2	1	18.8	1.3619	15.0130	0.7510
	2	18.6	1.3616	14.8571	0.7470
	3	18.8	1.3619	15.0130	0.7503
	4	18.7	1.3618	14.9610	0.7493
Average					0.7494
3	1	18.8	1.3619	15.0130	0.7500
	2	18.8	1.3619	15.0130	0.7484
	3	18.2	1.3609	14.4935	0.7516
	4	18.8	1.3619	15.0130	0.7505
	5	18.9	1.3621	15.1169	0.7553
	6	18.8	1.3619	15.0130	0.7513
	7	18.8	1.3619	15.0130	0.7521
	8	18.9	1.3621	15.1169	0.7563
	9	18.9	1.3621	15.1169	0.7546
Average					0.7522

Table A.5 Raw data of solubility measurement of DL-met·HCl aqueous solution
at 40°C.

Batch	Set	% Brix	RI	g DL-met·HCl/100 g solution ($C_{\text{calibrated}}^*$)	g DL-met·HCl/g solution (C_{actual}^*)
1	1	19.1	1.3624	15.2727	0.7697
	2	19.3	1.3628	15.4805	0.7751
	3	19.4	1.3629	15.5325	0.7806
	4	19.6	1.3632	15.6883	0.7804
Average					0.7765
2	1	19.3	1.3628	15.4805	0.7748
	2	19.6	1.3632	15.6883	0.7738
	3	19.4	1.3629	15.5325	0.7754
	4	19.2	1.3626	15.3766	0.7725
	5	19.3	1.3628	15.4805	0.7770
Average					0.7747
3	1	19.8	1.3636	15.8961	0.7943
	2	19.9	1.3637	15.9481	0.7952
	3	19.9	1.3637	15.9481	0.7951
	4	19.8	1.3636	15.8961	0.7967
	5	19.8	1.3636	15.8961	0.7981
	6	19.8	1.3636	15.8961	0.7958
	7	19.9	1.3637	15.9481	0.7969
	8	19.9	1.3637	15.9481	0.7988
	9	19.9	1.3637	15.9481	0.7979
Average					0.7965

Table A.6 Raw data of solubility measurement of L-met·HCl aqueous solution
at 5°C.

Batch	Set	% Brix	RI	g L-met·HCl/100 g solution ($C_{\text{calibrated}}^*$)	g L-met·HCl/g solution (C_{actual}^*)
1	1	16.3	1.3578	12.8831	0.6335
	2	16.1	1.3575	12.7273	0.6377
	3	14.9	1.3555	11.6883	0.5888
	4	15.0	1.3557	11.7922	0.5902
	5	15.0	1.3557	11.7922	0.5897
	6	15.0	1.3557	11.7922	0.5896
	7	15.0	1.3557	11.7922	0.5912
	8	15.0	1.3557	11.7922	0.5928
	9	15.1	1.3559	11.8961	0.5943
	10	15.0	1.3557	11.7922	0.5906
Average					0.5998
2	1	15.6	1.3567	12.3117	0.6179
	2	15.5	1.3565	12.2078	0.6105
	3	15.8	1.3570	12.4675	0.6218
	4	15.7	1.3568	12.3636	0.6201
	5	15.8	1.3570	12.4675	0.6233
	6	15.8	1.3570	12.4675	0.6245
Average					0.6197
3	1	15.4	1.3564	12.1558	0.6077
	2	15.4	1.3564	12.1558	0.6064
	3	15.4	1.3564	12.1558	0.6077
Average					0.6073

Table A.7 Raw data of solubility measurement of L-met·HCl aqueous solution
at 10°C.

Batch	Set	% Brix	RI	g L-met·HCl/100 g solution ($C_{\text{calibrated}}^*$)	g L-met·HCl/g solution (C_{actual}^*)
1	1	16.2	1.3577	12.8312	0.6301
	2	15.9	1.3572	12.5714	0.6278
	3	16.2	1.3577	12.8312	0.6284
	4	16.2	1.3577	12.8312	0.6264
Average					0.6282
2	1	15.3	1.3562	12.0519	0.6050
	2	15.8	1.3570	12.4675	0.6231
	3	15.8	1.3570	12.4675	0.6260
	4	15.8	1.3570	12.4675	0.6239
	5	15.5	1.3565	12.2078	0.6141
	6	15.9	1.3572	12.5714	0.6287
Average					0.6201
3	1	15.4	1.3564	12.1558	0.6090
	2	15.4	1.3564	12.1558	0.6102
	3	15.5	1.3565	12.2078	0.6111
	4	15.5	1.3565	12.2078	0.6105
	5	15.6	1.3567	12.3117	0.6150
Average					0.6112

Table A.8 Raw data of solubility measurement of L-met·HCl aqueous solution
at 25°C.

Batch	Set	% Brix	RI	g L-met·HCl/100 g solution ($C_{\text{calibrated}}^*$)	g L-met·HCl/g solution (C_{actual}^*)
1	1	16.4	1.3580	12.9870	0.6459
	2	16.2	1.3577	12.8312	0.6446
	3	16.4	1.3580	12.9870	0.6455
	4	16.5	1.3582	13.0909	0.6437
Average					0.6449
2	1	16.2	1.3577	12.8312	0.6406
	2	16.1	1.3575	12.7273	0.6354
	3	16.2	1.3577	12.8312	0.6429
	4	16.2	1.3577	12.8312	0.6419
Average					0.6402
3	1	16.5	1.3582	13.0909	0.6524
	2	16.5	1.3582	13.0909	0.6534
	3	16.4	1.3580	12.9870	0.6511
	4	16.5	1.3582	13.0909	0.6553
	5	16.6	1.3583	13.1429	0.6572
	6	16.6	1.3583	13.1429	0.6580
Average					0.6546

Table A.9 Raw data of solubility measurement of L-met·HCl aqueous solution
at 40°C.

Batch	Set	% Brix	RI	g L-met·HCl/100 g solution ($C_{\text{calibrated}}^*$)	g L-met·HCl/g solution (C_{actual}^*)
1	1	17.5	1.3598	13.9221	0.6894
	2	17.7	1.3601	14.0779	0.6876
	3	17.7	1.3601	14.0779	0.6941
	4	17.6	1.3600	14.0260	0.6906
Average					0.6904
2	1	17.7	1.3601	14.0779	0.6902
	2	17.3	1.3595	13.7662	0.6896
	3	17.4	1.3596	13.8182	0.6875
	4	17.3	1.3595	13.7662	0.6889
Average					0.6891
3	1	16.9	1.3588	13.4026	0.6721
	2	16.7	1.3585	13.2468	0.6623
	3	16.9	1.3588	13.4026	0.6707
	4	16.9	1.3588	13.4026	0.6724
Average					0.6694

Table A.10 Raw data of solubility measurement of the mixture compositions

(75% L-met·HCl : 25% D-met·HCl) aqueous solution at 5°C.

Batch	Set	% Brix	RI	g mixtures of met·HCl/ 100 g solution($C_{\text{calibrated}}^*$)	g mixtures of met·HCl/g solution(C_{actual}^*)
1	1	14.1	1.3543	11.0649	0.5538
	2	14.1	1.3543	11.0649	0.5519
	3	14.1	1.3543	11.0649	0.5533
	4	14.0	1.3541	10.9610	0.5501
	5	14.1	1.3543	11.0649	0.5535
	6	14.1	1.3543	11.0649	0.5550
	7	14.1	1.3543	11.0649	0.5545
Average					0.5532
2	1	13.8	1.3538	10.8052	0.5410
	2	13.8	1.3538	10.8052	0.5402
	3	13.8	1.3538	10.8052	0.5392
	4	13.8	1.3538	10.8052	0.5402
	5	13.8	1.3538	10.8052	0.5412
	6	13.7	1.3537	10.7532	0.5394
	7	13.8	1.3538	10.8052	0.5403
Average					0.5402
3	1	14.6	1.3551	11.4805	0.5758
	2	14.6	1.3551	11.4805	0.5773
	3	14.7	1.3553	11.5844	0.5794
	4	14.7	1.3553	11.5844	0.5806
	5	14.5	1.3549	11.3766	0.5772
	6	14.7	1.3553	11.5844	0.5791
	7	14.7	1.3553	11.5844	0.5797
	8	14.7	1.3553	11.5844	0.5810
	9	14.8	1.3554	11.6364	0.5813
Average					0.5790

Table A.11 Raw data of solubility measurement of the mixture compositions

(75% L-met·HCl : 25% D-met·HCl) aqueous solution at 10°C.

Batch	Set	% Brix	RI	g mixtures of met·HCl/ 100 g solution($C_{\text{calibrated}}^*$)	g mixtures of met·HCl/g solution(C_{actual}^*)
1	1	15.7	1.3568	12.3636	0.6195
	2	15.7	1.3568	12.3636	0.6167
	3	15.7	1.3568	12.3636	0.6191
	4	15.8	1.3570	12.4675	0.6222
	5	15.7	1.3568	12.3636	0.6183
	6	15.6	1.3567	12.3117	0.6154
	7	15.6	1.3567	12.3117	0.6145
	8	15.7	1.3568	12.3636	0.6168
Average					0.6178
2	1	15.1	1.3559	11.8961	0.5961
	2	15.1	1.3559	11.8961	0.5936
	3	15.1	1.3559	11.8961	0.5967
	4	15.1	1.3559	11.8961	0.5952
	5	15.1	1.3559	11.8961	0.5963
	6	15.1	1.3559	11.8961	0.5946
	7	14.9	1.3555	11.6883	0.5928
	8	15.1	1.3559	11.8961	0.5963
Average					0.5952
3	1	16.0	1.3573	12.6234	0.6298
	2	16.0	1.3573	12.6234	0.6293
	3	16.0	1.3573	12.6234	0.6305
	4	16.0	1.3573	12.6234	0.6294
Average					0.6298

Table A.12 Raw data of solubility measurement of the mixture compositions

(75% L-met·HCl : 25% D-met·HCl) aqueous solution at 25°C.

Batch	Set	% Brix	RI	g mixtures of met·HCl/ 100 g solution($C_{\text{calibrated}}^*$)	g mixtures of met·HCl/g solution(C_{actual}^*)
1	1	17.4	1.3596	13.8182	0.6910
	2	17.3	1.3595	13.7662	0.6912
	3	17.4	1.3596	13.8182	0.6903
	4	17.4	1.3596	13.8182	0.6924
	5	17.4	1.3596	13.8182	0.6924
	6	17.4	1.3596	13.8182	0.6903
	7	17.4	1.3596	13.8182	0.6906
Average					0.6912
2	1	17.4	1.3596	13.8182	0.6916
	2	17.4	1.3596	13.8182	0.6935
	3	17.4	1.3596	13.8182	0.6910
	4	17.5	1.3598	13.9221	0.6949
	5	17.4	1.3596	13.8182	0.6934
	6	17.5	1.3598	13.9221	0.6966
	7	17.5	1.3598	13.9221	0.6958
	8	17.4	1.3596	13.8182	0.6920
Average					0.6936
3	1	17.7	1.3601	14.0779	0.7024
	2	17.7	1.3601	14.0779	0.7020
	3	17.7	1.3601	14.0779	0.7037
	4	17.7	1.3601	14.0779	0.7048
	5	17.7	1.3601	14.0779	0.7057
	6	17.7	1.3601	14.0779	0.7027
Average					0.7036

Table A.13 Raw data of solubility measurement of the mixture compositions

(75% L-met·HCl : 25% D-met·HCl) aqueous solution at 40°C.

Batch	Set	% Brix	RI	g mixtures of met·HCl/ 100 g solution($C_{\text{calibrated}}^*$)	g mixtures of met·HCl/g solution(C_{actual}^*)
1	1	18.1	1.3608	14.4416	0.7225
	2	18.2	1.3609	14.4935	0.7232
	3	18.2	1.3609	14.4935	0.7252
	4	18.2	1.3609	14.4935	0.7244
	5	18.2	1.3609	14.4935	0.7245
	6	18.1	1.3608	14.4416	0.7220
	7	18.2	1.3609	14.4935	0.7244
	8	18.1	1.3608	14.4416	0.7234
Average					0.7237
2	1	18.4	1.3613	14.7013	0.7362
	2	18.5	1.3614	14.7532	0.7364
	3	18.2	1.3609	14.4935	0.7348
	4	18.5	1.3614	14.7532	0.7371
	5	18.4	1.3613	14.7013	0.7374
	6	18.5	1.3614	14.7532	0.7365
	7	18.5	1.3614	14.7532	0.7377
	8	18.4	1.3613	14.7013	0.7403
Average					0.7371
3	1	18.8	1.3619	15.0130	0.7513
Average					0.7513

Table A.2 to Table A.13 show the 3 average values for the actual concentration ($C_{\text{actual, Avg}}^*$) in units of g met·HCl/g solution of DL-met·HCl, L-met·HCl, and 75% L-met·HCl : 25% D-met·HCl at 5°C, 10°C, 25°C, and 40°C, respectively. The concentration units can be changed to g met·HCl/100 g H₂O as shown example in Table A.14. Likewise, the average actual concentration can be used to calculate the average mass fraction (\bar{w}) of the solubility data as shown example in Table A.15. All the calculated solubility results were shown in Chapter II (Table 2.2 and Table 2.3, respectively).

Table A.14 The change of concentration unit of the DL-met·HCl aqueous solution at 5°C (from Table A.2).

Batch	^a $C_{\text{actual, Avg}}^*$	DL-met·HCl(g)	H ₂ O(g)	^b $C_{\text{DL-met-HCl}}^*$	^b $C_{\text{DL-met-HCl, Avg}}^*$
1 st	0.7388	0.7388	0.2612	282.8	257.9 ≈ 258
2 nd	0.7129	0.7129	0.2871	248.3	
3 rd	0.7081	0.7081	0.2919	242.6	
Summation				773.7	

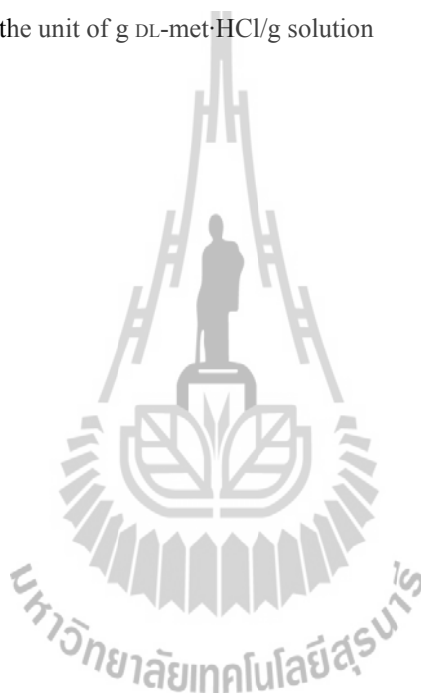
Remark: ^a $C_{\text{actual, Avg}}^*$ is in the unit of g DL-met·HCl/g solution

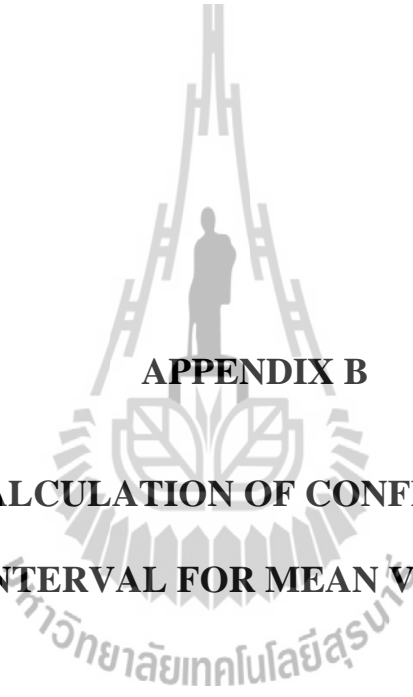
^b $C_{\text{DL-met-HCl}}^*$ and $C_{\text{DL-met-HCl, Avg}}^*$ is in the unit of g DL-met·HCl/100 g H₂O

Table A.15 Average solubility data in mass fraction (\bar{w}) of the DL-met·HCl aqueous solution at 5°C (from Table A.2).

Batch	${}^a C_{\text{actual, Avg}}^*$	DL-met·HCl (g)	H ₂ O (g)	$w_{\text{DL-met·HCl}}$	$\bar{w}_{\text{DL-met·HCl}}$
1 st	0.7388	0.7388	0.2612	0.7388	0.7199 \approx 0.720
2 nd	0.7129	0.7129	0.2871	0.7129	
3 rd	0.7081	0.7081	0.2919	0.7081	
Summation				2.1598	

Remark: ${}^a C_{\text{actual, Avg}}^*$ is in the unit of g DL-met·HCl/g solution



The logo of Sakon Nakhon Rajabhat University is a large, faint watermark in the background. It features a central figure of a person standing within a stylized, multi-tiered structure that resembles a traditional Thai architectural element or a modern emblem. The structure is composed of several vertical and horizontal lines forming a triangular shape with a central opening.

APPENDIX B
CALCULATION OF CONFIDENCE
INTERVAL FOR MEAN VALUES

มหาวิทยาลัยเทคโนโลยีสุรนารี

B.1 Confidence Interval for the Mean Value

This Appendix provides a framework and example to calculate experimental errors and determine uncertainty limits in laboratory measurements. In this work only the 95% confidence limits are considered and given as the uncertainty limit, the upper and lower boundaries of the error bar for the mean values, and values of a confidence interval. The t-distribution is used when the sample size less than 30 samples ($n < 30$), which is used in this work. If the sample size is greater than 30 samples ($n > 30$), the z-distribution is used instead of the t-distribution.

The t-distribution confidence interval for the mean value is defined by (Doebelin, 1995)

$$\text{Confidence interval} = \bar{x} \pm t_{\alpha/2, n-1} \sigma_{\bar{x}} \quad (\text{B.1})$$

The sample mean (\bar{x}) and the standard error of the mean ($\sigma_{\bar{x}}$) can be estimated by

$$\bar{x} = \frac{\sum_{i=1}^n x_i}{n} \quad (\text{B.2})$$

In this case, the sample size (n) is less than 30 samples. Thus, the standard deviation of the real distribution can be estimated by the standard deviation of measured values ($\sigma_x \cong s_x$).

$$\sigma_{\bar{x}} = \frac{\sigma_x}{\sqrt{n}} \cong \frac{s_x}{\sqrt{n}} \quad (\text{B.3})$$

The standard deviation of measured values (s_x) is given by

$$s_x = \left[\frac{\sum_{i=1}^n (x_i - \bar{x})^2}{n-1} \right]^{1/2} \quad (\text{B.4})$$

Substituting equation (B.3) into equation (B.1) becomes

$$\text{Confidence interval} \equiv \bar{x} \pm t_{\alpha/2, n-1} \frac{s_x}{\sqrt{n}} \quad (\text{B.5})$$

The t-distribution is described by the degree of freedom, $f = n-1$, and a parameter α is defined by

$$\alpha \equiv 1.00 - \text{decimal value of confidence value} \quad (\text{B.6})$$

The t is the percentage point of the t-distribution in equation (B.5) can be determined from Table B.1, which is located in the $(n-1)^{\text{st}}$ row and the $\alpha/2$ column.

Table B.1 The percentage points $t_{\alpha/2, n-1}$ of the t-distribution (Doebelin, 1995).

$n-1 \backslash \alpha/2$	0.150	0.100	0.050	0.025	0.010	0.005
1	1.963	3.078	6.314	12.706	31.821	63.657
2	1.386	1.886	2.920	4.303	6.965	9.925
3	1.250	1.638	2.353	3.182	4.541	5.841
4	1.190	1.533	2.132	2.776	3.747	4.604
5	1.156	1.476	2.015	2.571	3.365	4.032
6	1.134	1.440	1.943	2.447	3.143	3.707
7	1.119	1.415	1.895	2.365	2.998	3.499
8	1.108	1.397	1.860	2.306	2.896	3.355
9	1.100	1.383	1.833	2.262	2.821	3.250
10	1.093	1.372	1.812	2.228	2.764	3.169

Note: The full form of this table can be found in a number of references.

From Table A.14 (in Appendix A), the 95% confidence interval for the mean value of the solubility data of the DL-met·HCl aqueous solution at 5°C can be computed as follows:

1st step : An average DL-met·HCl solubility data (the sample mean, $C_{\text{DL-met-HCl, Avg}}^*$) was calculated by using equation (B.2),

$$C_{\text{DL-met-HCl, Avg}}^* = 257.9 \approx 258 \text{ g DL-met·HCl/100 g H}_2\text{O}$$

2nd step : Compute the standard deviation of the solubility data (s_x) by using equation (B.4),

$$s_x = \left[\frac{(282.8 - 257.9)^2 + (248.3 - 257.9)^2 + (242.6 - 257.9)^2}{3 - 1} \right]^{1/2}$$

$$s_x = 21.78 \text{ g DL-met}\cdot\text{HCl}/100 \text{ g H}_2\text{O}$$

3rd step : Compute a parameter α of 95% confidence interval by using equation (B.6),

$$\alpha = 1.00 - 0.95 = 0.05$$

$$\therefore \alpha/2 = 0.025$$

where the sample size (n) = 3, the degree of freedom (f) = $n-1 = 2$. From Table B.1, the value of $t_{\alpha/2, n-1}$ is given by $t_{0.025, 2}$ which is equal to 4.303. Therefore, 95% confidence interval for the mean value of the solubility data of DL-met·HCl aqueous solution at 5°C is

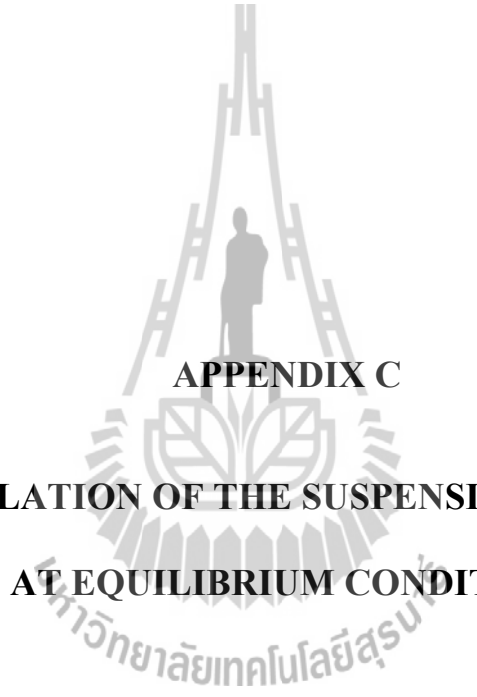
$$\text{Confidence interval} = 258 \pm (4.303) \frac{21.78}{\sqrt{3}} = 258 \pm 54 \text{ g DL-met}\cdot\text{HCl}/100 \text{ g H}_2\text{O}$$

This means that the best estimate of solubility data of DL-met·HCl aqueous solution at 5°C ($C_{\text{DL-met}\cdot\text{HCl}, \text{Avg}}^*$) is 258 g DL-met·HCl/100 g H₂O, and the true value of DL-met·HCl solubility data is somewhere between 204 and 312 g DL-met·HCl/100 g H₂O.

B.2 Reference

Doebelin, E. O. (1995). **Engineering experimentation: Planning, execution, reporting**. Singapore: McGraw-Hill.





APPENDIX C

CALCULATION OF THE SUSPENSION DENSITY

AT EQUILIBRIUM CONDITION

The suspension density (g crystal/g solution) of DL-met·HCl aqueous solution was measured with the relative supersaturation (σ) of 0.005 and 0.01 at 10°C aforementioned in Chapter IV. 40 g of total solution was used to represent the calculation of the suspension density at equilibrium condition of each of the relative supersaturation values.

C.1 The Suspension Density at Equilibrium Condition

with $\sigma = 0.005$

C.1.1 Calculation at Initial Condition ($t = 0$)

Data from Appendix A, Table A.3: relative supersaturation (σ) = 0.005, and total weight of DL-met·HCl aqueous solution = 40 g.

$$C_{\text{DL-met}\cdot\text{HCl, Avg}}^* \text{ at } 10^\circ\text{C} = \frac{0.7414 + 0.7436 + 0.7203}{3}$$

$$= 0.7351 \text{ g DL-met}\cdot\text{HCl/g solution}$$

In Chapter III, equation (3.1) and (3.3) can be defined as

$$\sigma = \frac{c_o - c^*}{c^*} \quad (\text{C.1})$$

Substituting σ and $C_{\text{DL-met}\cdot\text{HCl, Avg}}^*$ into equation (C.1), obtains

$$0.005 = \frac{c_o - 0.7351}{0.7351}$$

$$\therefore C_o = 0.7388 \text{ g DL-met}\cdot\text{HCl/g solution}$$

Thus, weight of DL-met·HCl and weight of water can be estimated as follow:

$$\begin{aligned}\text{Weight of DL-met}\cdot\text{HCl} &= C_o \times \text{Total weight of aqueous solution} \\ &= (0.7388 \text{ g DL-met}\cdot\text{HCl/g solution}) \times (40 \text{ g solution}) \\ &= 29.5520 \text{ g DL-met}\cdot\text{HCl}\end{aligned}$$

$$\begin{aligned}\text{Weight of water} &= (1-C_o) \times \text{Total weight of aqueous solution} \\ &= (1-0.7388) \text{ g H}_2\text{O/g solution} \times (40 \text{ g solution}) \\ &= 10.4480 \text{ g H}_2\text{O}\end{aligned}$$

C.1.2 Calculation at Equilibrium Condition ($t = \infty$)

Weight of DL-met·HCl can be estimated from

$$C_{\text{DL-met}\cdot\text{HCl, Avg}}^* = \frac{x}{x + \text{water}} \quad (\text{C.2})$$

where $C_{\text{DL-met}\cdot\text{HCl, Avg}}^* = 0.7351 \text{ g DL-met}\cdot\text{HCl/g solution}$

$x =$ weight of DL-met·HCl at equilibrium condition

$\text{water} =$ weight of water at equilibrium condition

$= 10.4480 \text{ g H}_2\text{O}$

Thus, weight of DL-met·HCl at equilibrium condition:

$$0.7351 = \frac{x}{x + 10.4480} \quad ; \quad \text{g DL-met}\cdot\text{HCl/g solution}$$

$$\therefore x = 28.9933 \text{ g DL-met}\cdot\text{HCl}$$

Weight of DL-met·HCl at initial condition ($t = 0$) and equilibrium condition ($t = \infty$) can be calculated from the weight of new crystal formed in the aqueous solution by:

$$\begin{aligned}
 \text{New crystal} &= \text{DL-met}\cdot\text{HCl at initial} - \text{DL-met}\cdot\text{HCl at equilibrium} \\
 &= 29.5520 - 28.9933 \text{ g} \\
 &= 0.5587 \text{ g}
 \end{aligned}$$

1.0000 g of seed crystal was used in the preferential crystallization:

$$\begin{aligned}
 \text{Total weight of crystal} &= \text{New crystal} + \text{Seed crystal} \\
 &= 0.5587 + 1.0000 \text{ g} \\
 &= 1.5587 \text{ g}
 \end{aligned}$$

Weight of liquid at equilibrium condition ($t = \infty$) can be determined from material balance of total weight at initial and equilibrium conditions:

$$\text{Total weight at initial} = \text{Total weight at equilibrium} \quad (\text{C.3})$$

$$\begin{aligned}
 \text{where Total weight at initial} &= \text{weight of seed crystal} + \text{weight of liquid} \\
 &= 1.0000 \text{ g} + 40 \text{ g}
 \end{aligned}$$

$$\begin{aligned}
 \text{Total weight equilibrium} &= \text{total weight of crystal} + \text{weight of liquid} \\
 &= 1.5587 \text{ g} + \text{weight of liquid (g)}
 \end{aligned}$$

Equation (C.3), becomes

$$\begin{aligned} \text{Total weight at initial} &= \text{Total weight at equilibrium} \\ 1.0000 \text{ g} + 40 \text{ g} &= 1.5587 \text{ g} + \text{weight of liquid (g)} \end{aligned}$$

$$\therefore \text{Weight of liquid at equilibrium} = 39.4413 \text{ g}$$

From equation (4.2) in Chapter IV, the suspension density at equilibrium condition, $M_{T,(t=\infty)}$ obtains

$$M_{T,(t=\infty)} = \left[\frac{\text{weight of crystal}}{\text{weight of crystal} + \text{weight of liquid}} \right]_{t=\infty} \quad (\text{C.4})$$

where weight of crystal = 1.5587 g
 weight of liquid at equilibrium = 39.4413 g

Substituting the values into equation (C.4),

$$M_{T,(t=\infty)} = \left[\frac{1.5587}{1.5587 + 39.4413} \right]_{t=\infty} ; \quad \text{g crystal/g solution}$$

$$\therefore M_{T,(t=\infty)} = 0.0380 \text{ g crystal/g solution}$$

Hence, the suspension density at the equilibrium condition, $M_{T,(t=\infty)}$, is 0.0380 g crystal/g solution for $\sigma = 0.005$ at 40 g of total aqueous solution.

C.2 The Suspension Density at Equilibrium Condition

with $\sigma = 0.010$

C.2.1 Calculation at Initial Condition ($t = 0$)

Data from Appendix A, Table A.3: relative supersaturation (σ) = 0.010, and total weight of DL-met·HCl aqueous solution = 40 g.

$$C_{\text{DL-met}\cdot\text{HCl, Avg}}^* \text{ at } 10^\circ\text{C} = 0.7351 \text{ g DL-met}\cdot\text{HCl/g solution}$$

Substituting σ and $C_{\text{DL-met}\cdot\text{HCl, Avg}}^*$ into equation (C.1), obtains

$$0.010 = \frac{C_o - 0.7351}{0.7351}$$

$$\therefore C_o = 0.7425 \text{ g DL-met}\cdot\text{HCl/g solution}$$

Thus, the weight of DL-met·HCl and the weight of water can be estimated as follow:

$$\begin{aligned} \text{Weight of DL-met}\cdot\text{HCl} &= C_o \times \text{Total weight of aqueous solution} \\ &= (0.7425 \text{ g DL-met}\cdot\text{HCl/g solution}) \times (40 \text{ g solution}) \\ &= 29.7000 \text{ g DL-met}\cdot\text{HCl} \end{aligned}$$

$$\begin{aligned} \text{Weight of water} &= (1 - C_o) \times \text{Total weight of aqueous solution} \\ &= (1 - 0.7425) \text{ g H}_2\text{O/g solution} \times (40 \text{ g solution}) \\ &= 10.3000 \text{ g H}_2\text{O} \end{aligned}$$

C.2.2 Calculation at Equilibrium Condition ($t = \infty$)

Weight of DL-met·HCl can be estimated from equation (C.2):

$$C_{\text{DL-met}\cdot\text{HCl, Avg}}^* = \frac{x}{x + \text{water}}$$

where $C_{\text{DL-met}\cdot\text{HCl, Avg}}^* = 0.7351 \text{ g DL-met}\cdot\text{HCl/g solution}$

$x =$ weight of DL-met·HCl at equilibrium condition

$\text{water} =$ weight of water at equilibrium condition

$= 10.3000 \text{ g H}_2\text{O}$

Thus, weight of DL-met·HCl at equilibrium condition:

$$0.7351 = \frac{x}{x + 10.3000} ; \text{ g DL-met}\cdot\text{HCl/g solution}$$

$$\therefore x = 28.5826 \text{ g DL-met}\cdot\text{HCl}$$

Weight of DL-met·HCl at initial condition ($t=0$) and equilibrium condition ($t = \infty$) can be calculated the weight of new crystal occurred in aqueous solution by:

$$\begin{aligned} \text{New crystal} &= \text{DL-met}\cdot\text{HCl at initial} - \text{DL-met}\cdot\text{HCl at equilibrium} \\ &= 29.7000 - 28.5826 \text{ g} \\ &= 1.1174 \text{ g} \end{aligned}$$

1.0000 g of seed crystal was used in the preferential crystallization:

$$\begin{aligned}\text{Total weight of crystal} &= \text{New crystal} + \text{Seed crystal} \\ &= 1.1174 + 1.0000 \text{ g} \\ &= 2.1174 \text{ g}\end{aligned}$$

Weight of liquid at equilibrium condition ($t = \infty$) can be determined from material balance of total weight at initial and equilibrium conditions as shown in equation (C.3), where

$$\begin{aligned}\text{Total weight at initial} &= \text{weight of seed crystal} + \text{weight of liquid} \\ &= 1.0000 \text{ g} + 40 \text{ g} \\ \text{Total weight equilibrium} &= \text{total weight of crystal} + \text{weight of liquid} \\ &= 2.1174 \text{ g} + \text{weight of liquid (g)}\end{aligned}$$

Equation (C.3), becomes

$$\begin{aligned}\text{Total weight at initial} &= \text{Total weight at equilibrium} \\ 1.0000 \text{ g} + 40 \text{ g} &= 2.1174 \text{ g} + \text{weight of liquid (g)}\end{aligned}$$

$$\therefore \text{Weight of liquid at equilibrium} = 38.8826 \text{ g}$$

The suspension density at equilibrium condition, $M_{T,(t=\infty)}$ can be estimated from equation (C.4), where

weight of crystal = 2.1174 g

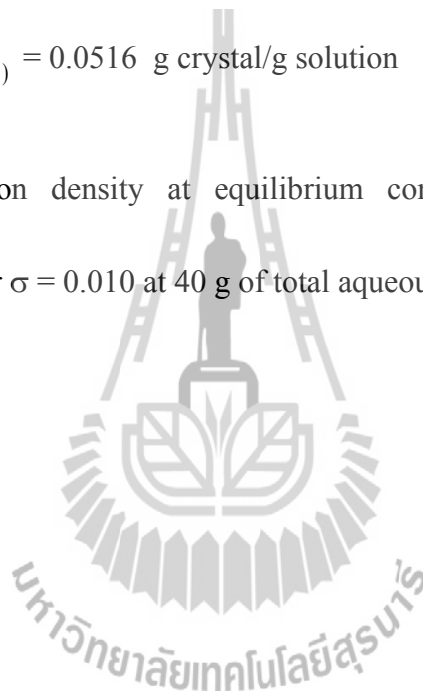
weight of liquid at equilibrium = 38.8826 g

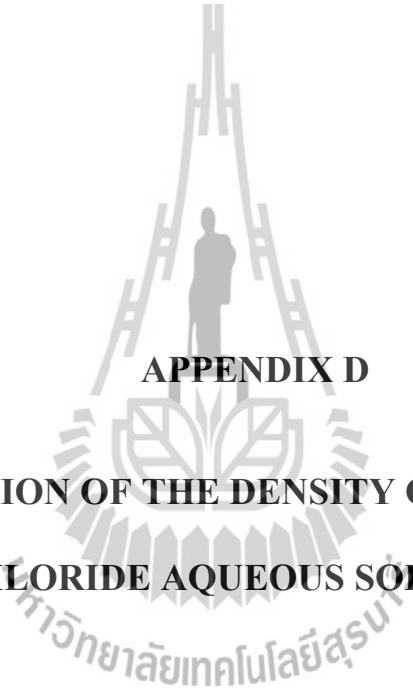
Substituting the values into equation (C.4),

$$M_{T,(t=\infty)} = \left[\frac{2.1174}{2.1174 + 38.8826} \right]_{t=\infty} ; \quad \text{g crystal/g solution}$$

$$\therefore M_{T,(t=\infty)} = 0.0516 \text{ g crystal/g solution}$$

Hence, the suspension density at equilibrium condition, $M_{T,(t=\infty)}$, is 0.0516 g crystal/g solution for $\sigma = 0.010$ at 40 g of total aqueous solution.





APPENDIX D

**DETERMINATION OF THE DENSITY OF DL-METHIONINE
HYDROCHLORIDE AQUEOUS SOLUTION AT 25°C**

D.1 Example of Calculation of Density Data

The density of DL-met·HCl aqueous solution was determined for use to change the concentrations units of met·HCl, from g met·HCl/g solution to g met·HCl/ml solution. A 2 ml of density bottle was used in this experiment as shown in Figure D.1. 6 g of total solution of DL-met·HCl was prepared for five concentration values (0.15, 0.30, 0.45, 0.60, and 0.75 g DL-met·HCl/g solution) at room temperature. These solutions were maintained in the water bath at 25°C for about an hour, to ensure the homogeneous temperature for the experiment. An example of density determination of DL-met·HCl aqueous solution at 25°C for a concentration of 0.15 g DL-met·HCl/g solution is shown as below.



Figure D.1 A 2 ml of density bottle.

For determination of the density bottle volume, it can be calibrated for the exact volume with pure distilled water at 25°C before starting the experiment. The density of pure water at 1 atmosphere and 25°C = 0.997048 g/ml (Haynes, 2010-2011).

The average weight of water in 2 ml of density bottle for 5 times measurement

$$= \frac{1.8705+1.8611+1.8783+1.8781+1.8729}{5} \quad ; \quad \text{g}$$

$$= 1.87218 \text{ g}$$

The exact total volume of a 2 ml density bottle

$$= \frac{\text{Average weight of water}}{\text{density of water at } 25^{\circ}\text{C, 1 atm}} \quad ; \quad \text{ml}$$

$$= \frac{1.87218 \text{ g}}{0.997048 \text{ g/ml}}$$

$$= 1.87772 \text{ ml}$$

The concentration of DL-met·HCl aqueous solution at 0.15 g DL-met·HCl/g solution was prepared for a 6 g of total solution.

$$\text{Weight of DL-met}\cdot\text{HCl} = 0.15 \times 6 = 0.9 \text{ g DL-met}\cdot\text{HCl}$$

$$\text{Weight of water} = (1-0.15) \times 6 = 5.1 \text{ g H}_2\text{O}$$

$$\text{Prepared weight of DL-met}\cdot\text{HCl} = 0.9003 \text{ g DL-met}\cdot\text{HCl}$$

$$\text{Prepared weight of water} = 5.1155 \text{ g H}_2\text{O}$$

The exact concentration of DL-met·HCl solution ($C_{\text{DL-met}\cdot\text{HCl}}$) is,

$$C_{\text{DL-met}\cdot\text{HCl}} = \frac{\text{g of DL-met}\cdot\text{HCl}}{\text{g of DL-met}\cdot\text{HCl} + \text{g of water}}$$

$$C_{\text{DL-met}\cdot\text{HCl}} = \frac{0.9003 \text{ g}}{0.9003 \text{ g} + 5.1155 \text{ g}}$$

$$\therefore C_{\text{DL-met}\cdot\text{HCl}} = 0.1497 \text{ g DL-met}\cdot\text{HCl/g solution}$$

A 0.9003 g of DL-met·HCl was dissolved into 5.1155 g of H₂O until dissolution was complete, and was kept in a water bath at 25°C for about an hour before weighing the DL-met·HCl solution in the density bottle on a balance.

Total weight of DL-met·HCl solution in the density bottle (size of total volume 1.87772 ml) = 1.9604 g

Thus, the density of DL-met·HCl aqueous solution at 25°C can be calculated as follows:

$$\rho_{\text{DL-met}\cdot\text{HCl}} @ 25^\circ\text{C} = \frac{\text{Total weight of solution}}{\text{Total volume of solution}}$$

$$\rho_{\text{DL-met}\cdot\text{HCl}} @ 25^\circ\text{C} = \frac{1.9604 \text{ g solution}}{1.87772 \text{ ml solution}}$$

$$\therefore \rho_{\text{DL-met}\cdot\text{HCl}} @ 25^\circ\text{C} = 1.04403 \text{ g solution/ml solution}$$

The experimental results of density of DL-met·HCl aqueous solution at 25°C for other concentrations are shown in Table D.1

Table D.1 The experimental results of density of DL-met·HCl aqueous solution at 25°C.

$C_{\text{DL-met}\cdot\text{HCl}}$ (g DL-met·HCl/g solution)	Weight of total solution (g)	$\rho_{\text{DL-met}\cdot\text{HCl}}$ (g solution/ml solution)
0.0000*	-	0.9970
0.1497	1.9604	1.0440
0.2999	2.0448	1.0890
0.4501	2.1418	1.1406
0.5988	2.2321	1.1887
0.7136	2.3032	1.2266

Remark : * The result of pure water at 25°C from the reference.

The data on Table D.1 can be plotted, graphing the relationship between the density of DL-met·HCl aqueous solution (g solution/ml solution) at 25°C versus the concentration of DL-met·HCl aqueous solution (g DL-met·HCl/g solution) as shown in Figure D.2. The density data of DL-met·HCl aqueous solution at 25°C in the concentration range of 0.00 – 0.80 g DL-met·HCl/g solution was fitted using a linear polynomial equation, with the result shown in equation (D.1).

$$\rho_{\text{DL-met}\cdot\text{HCl}@25^\circ\text{C}} = (0.3224)C_{\text{DL-met}\cdot\text{HCl}} + 0.9954 \quad ; \quad r^2 = 0.9996 \quad (\text{D.1})$$

where $C_{\text{DL-met}\cdot\text{HCl}}$ is the concentration of DL-met·HCl aqueous solution in g DL-met·HCl/g solution and $\rho_{\text{DL-met}\cdot\text{HCl}@25^\circ\text{C}}$ is the density of DL-met·HCl aqueous solution at 25°C in g solution/ml solution.

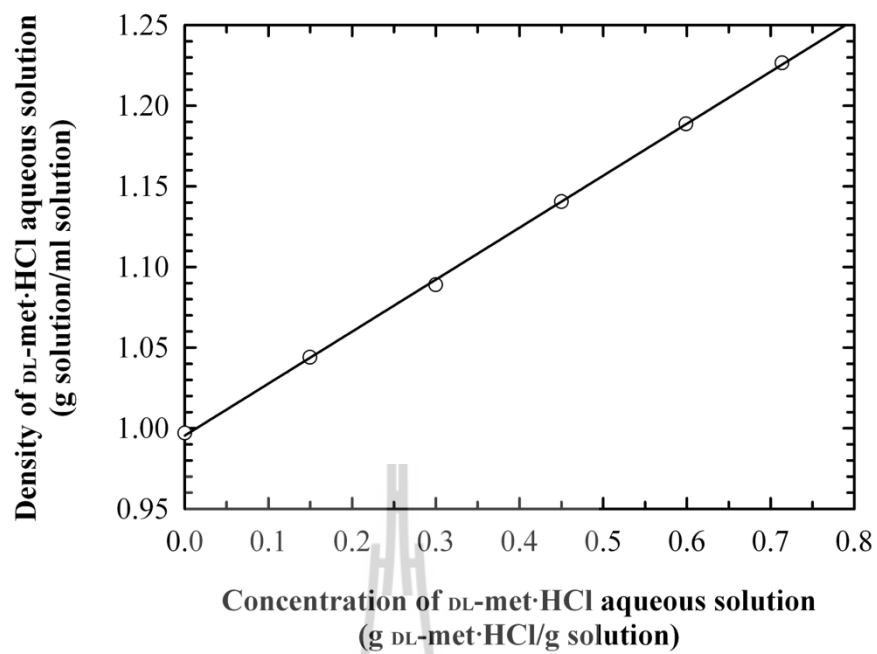


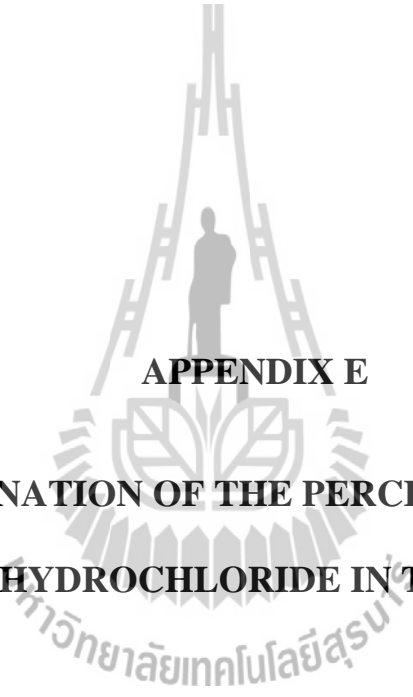
Figure D.2 The density of DL-met·HCl aqueous solution at 25°C.



D.2 Reference

Haynes, W. M. (2010-2011). **CRC Handbook of chemistry and Physics: A ready-reference book of chemical and physical data**. Boca Raton, Florida: CRC Press, Taylor & Francis Group.





APPENDIX E

**DETERMINATION OF THE PERCENT PURITY OF
L-METHIONINE HYDROCHLORIDE IN THE CRYSTAL PHASE**

The experimental data for preferential crystallization of DL-met·HCl aqueous solution with the relative supersaturation (σ) of 0.005 at 2 minutes of resolution time (1st batch) is used as an example to represent determination of the percent purity of L-met·HCl in the crystal phase. It can be divided into 2 parts; the first is calculation of the concentration of dissolved crystal in solution, and the second part is calculation of the percent purity of L-met·HCl in the crystal.

E.1 Calculation of Concentration of Crystal Solution

A sample of crystal obtained from an experiment of preferential crystallization was prepared to a DL-met·HCl aqueous solution at 25°C to measure the concentration and optical rotation, respectively. Data from Table 4.5 in Chapter IV:

Relative supersaturation (σ) = 0.005

Resolution time = 2 minutes (1st batch)

% Brix at 25°C = 8.5

Optical rotation (α) at 25°C = +01.56°

From Table A.1 in Appendix A the result can be converted from % Brix to RI, giving

Refractive index (RI) at 25°C = 1.3456

The concentration of DL-met·HCl aqueous solution ($C_{\text{DL-met·HCl}}$) was calculated using equation (2.1) in Chapter II:

$$RI = (1.925 \times 10^{-3})C_{\text{DL-met}\cdot\text{HCl}} + 1.3330$$

$$C_{\text{DL-met}\cdot\text{HCl}} = 6.5299 \text{ g DL-met}\cdot\text{HCl}/100 \text{ g solution}$$

$$= 0.065299 \text{ g DL-met}\cdot\text{HCl}/\text{g solution}$$

Equation (D.1) in Appendix D was used to change the concentration units of the DL-met·HCl aqueous solution at 25°C from g DL-met·HCl/g solution to g solution/ml solution:

$$\rho_{\text{DL-met}\cdot\text{HCl}@25^\circ\text{C}} = (0.3224)C_{\text{DL-met}\cdot\text{HCl}} + 0.9954 \quad (\text{E.1})$$

Substituting $C_{\text{DL-met}\cdot\text{HCl}} = 0.065299 \text{ g DL-met}\cdot\text{HCl}/\text{g solution}$ into equation (E.1):

$$\therefore \rho_{\text{DL-met}\cdot\text{HCl}@25^\circ\text{C}} = 1.0165 \text{ g solution/ml solution}$$

Thus, the concentration of crystal solution (C_{crystal}) is

$$C_{\text{crystal}} = C_{\text{DL-met}\cdot\text{HCl}} \times \rho_{\text{DL-met}\cdot\text{HCl}@25^\circ\text{C}}$$

$$= \left[0.065299 \frac{\text{g DL-met}\cdot\text{HCl}}{\text{g solution}} \right] \times \left[1.0165 \frac{\text{g solution}}{\text{ml solution}} \right]$$

$$= 0.066376 \text{ g DL-met}\cdot\text{HCl}/\text{ml solution}$$

$$= 6.6376 \text{ g DL-met}\cdot\text{HCl}/100 \text{ ml solution}$$

Hence, the concentration of crystal solution at 25°C is 6.6376 g DL-met·HCl/100 ml solution.

E.2 Calculation of the Percent Purity of L-met·HCl in Crystal

The percent purity of L-met·HCl in the crystal can be calculated from equation (4.9) in Chapter IV:

$$\% \text{ Purity of L - crystal} = \left[[\alpha]_D^{25} + (18.26^\circ) \right] \times \left[\frac{(100-0)}{(2) \times (18.26^\circ)} \right] \quad (\text{E.2})$$

From equation (4.1) in Chapter IV, the specific rotation at 25°C, $[\alpha]_D^{25}$, is given by

$$[\alpha]_D^{25} = \frac{100 \times \alpha}{c \times l} \quad (\text{E.3})$$

where α = the optical rotation at 25°C
 = + 01.56°
 c = the concentration of crystal solution at 25°C
 = 6.6376 g DL-met·HCl/100 ml solution
 l = the length of the polarimeter tube
 = 2 dm

Substituting all values into equation (E.3), gives

$$[\alpha]_D^{25} = \frac{100 \times (+ 01.56^\circ)}{\left(6.6376 \frac{\text{g DL - met} \cdot \text{HCl}}{100 \text{ ml solution}} \right) \times (2 \text{ dm})}$$

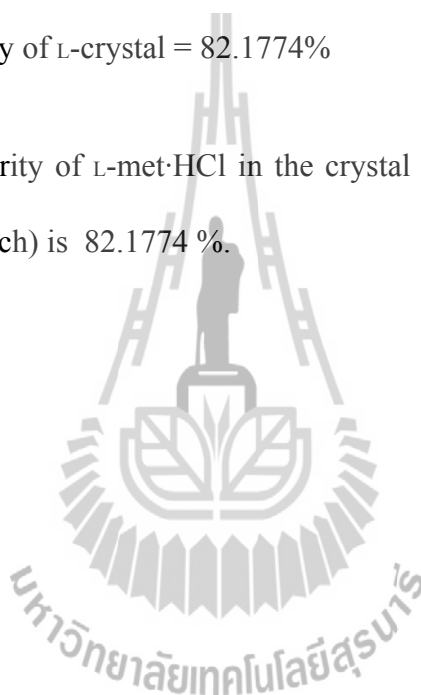
$$\therefore [\alpha]_D^{25} = +11.7512^\circ$$

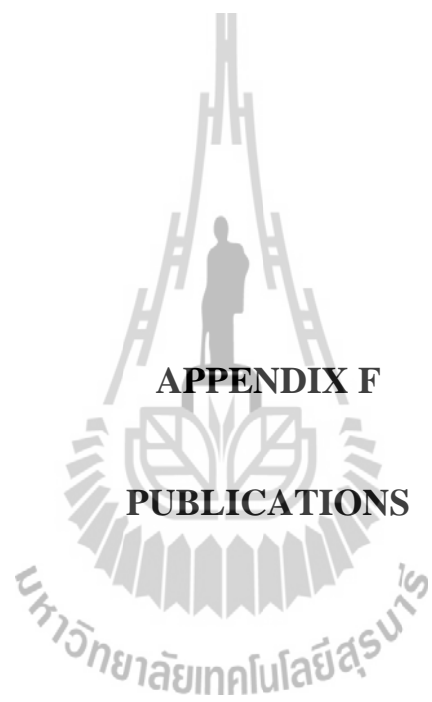
Substituting $[\alpha]_D^{25} = +11.7512^\circ$ into equation (E.2), gives

$$\% \text{ Purity of L-crystal} = [(+11.7512^\circ) + (18.26^\circ)] \times \left[\frac{(100-0)}{(2) \times (18.26^\circ)} \right]$$

$$\therefore \% \text{ Purity of L-crystal} = 82.1774\%$$

Hence, the percent purity of L-met·HCl in the crystal for $\sigma = 0.005$ at 2 minutes of resolution time (1st batch) is 82.1774 %.





APPENDIX F

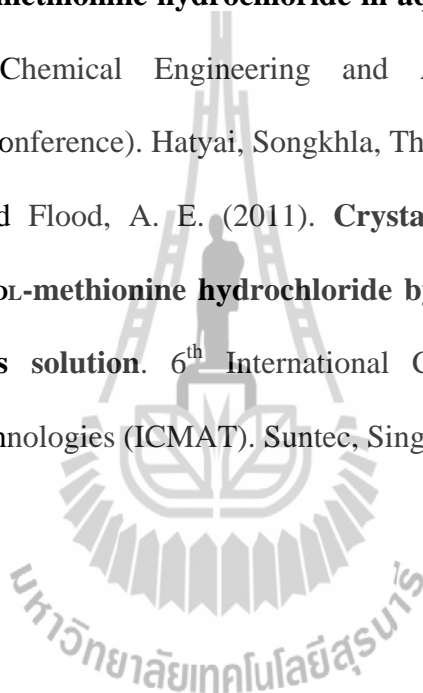
PUBLICATIONS

List of Publications

Srimahaprom, W. and Flood, A. E. (2011). **Crystal growth rates and optical resolution of DL-methionine hydrochloride by preferential crystallization from aqueous solution.** Journal of Crystal Growth, Article in Press.

Srimahaprom, W. and Flood, A. E. (2011). **Solubility equilibria measurements of enantiomeric methionine hydrochloride in aqueous solution.** The 21st Thai Institute of Chemical Engineering and Applied Chemistry (TIChE International Conference). Hatyai, Songkhla, Thailand.

Srimahaprom, W. and Flood, A. E. (2011). **Crystal growth rates and optical resolution of DL-methionine hydrochloride by preferential crystallization from aqueous solution.** 6th International Conference on Materials for Advanced Technologies (ICMAT). Suntec, Singapore.





Contents lists available at SciVerse ScienceDirect

Journal of Crystal Growth

journal homepage: www.elsevier.com/locate/jcrysgr

Crystal growth rates and optical resolution of DL-methionine hydrochloride by preferential crystallization from aqueous solution

Watcharakarn Srimahaprom, Adrian E. Flood*

School of Chemical Engineering, Suranaree University of Technology, 111 University Avenue, Muang District, Nakhon Ratchasima, Thailand

ARTICLE INFO

Keywords:

A2. Growth from solutions
A2. Preferential crystallization
B1. DL-methionine hydrochloride

ABSTRACT

Optical resolution of DL-methionine hydrochloride (DL-met·HCl) by preferential crystallization was studied for the purification of L-met·HCl (the desired enantiomer) from supersaturated solutions of DL-met·HCl. The nucleation thresholds (NT) of DL-met·HCl affect the maximum resolution time suitable for preferential crystallization and also the percentage purity of the product crystals. Crystal growth rates of L-met·HCl single crystals both in supersaturated solutions of DL-met·HCl and in supersaturated solutions of pure L-met·HCl were measured in order to model the preferential crystallization more effectively. Results showed that the growth rate depends strongly on the relative supersaturation (especially from pure L-met·HCl solutions), that there is a wide crystal growth rate distribution in growth from both types of solution, and that the growth is faster from pure L-met·HCl solutions, as expected. A batch crystallizer seeded with L-met·HCl crystals was used to study the preferential crystallization, and to study the behavior of purity decrease of the product crystals during the crystallization process. The purity of the L-met·HCl product decreased to the equilibrium value over time, with almost no plateau at 100% purity (as is hoped for in preferential crystallizations). This is explainable by the very short induction times for nucleation in these solutions, and also that the L-met·HCl seed crystals may act as a template for the nucleation of the counter-enantiomer.

© 2011 Elsevier B.V. All rights reserved.

1. Introduction

The separation of enantiomers of organic compounds into pure chiral species has received increasing interest recently, largely due to their importance in the pharmaceuticals industry [1]. More than 50% of active pharmaceutical ingredients produced and many food additives are chiral compounds. Hence, enantioseparation and recovery of a pure enantiomer from solution are of significant interest [2,3].

Methionine occurs naturally as L-methionine (L-met). It is one of the essential amino acids, and is a major source of sulfur, which is required in the human diet for normal metabolism and growth, since it is not synthesized in humans. Methionine is often used as an additive in animal feedstuffs, and it is also used in production of medicines and active pharmaceutical ingredients, and as a precursor to other amino acids.

Crystallization is one of the most important separation and purification processes in the pharmaceutical and chemical industries. One method for racemate separation is "resolution by entrainment", which is usually referred to as preferential crystallization [4]. Preferential crystallization is a separation method that is very useful

for the production of optically active amino acids [5] and other chiral materials, and is low cost compared with other separation methods (e.g. chromatography, membrane processes) [6]. However the method is most useful when a racemic solution crystallizes to a conglomerate, i.e. for those systems in which the enantiomers are immiscible in the solid phase [7]. However, this method is a simple and useful method for large scale separation of enantiomers. Although racemic solutions of DL-methionine crystallize into a racemic crystal, DL-methionine hydrochloride (DL-met·HCl) forms a conglomerate [8], thus making the preferential crystallization a potential separation process. Optical resolution of DL-met·HCl by preferential crystallization from ethanolic solutions has already been demonstrated [8], although so far it has not been demonstrated from aqueous solutions. Due to the advantages of using water as a solvent for food and pharmaceutical materials it is useful to determine the feasibility of preferential crystallization from aqueous solutions.

The major objective of this study was to determine the growth rate distribution of L-met·HCl crystal in both pure L-met·HCl aqueous solutions and DL-met·HCl aqueous solutions. A second objective was to study the viability of the preferential crystallization of L-met·HCl in aqueous solution. The growth rate distributions together with the SNT data can be used to optimize operation of the preferential crystallization of DL-met·HCl from aqueous solution. The study was performed in an attempt to

* Corresponding author. Tel.: +66 44224497; fax: +66 44224609.
E-mail address: adrianf@g.sut.ac.th (A.E. Flood).

improve the efficiency and economics of the optical resolution of methionine.

2. Materials and methods

2.1. Materials

DL-met and L-met (>99% and >98%, Acros Organics), hydrochloric acid (37% analytical reagent grade, Carlo Erba), and deionized water (18.2 M Ω cm) were used to prepare DL-met·HCl and L-met·HCl based on the method of Shiraiwa et al. [8]. The two forms of methionine were reacted to form methionine hydrochloride using hydrochloric acid; 208.95 g of DL-met (or 101.49 g of L-met) was dissolved in 350 cm³ (or 170 cm³ for preparation of L-met) of 37% hydrochloric acid in a 0.5-L glass batch crystallizer until dissolution was complete. The solution was continuously agitated using a four-bladed pitch-blade impeller at 350 rpm, and the solution was cooled to 10 °C and maintained at this temperature for 24 h. The precipitated DL- or L-met·HCl was collected by filtration, washed with 5 ml of hydrochloric acid 37% at 10 °C, and dried over silica gel in a desiccator. The pure L-met·HCl crystals were sieved, and the cut between 100 and 600 μ m was used as seed crystals for crystal growth rate measurement.

2.2. Crystal growth rate measurement

These experiments were performed in the small-cell crystallizer depicted in Fig. 1. The supersaturated solution was held in the upper section (the growth section), which had a capacity of approximately 70 ml, and contains a glass cover slip upon which a set of single crystals grows. The supersaturated solution in the upper section was maintained at a temperature of 10 \pm 0.5 °C by circulation of water from a cooling bath in the lower section. The temperature in the growth section was confirmed using a thermometer inserted into the growth cell.

Aqueous solutions (50 ml) of DL- and L-met·HCl were prepared at relative supersaturations (σ) of 0.005, 0.01, and 0.02 (corresponding to the solubility data for racemic solutions of met·HCl

and pure L-met·HCl, respectively, at 10 °C) at a temperature of 45–50 °C to ensure complete dissolution. Nine samples of L-met·HCl seed crystals (sieved to 200–500 μ m) were attached with a very small amount of latex glue onto a 20 \times 20 mm glass cover slip. The glass cover slip was set into the solution chamber of the small-cell crystallizer, which contained the supersaturated L-met·HCl or DL-met·HCl solutions. The crystal size was monitored directly throughout the experiment using a stereomicroscope (model SZX9, Olympus Optical Co., Ltd., Japan) equipped with a microscope digital camera (model DP11 type C-mount CCD camera plus hand switch, Olympus Optical Co., Ltd., Japan) connected to a computer to operate the software for image processing and analysis (Olympus Camedia Master version 1.11). The crystal size was measured using a scale calibrated against a standard wire measured at magnifications of 6.3 \times , 16 \times , 25 \times , and 40 \times . In this experiment, the measurement of the crystal size to determine the growth rate is done only on the crystal dimension that significantly changes and is most easily measured, which is the width of the single crystals. Growth rates based on other faces can be predicted using measured aspect ratios for the crystals. After the growth experiments, data on the number of crystals in the cell, the initial and final sizes of the crystals, and the aspect ratios of the crystals were used to confirm that the supersaturation did not change significantly during the batch. In all cases the decrease in supersaturation was less than 1% relative to the initial supersaturation; for instance an experiment initiated at an initial relative supersaturation of 0.01 had a predicted final supersaturation in excess of 0.0099. The reason for this very small change is that only a very small number of crystals were growing in a large volume of solution. The change in supersaturation predicted is too small to detect using measurement of solution concentration.

2.3. Optical resolution by preferential crystallization

A 100 ml glass vessel (Schott Duran, Germany) was used as a seeded batch crystallizer for preferential crystallization of L-met·HCl from initially racemic solutions of DL-met·HCl. Supersaturated solutions of DL-met·HCl in water were prepared at 0.005 and 0.01 relative supersaturation (σ) (corresponding to the solubility data at 10 °C) by dissolving the solute at a higher temperature than the saturation point until the solution was homogeneous. The solution was quickly cooled down to 10 °C and maintained at the crystallization temperature to within \pm 0.5 °C. Approximately 1 g of L-met·HCl as seed crystals was added to the DL-met·HCl aqueous solution to initiate the batch, and solution and crystal samples were taken at 2, 5, 8, and 10 min after the start of the batch. The suspension in the seeded batch crystallizer was agitated by a centrally located, four-blade impeller driven by an overhead stirrer at 350 rpm. After the required resolution time is reached, the suspension of met·HCl was filtered rapidly through a wire mesh sieve (61 μ m to 104 μ m) to separate the solids from liquids. This was sufficient for good separation of the phases due to the use of large seed crystals. The remaining solution was clear, which indicated that if the counter-enantiomer, D-met·HCl, did nucleate then it is nucleated via a surface-nucleation mechanism. Both solid and liquid contents were weighed on an electronic balance (Sartorius model BP221S, USA) to determine the suspension density (M_T). The solid product was dried over silica gel until the weight of solid was constant.

Between 2 and 5 g of solid (depending on the amount available from the sample) was dissolved to 15 or 20 ml of total aqueous solution to prepare sufficiently concentrated samples for accurate optical rotation measurement. These were kept in a constant temperature bath at 25 \pm 0.5 °C for an hour before the optical activity measurement. The concentration of met·HCl in the samples was monitored using an automatic digital refractometer (RFM

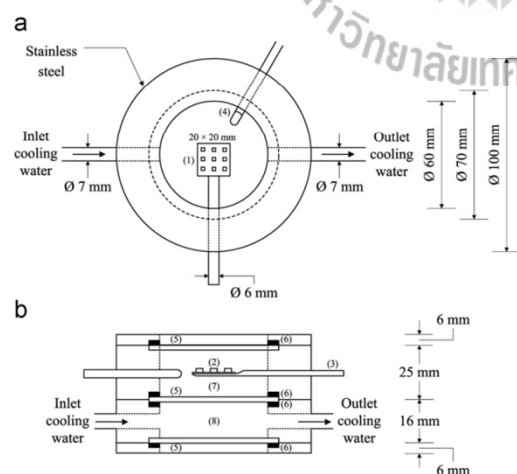


Fig. 1. Schematic diagram of the small-cell crystallizer for use with an optical microscope: (a) top view, (b) side view; (1) glass cover-slip, (2) single crystals, (3) supported rod, (4) thermometer, (5) O-ring seal, (7) sample solution compartment, and (8) constant temperature water circulation compartment.

340, Bellingham and Stanley Limited, UK) with a discrimination of ± 0.00001 RI unit. A calibration curve of known concentration solutions was used to determine total met·HCl concentrations from the refractive index measurement. The optical rotation (α) of solid solutions at various resolution times was determined using a polarimeter (P20, Bellingham and Stanley Limited, UK) at 25 °C. The optical rotation was used to calculate the specific rotation, $[\alpha]_D^T$, of the met·HCl solid sample based on the measured concentration value using the relationship:

$$[\alpha]_D^T = \frac{100\alpha}{cl} \quad (1)$$

where $[\alpha]_D^T$ is the specific rotation, T is the temperature of the measurement, λ is the wavelength of light used (here the sodium D-line, $\lambda=589$ nm is used), c is the concentration of the sample (g/100 mL of solution), and l is the length of the polarimeter tube in decimeters (dm). α is the rotation of the polarized light.

3. Results and discussion

3.1. Growth rate distribution and mean growth rate

Examples of photomicrographs of the crystal growth behavior of L-met·HCl seed crystals in supersaturated solutions of L-met·HCl ($\sigma=0.005$) at 10 °C are shown in Fig. 2. Growth from solutions of different supersaturation levels and growth from D-met·HCl solutions showed similar features, and are not shown here due to space limitations. The seed crystals grew in both visible directions (the width and the length), and small particles that were attached to the single crystal at the initial time (which could not be seen with the naked eye) also grew. However, the growth of small crystals on the seed crystals in L-met·HCl supersaturated solutions was more orderly (and resulted in better shape) than in the growth in supersaturated solutions of DL-met·HCl. This is likely due to the impurity effect that the D-met·HCl had on the growth of the L-met·HCl crystals. L-met·HCl crystals in supersaturated solutions of DL-met·HCl grow mainly in the direction of the longest axis of the crystal. This is likely a growth inhibition effect caused by D-met·HCl acting as an inhibitor.

All growth rate data (321 growth kinetic data representing 54 seed crystals and multiple secondary crystals at the 6 experimental

conditions) were fitted with log-normal distributions using Sigma-Plot® version 9.0. This allows for mean growth rates and standard deviations of the growth rate distributions to be calculated, and these are shown in Table 1. When L-met·HCl crystals are grown in supersaturated solutions of L-met·HCl the crystal growth rates depend strongly on relative supersaturation with very large growth rates evident at a relative supersaturation of 0.02. The measured mean growth rate at a relative supersaturation of 0.01 was slightly smaller than that measured for a relative supersaturation of 0.005; however this is likely to relate to small differences in the quality of the seeds, or differences in the proportions of seed crystals and secondary crystals measured. The mean growth rate of L-met·HCl crystals in DL-met·HCl solutions shows almost no dependence on supersaturation at or above a relative supersaturation of 0.005, although there must be a dependence for lower values of the supersaturation since the growth rate is already 2 $\mu\text{m}/\text{min}$ at $\sigma=0.005$. The growth rate of L-met·HCl crystals from pure L-met·HCl solutions is significantly higher, for the same supersaturation, than the growth of L-met·HCl crystals from DL-met·HCl solutions. The results of the growth rate analysis suggest that D-met·HCl acts as a strong inhibitor to crystal growth of L-met·HCl, as has been seen with counter-enantiomers in other preferential crystallizations [9]. It was noted that the aspect ratios of the crystals grown from DL-met·HCl solutions were slightly more elongated (or narrower) than those grown from L-met·HCl solutions, although this effect was slight.

Table 1
Mean and standard deviation of the crystal growth rate distributions of L-met·HCl crystals grown in DL-met·HCl and L-met·HCl solutions.

Number of growth rate data	Relative supersaturation (σ)	Mean growth rate \bar{G} ($\mu\text{m}/\text{min}$) \pm S.D.
<i>Growth in DL-met·HCl solution</i>		
45	0.005	2.01 \pm 0.86
43	0.01	2.01 \pm 0.91
60	0.02	2.73 \pm 0.92
<i>Growth in L-met·HCl solution</i>		
38	0.005	5.13 \pm 2.31
57	0.01	3.58 \pm 3.57
78	0.02	18.42 \pm 7.03

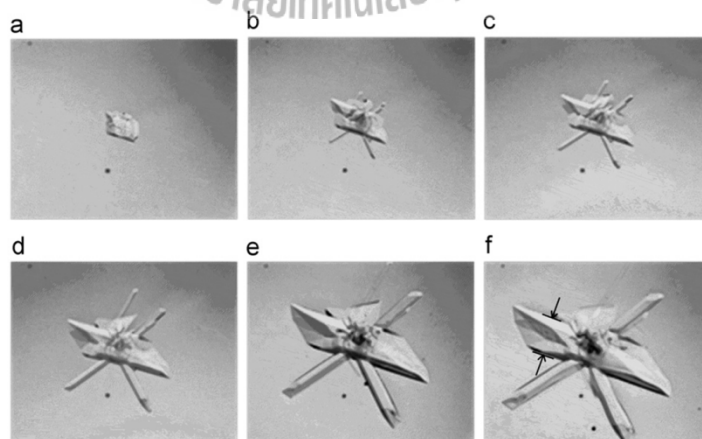


Fig. 2. Photomicrographs of crystal growth of L-met·HCl single crystal in L-met·HCl solution ($\sigma=0.005$) at 10 °C, magnification 25 \times . The measured dimension of the crystal is indicated.

3.2. Optical active and percent purity of *l*-methionine hydrochloride crystal

Preferential crystallization experiments were performed in an isothermal seeded batch process called seeded isothermal preferential crystallization (SIPC). The experiments were repeated at least 4 times at each condition to confirm the accuracy of the experimental results.

Fig. 3 shows the increase in the suspension density as a function of resolution time for the batch initiated at a relative supersaturation of 0.005. The crystallization is rapid, likely because the amount of seed crystal is approximately 1 g, which is a significant fraction of the 3.28 g of product (including seed crystals) expected based on the yield predicted by the solubility. Since there is a relatively large surface area of *l*-met·HCl crystal at the start of the experiment then the de-supersaturation of the solution is rapid. Based on suspension density measurements, the batch initiated at a supersaturation of 0.01 is predicted to be near equilibrium after approximately 30 min, significantly slower than the batch initiated at 0.005 since the amount of seed used was the same, but the required increase in crystal mass to reach equilibrium was larger.

The percent purity of *l*-met·HCl crystal was determined using polarimetry and the results are given in Table 2 for all conditions studied. The relationship between the percent purity of *l*-met·HCl in crystals and resolution time at an initial relative supersaturation of 0.005 is shown in Fig. 4. The result for the batch initiated at 0.01 relative supersaturation is similar, and is not shown here. The percent purity of the *l*-met·HCl crystal decreased rapidly from 100% pure *l*-met·HCl crystal to the equilibrium value (around 60–55% purity, depending on the supersaturation and the amount of *l*-met·HCl seed crystal used) over time. The percent purity of *l*-met·HCl decreased rapidly starting almost from the time of seeding, with no plateau at the 100% purity state, as is desirable in preferential crystallizations. This indicates that the *D*-enantiomer and *L*-enantiomer have nucleated simultaneously at a very early point in the experiment, which causes the percent purity of the *l*-met·HCl crystal to decrease rapidly at the initial state. This can be explained by the very short induction time for nucleation in these solutions; induction times for this system have been measured by our group using an isothermal solution in a 400 mL jacketed batch crystallizer at 10 ± 0.5 °C, with a 4-blade impeller driven by an overhead stirrer operating at 350 rpm. The induction times are typically less than 10 min. Perhaps the seed crystals may act to induce nucleation of the other enantiomer of met·HCl. This seems likely,

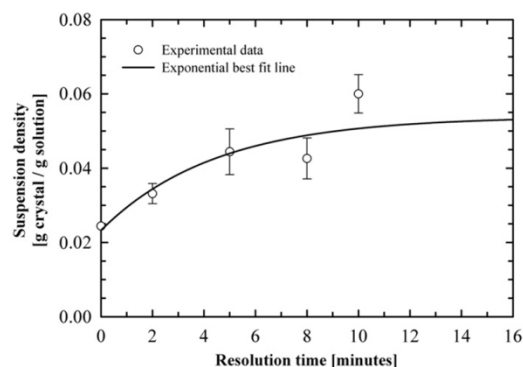


Fig. 3. Suspension density changes during preferential crystallization from *D*-met·HCl solutions (initial $\sigma=0.005$).

Table 2

Optical activity results and percent purity of *l*-met·HCl crystal in *D*-met·HCl aqueous solution ($\sigma=0.005$ and 0.01), measured by the polarimeter at 25 °C.

t (min)	Runs	$[\alpha]_D^{25}$ (deg.)	%-crystal $\pm 2\sigma$
Relative supersaturation = 0.005			
2	4	(+) 11.81	82.34 \pm 2.89
5	4	(+) 9.26	75.36 \pm 1.56
8	4	(+) 3.87	60.60 \pm 3.22
10	4	(+) 2.73	57.46 \pm 2.02
Relative supersaturation = 0.01			
2	4	(+) 11.96	82.75 \pm 1.05
5	4	(+) 6.50	67.81 \pm 5.49
8	4	(+) 4.38	62.00 \pm 2.34
10	5	(+) 2.79	57.63 \pm 2.01

^a Average values.

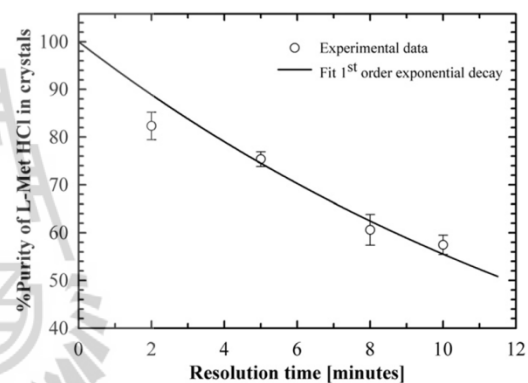


Fig. 4. Optical purity of the *l*-met·HCl crystal during resolution by preferential crystallization from *D*-met·HCl aqueous solution ($\sigma=0.005$). Total solution: 40 g. Solvent: 10.25 cm³ of deionized water. Seed crystals: 1 g of *l*-met·HCl. Crystallization temperature: 10 ± 0.5 °C.

since nucleation of *D*-met·HCl must have occurred to result in the purity decrease; yet when samples were filtered through a mesh of 61 μ m the result was a clear solution and a crystal phase of particles larger than 61 μ m containing the nucleated *D*-met·HCl. In addition, in the small cell crystallization experiments nucleation was not evident in the bulk solution, but many nuclei appeared on the surface of the seed crystals. This mechanism has already been discussed in the literature [9]. Doki et al. studied preferential crystallization of asparagine in which they used a tailor made additive to suppress nucleation [10]. They found that the systems containing little or no additive nucleated the counter-enantiomer very rapidly and this led to the purity of the crystals decreasing rapidly from the initiation of the batch. Adding a nucleation inhibitor greatly increased the time that crystals of essentially pure *D*-asparagine could be produced.

4. Conclusions

The crystal growth rate of *l*-met·HCl depends strongly on the relative supersaturation from supersaturated solutions of pure *l*-Met·HCl but not from racemic solutions. The mean growth rate of *l*-met·HCl seed crystals is significantly faster from pure *l*-met·HCl supersaturated solutions than from racemic solutions,

ARTICLE IN PRESS

W. Srimahaprom, A.E. Flood / Journal of Crystal Growth (2011) 311–315

5

and there is a large degree of growth rate dispersion in both systems. The suspension density (M_T) during the preferential crystallization of D,L-met-HCl aqueous solution increases rapidly with resolution time in the current experiments partly due to the relatively large growth rates but also due to the large amount of seed crystal. The purity of the L-met-HCl crystal decreased rapidly to the equilibrium value over time, due to the influence of the nucleation threshold of the counter-enantiomer being small. Using preferential crystallization to separate the enantiomers of met-HCl from an aqueous solution to obtain a high purity product appears to be very difficult; this study cannot separate the desired enantiomer to close to 100% purity. A process in which a tailor-made additive agent is used to inhibit the primary nucleation of the undesired enantiomer may enable the optical resolution from aqueous solution to be more effective.

Acknowledgment

This research was supported by the SUT Research Fund, Grant no. SUT7-706-51-36-31.

References

- [1] A.N. Collins, G.N. Sheldrake, J. Crosby, *Chirality in Industry: The Commercial Manufacture and Applications of Optically Active Compounds*, Wiley, Chichester, 1992.
- [2] H. Lorenz, A. Seidel-Morgenstern, Binary and ternary phase diagrams of two enantiomers in solvent systems, *Thermochim. Acta* 382 (2002) 129–142.
- [3] S.K. Tulashie, H. Lorenz, C.R. Malwade, A. Seidel-Morgenstern, Ternary solubility phase diagrams of mandelic acid and N-methylephedrine in chiral solvents with different carbon chain lengths, *Cryst. Growth Des.* 10 (2010) 4023–4029.
- [4] J. Jacques, A. Collet, S.H. Wilen, *Enantiomers, Racemates and Resolutions*, John Wiley & Sons, New York, 1981, pp. 217–250.
- [5] S. Yamada, M. Yamamoto, I. Chibata, Optical resolution of α -amino acids by preferential crystallization procedure, *J. Org. Chem.* 38 (1973) 4408–4412.
- [6] H. Lorenz, A. Perlberg, D. Sapoundjiev, M.P. Elsner, A. Seidel-Morgenstern, Crystallization of enantiomers, *Chem. Eng. Process.* 45 (2006) 863–873.
- [7] A. Seidel-Morgenstern, H. Lorenz, D. Polenske, Method for separating compound-forming chiral systems, U.S. Patent 7,820,860 B2, October 26, 2010.
- [8] T. Shiraawa, H. Miyazaki, T. Watanabe, H. Kurokawa, Optical resolution by preferential crystallization of α -methionine hydrochloride, *Chirality* 9 (1997) 48–51.
- [9] G. Coquerel, Preferential crystallization, *Top. Curr. Chem.* 269 (2007) 1–51.
- [10] N. Doki, M. Yokota, S. Sasaki, N. Kubota, Simultaneous crystallization of D- and L-Asparagines in the presence of a tailor-made additive by natural cooling combined with pulse heating, *Cryst. Growth Des.* 4 (2004) 1359–1363.



Paper Code: sp001

Solubility Equilibria Measurements of Enantiomeric Methionine Hydrochloride in Aqueous Solution

Watcharakarn Srimahaprom, Adrian E. Flood*

School of Chemical Engineering, Institute of Engineering,
Suranaree University of Technology, Nakhon Ratchasima, 30000, Thailand
*e-mail: adrianfl@g.sut.ac.th

Abstract – The solubilities of three fixed enantiomeric mixtures of methionine hydrochloride (met-HCl) in pure water (pure enantiomer, racemic mixture, and an intermediate composition) were measured as functions of temperature between 5°C and 40°C by means of the classical isothermal method in an equilibrium apparatus for measuring solubilities in the entire ternary system. A refractive index technique using a refractometer was employed to analyze the concentration of methionine hydrochloride. The results show that the solubilities of the enantiomeric mixture of methionine hydrochloride increased with increasing temperature, and also methionine hydrochloride exhibits high solubility in water. Moreover, the ternary solubility phase diagram of enantiomeric methionine hydrochloride species in aqueous solution is in agreement with the typical ternary phase diagram of a conglomerate system, demonstrating that DL-methionine hydrochloride does not form a racemic crystal.

Keyword: *Amino Acid, Methionine Hydrochloride, Ternary Phase Diagram, Conglomerate, Racemic Mixture*



มหาวิทยาลัยเทคโนโลยีสุรนารี

1. Introduction

Chemical synthesis of chiral substances usually provides 50:50 mixtures of the two enantiomers that are generally called racemates or racemic mixtures. The pure enantiomer form is often synthesized from optically pure substances in the pharmaceutical industry [1]. To design crystallization processes it is necessary to describe the physical and chemical properties of the crystal products, for which the solubility data is perhaps the most significant property. Results of solubility are necessary for the study of any rates in crystallization processes; for example primary and secondary nucleation thresholds, growth rate of crystals, and the optimization of the crystallization of chiral compounds.

Currently the solubility data in water of amino acids are usually obtained by means of the classical solubility measurement techniques. There are broadly classified into isothermal and nonisothermal or polythermal methods. The solubility measurement with isothermal method tends to be more accurate, and the results are usually dependent on the concentration measurement or weighing accuracy achieved [2]. Moreover, the solid-liquid equilibria (SLE) data expressed in binary (melting point defined) and ternary (solubility behavior of the system) phase diagrams are necessary and required to allow optimization of separation of enantiomers and also increase the productivity [3, 4].

The present work is concerned with the determination and analysis of the solubility data and the ternary solubility phase diagram of methionine hydrochloride (a conglomerate-forming system) in three fixed enantiomeric mixtures at different temperatures. The results can be extended to study any properties in the crystallization process, e.g. primary and secondary nucleation threshold, mean growth rate of crystals, and also the optimization of preferential crystallization to gain the pure enantiomer(s) of methionine.

2. Experimental Procedure

The methionine hydrochloride ($\text{met} \cdot \text{HCl}$) concentration of the experimental batch crystallization solution was monitored using an automatic digital refractometer (RFM340, Bellingham and Stanley Limited, UK) at a controlled temperature of 25°C. The discrimination of the refractive index (RI) value is ± 0.00001 RI units. A calibration curve of known $\text{met} \cdot \text{HCl}$ concentration solutions at 25°C was used to determine total $\text{met} \cdot \text{HCl}$ concentrations from the refractive index measurements.

2.1. Materials

DL-methionine (DL-met) and L-methionine (L-met) were purchased from Acros Organics (with 99+% and 98+% purity respectively), and hydrochloric acid (37%

analytical reagent grade) was purchased from Carlo Erba. These two methionine amino acids and hydrochloric acid were used to prepare the DL-methionine hydrochloride compound ($\text{DL-met} \cdot \text{HCl}$) and L-methionine hydrochloride crystal ($\text{L-met} \cdot \text{HCl}$), which has been prepared based on the experimental method of Shiraiwa et al. [5]. Deionized water (18.2 M Ω -cm) was used to prepare all aqueous solutions throughout the experiments.

2.2. Methionine Hydrochloride Preparation

The two forms of methionine (enantiopure L-met and racemic DL-met) were reacted to form $\text{met} \cdot \text{HCl}$ in sealed batch crystallization experiments, as shown in Fig. 1, using hydrochloric acid 37% as a reagent. 5.97 g of DL- or 5.97 g of L-met was dissolved in 10 cm³ of hydrochloric acid 37% in a 0.5 liter glass vessel with a sealed glass lid (to reduce solution loss at higher than room temperature) until complete dissolution, and then the solution was kept in a water bath at 10°C with agitation at 350 rpm by a centrally located four-blade propeller driven by an overhead mixer for around 24 hours. The precipitated DL- or L-met·HCl was collected by filtration with a filter paper (number 42 ashless 110 mm diameter, Whatman). The solution was filtered through a buchner funnel using an aspirator (Eyela model A-3S, Tokyo Rikakikai Company Limited, Japan) and washed with 5 ml of hydrochloric acid 37% at 10°C. Both solid products were dried over silica gel in a desiccator.

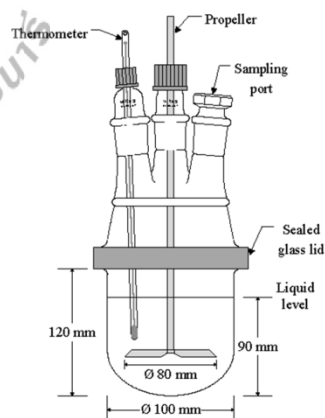


Fig. 1. The 0.5 liter glass batch crystallizer

2.3. Concentration Calibration Curve of $\text{DL-met} \cdot \text{HCl}$

DL-met·HCl samples were dissolved in water by varying the mass of DL-met·HCl for 100 g solution at 25 \pm 0.5°C. The solutions were stirred constantly with a magnetic stirrer bar. The solution samples were removed after 24, 29, 34, and 39 hours and they were

filtered through a 0.45 μm cellulose acetate membrane filter in a 47 mm filter holder connected to a 20 ml disposable syringe. The solutions were analyzed for DL-met·HCl content by refractometry and pH values using a pH meter (CyberScan pH510, Eutech Instrument Private Company Limited, Singapore).

2.4. Solubility Measurement

The solubility data of the conglomerate (DL-met·HCl), pure L-methionine hydrochloride enantiomers (L-met·HCl), and also a 75% L- and 25% D-met·HCl mixture were measured at 5, 10, 25, and 40°C by means of the isothermal method based on the classical solubility measurement. The experimental procedure uses a concentration calibration curve of DL-met·HCl. The experimental equipment setup is shown in Fig. 2. Excess solid met·HCl was added into 20 ml of deionized water in a 100 ml laboratory glass bottle with a screw cap which was placed into a 3 liter beaker on a magnetic stirrer plate. Constant temperature water from a water bath was circulated through the 3 liter beaker to maintain a constant solution temperature. The met·HCl compounds were maintained at constant temperature with stirring at all times until dissolution was complete; about 48 hours. 2 ml of solution was taken to separate the liquids from solids through a 0.45 μm cellulose acetate membrane filter. The liquid sample was diluted at a ratio of 1:4 by mass and was kept at 25°C for an hour before measuring the solution concentration at 25°C by the refractive index method. These experiments were started at 40°C, then were continued at 25, 10, and 5°C using the same samples of DL-met·HCl. L-met·HCl solubilities were first determined at 5°C for then also 10, 25, and 40°C, adding small amounts of solute until the solubility was reached. The two solubility measurement techniques give results that are consistent with each other. Solubility measurements of L-met·HCl were started at low temperature because this can conserve the raw material (L-met·HCl). The solubility of an equimolar mixture of DL- and L-met·HCl was determined using the same method as for L-met·HCl. All experiments were made at least three times, and results were averaged.

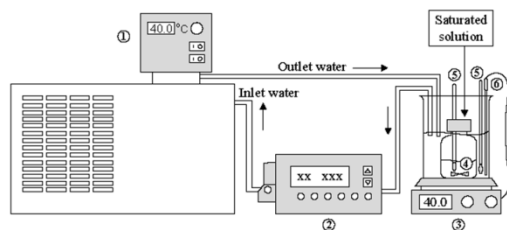


Fig. 2. The design of solubility experimental setup of met·HCl three fixed enantiomeric mixtures in water, which consists of (1) thermostat, (2) feed pump drive, (3) magnetic stirrer with hot plate, (4) magnetic bar, (5) thermometer, and (6) temperature probe

3. Results and Discussion

The concentration calibration curve of DL-met·HCl solution at 25°C for use in calculating the met·HCl content is shown in Fig. 3. There is a straight line relationship ($r^2 = 0.9997$) and the fitted line is shown in equation 1, where C represents the met·HCl concentration and RI represents the refractive index (n_D). The calibration curve has a y-axis intercept of 1.3330 which is the refractive index of pure water. The refractive index of DL-met·HCl solutions is linearly dependent on the DL-met·HCl concentration in a range between 0.0 to 20.0 g met·HCl / 100 g solution.

$$RI = 1.925 \times 10^{-3} C + 1.3330 \quad (1)$$

The measured pH value is strongly affected by the amount of met·HCl, however the data is not shown here. The pH value decreases with an increasing amount of met·HCl in water; the met·HCl solutions are strongly acidic solutions.

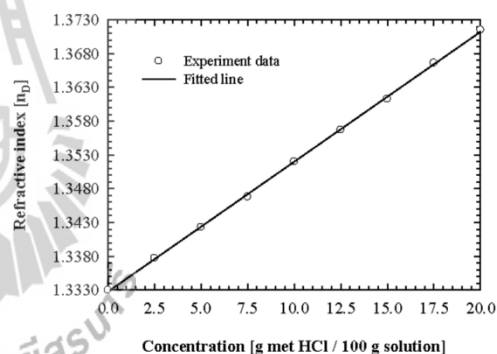


Fig. 3. Refractive index for calibration curve of DL-methionine hydrochloride (DL-met·HCl) in water at 25°C

Table 1 shows the solubility data of conglomerate met·HCl, pure enantiomer met·HCl (L- and D-met·HCl are enantiomorphs where the physical and chemical properties shown here are identical), and the 1:1 mixtures of L- and DL-met·HCl in water as a function of temperature. Solubilities of DL- and L-met·HCl in water show an increasing tendency with increasing temperature as shown in Fig. 4 and Fig. 5 respectively.

Table 1. Average value of solubility results, and standard deviation (2σ) of three enantiomeric methionine hydrochloride in water at different equilibrium temperature

T, °C	Run	g/100 g H ₂ O $\pm 2\sigma$		
		DL-met·HCl	L-met·HCl	*mixture
5	3	262 \pm 33	168 \pm 17	129 \pm 13
10	3	284 \pm 35	170 \pm 12	162 \pm 17
25	3	315 \pm 10	191 \pm 12	235 \pm 5
40	3	387 \pm 53	224 \pm 21	284 \pm 22

*75% L-met·HCl + 25% D-met·HCl

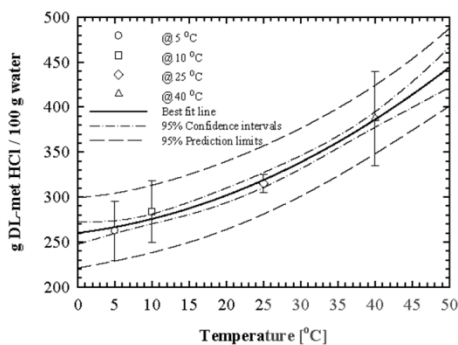


Fig. 4. Solubility data of the conglomerate DL-methionine hydrochloride (DL-met·HCl) in water

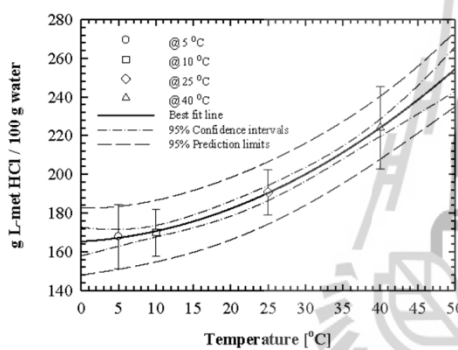


Fig. 5. Solubility data of pure enantiomer L-methionine hydrochloride (L-met·HCl) in water

Fig. 6 shows a comparison between the solubility of the conglomerate met·HCl in water and the racemic compound form of methionine in water in the temperature range of 0°C to 50°C.

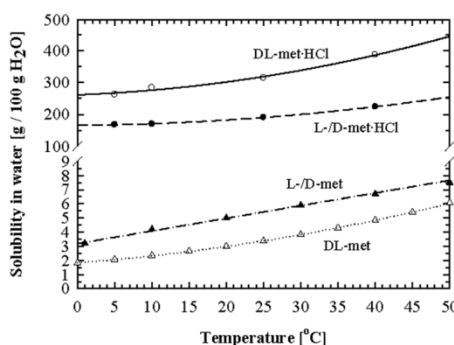


Fig. 6. Solubility of (○) conglomerate DL-met-HCl (from this work) and (●) L-/D-met-HCl (from this work) in water compared to solubility literature data of (Δ) DL-met (replotted from Dalton and Schmidt, 1935) and (▲) L-/D-met (replotted from Polenske and Lorenz, 2009) in water

This shows that the solubility of DL-met [6] is lower than the two enantiomeric forms (L- and D-met [7]), but

the solubility of DL-met·HCl form is higher than that of L- and D-met·HCl, which makes the conglomerate more stable than the racemic compound, as theoretically expected [8]. Both the solubility of the conglomerate and racemic crystals were increased with increasing temperature, and the solubility of the conglomerate of the hydrochloride form of methionine is very much higher than the solubility of the racemate form of methionine.

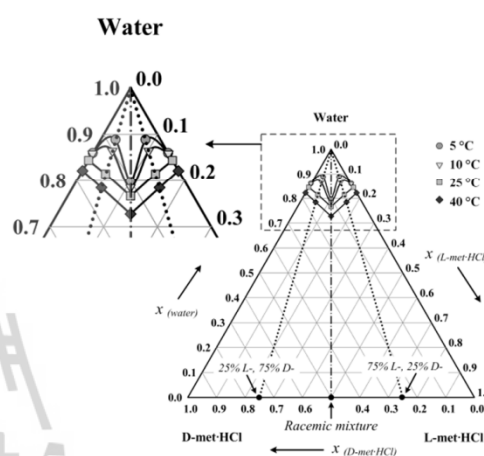


Fig. 7. Ternary solubility phase diagram of L-methionine hydrochloride (L-met·HCl) + D-methionine hydrochloride (D-met·HCl) + water. The phase diagram is shown for isotherms at 5°C, 10°C, 25°C, and 40°C (from top to bottom). The isotherm lines are just guides to the eye

The ternary solubility phase equilibria of enantiomeric methionine hydrochloride in water (in mole fraction) is presented in Fig. 7. These consist of all measured solubility data of the pure enantiomers of methionine hydrochloride (L-/D-met·HCl), the racemic conglomerate (DL-met·HCl), and mixture compositions (75% L-met·HCl + 25% D-met·HCl and 75% D-met·HCl + 25% L-met·HCl) in water in the ternary phase diagram.

The equilateral triangular form consists of the vertices of the triangle which represent the pure components of water (on top), and L- and D-met·HCl (right and left). The triangle sides show content in mole fraction which represents the binary systems, for example L-met·HCl / water, L-met·HCl / D-met·HCl, and D-met·HCl / water. Each point inside the phase diagram describes a ternary mixture consisting of all three components. The solubility isotherms of enantiomeric methionine hydrochloride exhibit the typical shape of a conglomerate forming chiral system with a maximum solubility at the racemic composition (DL-met·HCl).

The four solubility isotherms at 5°C, 10°C, 25°C, and 40°C are strongly dependent on temperature with an increase in temperature resulting in a rapid rise in solubility. All solubility data has mirror image

TICHe International Conference 2011
November 10 – 11, 2011 at Hatyai, Songkhla THAILAND

symmetry with respect to the racemic compound line but the solubility lines at 5°C and 10°C are curved which is different to the solubility lines at 25°C and 40°C. Solubility results at 5°C and 10°C indicate non-ideal solution behavior at the solubility at 5°C and 10°C. The solubility results at 25°C and 40°C displayed ideal behavior in the solutions.

4. Conclusions

The refractive index method is a convenient and simple measurement of solid content in liquids. The refractive index can well determine the solubility values. The solubility of three fixed enantiomeric mixtures in water (pure enantiomer, racemic conglomerate, and 75% L- and 25% D-met·HCl mixture) are strongly dependent on the temperature and solubility increased with increasing temperature. More specially, it has been found that, when DL-met is converted into crystals of DL-met·HCl the resulting species has a much higher solubility in water than the free form (see Fig. 6). On the other hand, the L-form or D-form of met·HCl has a lower solubility in water than DL-met·HCl (see Fig. 6). Thus, it becomes possible to separate crystals of the L-form or D-form of met·HCl from DL-met·HCl using the preferential crystallization process. The ternary solubility phase diagram of L-met·HCl + D-met·HCl + water is in accordance with the typical ternary phase diagram for a conglomerate type compound. The solubility equilibrium points on the ternary phase diagram can define the phase regions on the phase diagram; hence the state condition of the substance can be determined.

Acknowledgement

This research was supported by the SUT Research Fund, Grant no. SUT7-706-51-36-31.

References

- [1] D. Sapoundjiev, H. Loran, A. Seidel-Morgenstern, Solubility of chiral threonine species in water/ethanol mixtures, *J. Chem. Eng. Data* 51 (2006) 1562-1566.
- [2] R. Mohan, H. Lorenz, A. S. Myerson, Solubility measurement using differential scanning calorimetry, *Ind. Eng. Chem. Res.* 41 (2002) 4854-4862.
- [3] H. Lorenz, A. Seidel-Morgenstern, Binary and ternary phase diagrams of two enantiomers in solvent systems, *Thermochim. Acta* 382 (2002) 129-142.
- [4] H. Lorenz, A. Perlberg, D. Sapoundjiev, M. P. Elsner, A. Seidel-morgenstern, Crystallization of enantiomer, *Chem. Eng. Process.* 45 (2006) 863-873.
- [5] T. Shiraiwa, H. Miyazaki, T. Watanabe, H. Kurokawa, Optical resolution by preferential crystallization of DL-methionine hydrochloride, *Chirality* 9 (1997) 48-51.
- [6] J. B. Dalton, C. L. A. Schmidt, The solubilities of certain amino acids and related compounds in water, the densities of their solutions at twenty-five degrees, and the calculated heats of solution and partial molal volume. II, *J. Biol. Chem.* 109 (1935) 241-248.

- [7] D. Polenske, H. Lorenz, Solubility and metastable zone width of the methionine enantiomers and their mixtures in water, *J. Chem. Eng. Data* 54 (2009) 2277-2280.
- [8] A. E. Flood, Recent patents on the optical resolution of amino acid enantiomers by crystallization from solution, *Recent Patents on Materials Sciences* 1 (2008) 98-115.

BIOGRAPHY

Mr. Watcharakarn Srimahaprom was born on January 20, 1985 in Phu Khiao District, Chaiyaphum Province. He graduated with the Bachelor of Engineering Degree of Chemical Engineering in 2008 from Suranaree University of Technology (SUT), Nakhon Ratchasima, Thailand. He was very well taken care and educated under the supervision of Assistant Professor Dr. Chalongsri Flood, which is an undergraduate advisor.

Among the studying, he was an occupational trainee in Chemical Engineering at Pipeline Maintenance and Engineering Division, Transportation Management and Technical Service Department, Chonburi Operation Center, PTT Public Co., Ltd. during his SUT Cooperative Education Program in 2007. His responsible is research and monitoring the internal corrosion of offshore natural gas pipeline systems (eastern seashore).

After graduating, he has received the scholarship for research from the SUT Institute of Research and Development Fund to study the Master of Engineering Degree in Chemical Engineering at SUT since year 2008. He has special studied in the industrial crystallization research group, with thesis advisor is Professor Dr. Adrian E. Flood. His research interests cover the area of chiral resolution of amino acids via preferential crystallization through the investigation of relevant thermodynamic and kinetic properties for efficient design of preferential crystallization in pharmaceutical and food industries. During the studying, he has received the scholarship for a teacher assistant at SUT since year 2008 to 2009.